Abstract

Title of Thesis: Hardware Design of a Wearable System for Gesture-Based

Teleoperation of a Robotic Manipulator

Degree candidate: Brooke Teresa Buchholz

Degree and year: Master of Science, 2007

Thesis directed by: Associate Professor David L. Akin

Department of Aerospace Engineering

To overcome some of the difficulties of robotic teleoperation using hand controllers, a new approach is necessary, namely gesture-based control. A review of sensors currently in use for human joint angle measurement is presented. Based on this review, a method was chosen that uses a variable-length fiber optic sensor. Several different types of optical fibers, along with a variety of test configurations, were initially evaluated, and the most promising of these were selected for further testing. This thesis describes these methods of evaluation and the final system design and testing of a wearable system for gesture-based control of a robotic manipulator, including a discussion of sensor placement to obtain improved results. The final system presented requires improvements and continued research to become usable for robotic control. However, the basic concept and design are shown to provide reliable information regarding relative human joint motion.

Hardware Design of a Wearable System for Gesture-Based
Teleoperation of a Robotic Manipulator

by

Brooke Teresa Buchholz

Thesis submitted to the Faculty of the Graduate School of the
University of Maryland, College Park in partial fulfillment
of the requirements for the degree of
Master of Science
2007

Advisory Committee:
Dr. Dave Akin, Chair/Advisor
Dr. Mary Bowden
Dr. Sean Humbert

Dedication

This thesis is dedicated to

My Dad

who bought me my first robot kit and taught me how to solder and

who always asks lots of questions and tries to understand what I do

Acknowledgments

Do not fear, for I have redeemed you; I have called you by name, you are mine. When you pass through the waters, I will be with you; and through the rivers, they shall not overwhelm you; when you walk through fire you shall not be burned, and the flame shall not consume you. For I am the Lord your God, the Holy One of Israel, your Savior.

Isaiah 43:1-3

I have to start my thanks with Kim, Kate, and Chett, without whom I probably would not have made it through the past three years. Of course, I must also thank my parents and my sister, who provided unfailing encouragement and support, not just during the past three years, but throughout my life. I would also like to thank my roommates, Emily and Ginny, for smiling and nodding when I would come home excitedly yammering on about my project, which they don't really understand.

Thank you, Dave, for picking me out of the pile of applications to be your grad student. Thank you for finding money to keep paying me all the way through my third year. Thanks for putting up with my initial lack of focus and switching projects until we found one that would sufficiently excite and motivate me.

Thank you, Dr. Bowden and Dr. Humbert, for being on my thesis committee. With eight other students just from the SSL graduating, I know you have a busy couple of months of thesis defenses. Thanks for letting mine be one of them.

Last, but certainly not least, I want to thank all of the wonderful people at the SSL, particularly Heather for being a wonderful, helpful assistant, for being the first and primary guinea pig for the JAMSTORM Vest of Science, and for being

excessively excited about everything in life; Rico for machining things for me and saying nice things when I would freak out about my thesis and life; Shane for knowing where the old JAMS equipment could be found and for always being really excited about the future potential of my research to be used with MARS suit; Nick for being another EE to bounce ideas off of; and Kiwi for being amazingly helpful in so many ways they can't be listed here.

Table of Contents

List of Tables

List of Figures

List of Abbreviations

ADC – Analog-to-Digital Converter
DOF – Degrees of Freedom
EAM – Exoskeletal Arm Measurement
EMG – Electromyography
EVA – Extra-Vehicular Activities
FES – Functional Electrical Stimulation
FSR – Force Sensitive Resistor
JAMS – Joint Angle and Muscle fatigue Sensor
JAMSTORM – Joint Angle Measurement System for TeleOperation
of a Robotic Manipulator
LED – Light Emitting Diode
MARS Suit – Maryland Advanced Research/Simulation Suit
MGA – Maryland-Georgetown-Army
NBRF – Neutral Buoyancy Research Facility
RMS – Remote Manipulator System
ROM – Range of Motion
SSL – Space Systems Laboratory
USB – Universal Serial Bus

Chapter 1

Introduction

1.1 Motivation

To date, the primary method for teleoperation of a robotic manipulator consists of using joysticks and a multitude of camera views. The space shuttle setup requires two joysticks and two astronauts to operate the Remote Manipulator System (RMS). One joystick is used to translate forward/backward, up/down, and left/right and the other is used to control yaw, roll, and pitch. One astronaut uses these joysticks to control the RMS, while a second astronaut manipulates the available camera views. In addition to the closed-circuit television monitors, the astronauts also observe RMS operation through overhead windows [1]. Even given all of these viewing options, it can be extremely difficult, sometimes impossible, to obtain adequate camera views, either for extravehicular activity (EVA) monitoring or for vehicle inspection [2]. This problem of sufficient camera views also applies to robotic teleoperation. Depending on the available views of the manipulator and target, it can be extremely difficult to determine the joystick movements necessary to move the manipulator to the desired position and orientation without running into objects or singularities.

Another drawback to the use of hand-controllers is that they need to be mounted, for example to a control panel in the space shuttle or space station. As

Figure 1.1: Space Shuttle Aft Flight Deck Mockup at the University of Maryland SSL, showing joysticks and closed-circuit television monitors for teleoperation of a robotic manipulator [3]

humans return to the moon and continue on to Mars, joysticks for robotic teleoperation could be mounted on a table inside the astronauts' habitat or on the dashboard of a rover. This need to attach hand-controllers to some sort of console means that the user has to either remain at or return to a control station to be able to teleoperate the robot. In future space exploration, it will be beneficial for humans to be able to work alongside robots, interacting with them while, at the same time perhaps, teleoperating them. In this case, it will be less work for the humans if they can remain in their current working positions during teleoperation, instead of returning to a control station.

These issues can be dealt with by employing a gestural control system for teleoperation. This type of system makes teleoperation much more intuitive than using hand-controllers by allowing the user to simply move his or her arm in the

manner of the desired robot movement. The system measures the position and orientation of the user's arm and translates this information into control data for the robotic manipulator. The manipulator is then instructed to move to the position and orientation corresponding to the user's motion.

1.2   Thesis Objective and Overview

The purpose of the Joint Angle Measurement System for TeleOperation of a Robotic Manipulator (JAMSTORM) project is to evaluate the feasibility of using fiber optic cables to measure human joint angles during shoulder abduction/adduction, shoulder flexion/extension, and elbow flexion/extension. To this end, a variety of optical fibers were tested in a progression of test configurations to determine the most likely candidates for joint angle measurement. Once the optical fiber and necessary electronics were selected, the cables and light emission and detection electronics were a vest and armbands to create a wearable system. This collective system was then tested further to verify that the hardware would function in a realistic, human-worn configuration the same way it did during initial testing.

The joint angle data collected by JAMSTORM is currently stored in text files for later, offline analysis. However, for use in gestural control, this data will need to be analyzed in real-time and be sent to the robotic control software, which will move the manipulator to mimic the human user's motions. Integration of the JAMSTORM data with robotic control software is beyond the scope of this thesis. Future plans include supplying the output of the JAMSTORM sensors to the control system

Figure 1.2: Maryland Advanced Research/Simulation Suit at the University of Maryland Space Systems Laboratory[6]

for the Ranger dexterous manipulator and integrating the JAMSTORM hardware into the Maryland Advanced Research/Simulation (MARS) suit at the University of Maryland Space Systems Laboratory (SSL). Ranger is a robotic manipulator originally designed for operation on the space shuttle. It has two arms, each with 8 degrees of freedom (DOF), and a 6-DOF positioning leg [4]. Ranger is currently controlled using translational and rotational hand-controllers in a setup similar to the setup on the space shuttle for the RMS. MARS suit is test bed used for neutral buoyancy testing and research related to space suit design and extravehicular activity (EVA) operations [5].
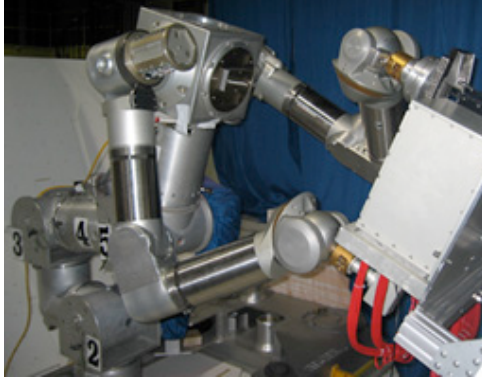
Figure 1.3: Ranger Dexterous Manipulator at the University of Maryland Space Systems Laboratory[7]

Chapter 2 provides an overview of several methods that have been used for measuring joint angles. Some of these are wearable systems, while some are not. Chapter 3 introduces the Joint Angle and Muscle fatigue Sensor (JAMS) system that was developed at the SSL. JAMS uses etched optical fibers sewn into a glove to measure finger joint angles during pressurized EVA tasks. While JAMSTORM is not a direct continuation of the JAMS project, the two systems use related technology, so some of the JAMS hardware and software were used as an initial proving ground for the current JAMSTORM project. Chapter 4 describes the design process and various test phases. Chapter 5 describes the final system and test setup. Methods of data analysis are discussed and test results are provided. Finally, Chapter 6 discusses the conclusions of this thesis and the remaining research required to integrate JAMSTORM with the Ranger dexterous manipulator and MARS suit at the SSL.

Chapter 2

Background and Literature Review

2.1 Human Joint Movement

Marcus, An, and Eberman [8] looked at the different arm motions that should be used for robot control and how to map the human movements to robot movements. They compiled a set of range-of-motion (ROM) requirements was compiled for both unsuited and suited human movement. Medical literature was explored to determine the unsuited ROM, and NASA studies were consulted for the ROM of a person in a spacesuit.

Joint Motion	Normal ROM	Suited ROM
Shoulder Abduction/Adduction	150 deg	150 deg
Shoulder Medial/Lateral Rotation	130 deg	120 deg
Shoulder Horizontal Flexion/Extension	170 deg	150 deg
Scapula Elevation/Depression	10-12 cm	N/A
Scapula Medial/Lateral Movement	15 cm	N/A
Scapula Rotation	60 deg	N/A
Elbow Flexion/Extension	145 deg	130 deg
Forearm Supination/Pronation	180 deg	180 deg
Wrist Flexion/Extension	170 deg	N/A
Wrist Radial/Ulner Deviation	60 deg	N/A

Table 2.1: Suited and Unsuited Ranges of Motion [8]
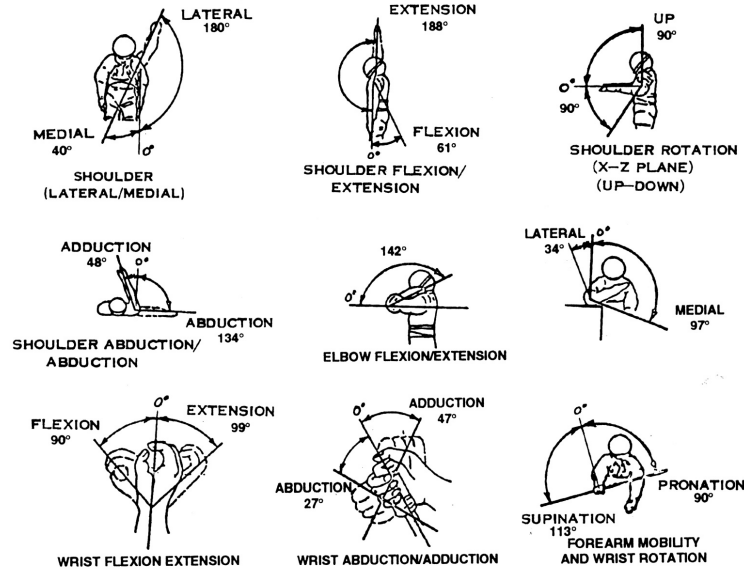
Figure 2.1: Human Ranges of Motion [9]

However, not all of these human arm movements easily correspond to those of a robotic manipulator. Table 2.1 provides ranges of motion for the joints of some robotic manipulators that are meant to closely match human motion capabilities. At the shoulder, robotics arms tend to have only two or three degrees of freedom – pitch, yaw, and sometimes roll – equivalent to the human shoulder motions of abduction/adduction, flexion/extension, and medial/lateral rotation (Fig 2.1). This means there is no robotic equivalent of the scapula elevation/depression, rotation and medial/lateral motions; therefore, for teleoperation of this type of manipulator, these human movements can be ignored. The rest of the joint motions of the human arm can be associated with robotic manipulator degrees of freedom: elbow medial/lateral rotation, elbow flexion/extension, forearm supination/pronation, wrist flexion/extension, and wrist ulner/radial deviation in a human can be mapped to

7

elbow roll, elbow pitch, wrist roll, wrist pitch, and wrist yaw in a robotic arm, respectively.
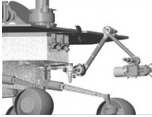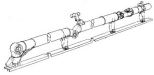
Joint	Manipulator Limits (deg)				
	MER [10]	SRMS [11]	Ranger [12]	WABIAN-2 [13]	HRP-2 [14]
Shoulder Pitch	70	+145 to -2	-220 to 220	-180 to 180	-180 to 60
Shoulder Yaw	160	±180	-107 to 107	-180 to 180	-90 to 90
Shoulder Roll	N/A	N/A	-220 to 220	-17 to 196	-95 to 10
Elbow Pitch	290	+2 to -160	-1 to 169	-10 to 130	-135 to 0
Elbow Roll/Yaw	N/A	N/A	-310 to 130	-180 to 180	-90 to 90
Wrist Pitch	340	±120	-110 to 290	-47 to 47	-90 to 90
Wrist Roll	350	±447	-811 to 811	-115 to 41	N/A
Wrist Yaw	N/A	±120	-105 to 105	N/A	N/A

Table 2.2: Ranges of Motion for Selected Manipulators

2.2 Joint Angle Measurement Systems

There are many different methods for measuring joint angles during human movement. Each method has both benefits and drawbacks. This section provides an overview of several types of joint angle measurement systems.

2.2.1 Vision Systems

One way to measure joint angles is to use a vision system. These systems capture motion data using cameras. One type of visual motion analysis system relies on computer software to first detect relevant objects, such as humans, in the images, then track these objects as they move through consecutive images, and finally categorize the motion of these objects to enable some understanding of the motion [15]. Each of these three tasks is performed strictly in software and is extremely complicated. Recognizing and understanding motions are the most difficult tasks to perform accurately. However, object detection and tracking are not simple tasks either. Difficulties arise when an object becomes partly or entirely hidden behind another object in the scene. This problem can be reduced by using images from multiple cameras, but this introduces new complications and requires further research.

Another type of optical motion analysis system is currently in use in the entertainment industry for building computer models of humans for animation. The cameras in these systems track retro-reflective markers placed on various parts of a person's body. This technique has been used by Weta Digital to create characters such as Gollum in the "Lord of the Rings" trilogy [16], [17] and by Imageworks for entire motion pictures like "The Polar Express" [18]. These commercially-available optical motion analysis systems are considered to be somewhat of a "gold standard" against which new types of motion analysis systems are compared [19], [20], [21]. However, optical systems also tend to be quite large and expensive and cannot be

used outside of the laboratory environment.

2.2.2 Exoskeletons

Another way to measure arm joint angles is through the use of an exoskeleton. Exoskeletons are generally designed for rehabilitation or strength enhancement, as well as teleoperation. In 1990, Repperger, Remis, and Merrill performed tests using a 7-DOF passive exoskeleton. Each joint has an optical encoder with an accuracy of 1024 parts per revolution and a frequency response of $100\,\mathrm{kHz}$ for obtaining position information [22]. The Maryland-Georgetown-Army (MGA) exoskeleton uses optical incremental encoders to measure motor position. Optical absolute encoders are also used in the system to determine the position of the exoskeleton at system start up and as a check of the operation of the incremental encoders [23].

As shown by these examples, exoskeletons tend to use optical encoders, both absolute and relative, to determine joint angles. The main drawback to exoskeletons for angle measurement in teleoperation is their size. The bulk of exoskeletons is created by all of the actuators and electronics needed to power the arm for rehabilitation or strength augmentation; however, for pure angle measurements, actuators are not needed, so a smaller, simpler design could be found.

2.2.3 Gyroscopes and Accelerometers

Many wearable motion detecting systems use gyroscopes and accelerometers to measure angular velocities and accelerations, respectively. Perng, et al [24] de-

signed a glove that uses accelerometers to measure hand motions. This device contains/consists of six accelerometers – one on each of the fingertips and one on the back of the hand. The glove was shown to work well as a mouse pointing device with Windows NT and 98.

Most other systems that use accelerometers and gyroscopes for motion sensing are developed for use in gait analysis and/or functional electrical stimulation (FES). In 1999, Tong and Granat [19] designed a system that used only two gyroscopes, one attached to the subject's shank, the other attached to the thigh, to measure angular velocities during walking. By integrating these velocities, the inclination of the shank and thigh could be calculated; the knee joint angle can then be found from these inclinations. The results of this system were shown to correlate well with the signals obtained from the Vicon optical motion analysis system.

Instead of gyroscopes, Williamson and Andrews [25] used a cluster of three uni-axial accelerometers attached to the subject's shank. Force sensing resistors (FSRs) were placed on the shoe insole and were used as gait phase reference signals. Five gait phases were defined – loading response, mid-stance, terminal stance, pre-swing, and swing – and all phases were successfully detected with an accuracy of approximately 98%.

A 2001 system uses force sensitive resistors (FSRs) and a gyroscope for gait detection [20]. Three FSRs are used to measure the forces exerted by the foot on the shoe insole during walking and standing activities. The gyroscope is attached to the heel of the shoe with its sensing axis oriented to measure rotational velocity of the foot. The gait cycle is divided into four gait phases: stance, heel-off, swing,

and heel-strike.

First, the delay and accuracy of the system were compared to a reference gait signal obtained using a Vicon 370 optical motion analysis system. The experimental system compared well to the optical motion analysis system, though there was some time delay in the experimental system. The worst case gait phase detection delay was about 90 ms. These delays can be explained by the fact that two different types of systems were used to measure gait phase transitions – the visual system identifies the change from swing to heel-strike at the point of initial contact, whereas the force-sensor system identifies that change at the point when the heel sensor is loaded with weight.

The second set of experiments involved testing the performance of the system during a variety of walking tasks – level ground, slopes, stairs, and irregular surfaces. The system showed high reliability in gait detection over a variety of walking tasks, with a worst-case success rate of 96%. System performance during non-walking tasks was also examined. The system performed extremely well during non-walking tasks, never detecting gait phases when subjects stood up, sat down, or shifted weight while standing. The final set of experiments determined the range of walking speeds for which the system is reliable. Again, the system demonstrated excellent reliability (100%) during speed tests from slow walking at 0.5 km/hr to fast jogging at 13 km/hr.

Another system used two sensing units, each composed of both a uni-axial and a bi-axial accelerometer [26]. The worst-case accuracy determined for this system was 3 deg, which means that the system can recognize at least 60 distinct positions

for a 180-deg movement. The system was also shown to provide correct position tracking for motions at speeds of up to 3 radians/s. Similarly, another system also used two sensing units, one attached to the thigh and one to the shank, but these units contained two accelerometers and one gyroscope [27]. This system showed good results when compared to an ultra-sound-based motion tracking system, achieving a correlation coefficient of 0.997 and an average root mean squared error of 1.30 deg.

Liu, et al [21] developed two systems, the first for sensing motion of the foot and the second to detect motion of the leg and foot. The purpose of these two systems was to detect four gait phases: stance, toe-rotation, swing, and heel-rotation. The first system consists of two gyroscopes to measure rotational velocities of the foot in two directions and a two-axis accelerometer chip to measure accelerations of the foot. To prove the abilities of this wearable, foot-tracking system, results were compared to those of Hi-DCam, a commercial optical motion analysis system used to track 3-dimensional trajectories of retro-reflective markers that, for this experiment, were placed on the subject's toe, heel, ankle, and knee. From this data, the experimental system was determined to perform as well as the commercial optical system, so system development progressed to track the motions of the entire leg. The new system contains three gyroscopes, one attached to foot, one to the shank, and one to the thigh, to measure those angular velocities. There is also a two-axis accelerometer attached to side of thigh to measure accelerations.

Many systems using combinations of gyroscopes and accelerometers for motion detection and tracking have been developed. These systems have been shown to work well for detecting four or five specific phases of the human walking cycle. One

system was shown to be capable of distinguishing between 60 different positions [26], so a similar system might be useable for detecting arm motions for teleoperation.

2.2.4   EMG signals

Electromyography (EMG) uses electrodes placed on the skin to measure the changing electrical properties of human muscle fibers as the muscle extends and contracts. These changes can be correlated to both muscle fatigue [28] and joint motion.

One EMG system developed for teleoperation uses EMG patterns to detect wrist and hand movements and a 3-D position sensor for tracking larger arm movements [29]. The primary difficulties with using EMG signals for motion detection are that the EMG patterns will be different for different individuals and locations of the electrodes and the patterns will change over the time of a test due to user fatigue and sweat on the skin. To deal with these issues, machine learning and neural networks are employed, which adds a level of complexity to the system.

Artemiadis and Kyriakopoulos, however, did develop a system that uses EMG signals from the biceps and triceps, along with a position tracker, without using a neural network [30]. The system requires a 10-minute calibration for each new user. However, once in operation, the system achieved errors of less than $0.02\,\mathrm{m}$ for catching motions when/as compared with an optical motion measurement system.

2.2.5 Conductive Fibers

Conductive fibers change electrical resistance as the length of the fiber changes; therefore if this change is associated with changes in a joint's angle, conductive fibers can be used to measure human joint movements. Epitropic fibers have extremely high resistances, while metal-clad fibers have lower resistances. Gibbs and Asada [31] chose silver-plated nylon for a wearable joint motion measurement system. Since the conductive fibers are inelastic, they were not sewn directly into the spandex sleeve worn over the joint, but were instead attached to the sleeve above the joint, then attached to an elastic strip, which is then attached to the sleeve below the joint. Therefore, as the joint bends, the elastic stretches quite a bit, and the conductive fibers stretch enough to measure the changing resistance. The signal from this system was compared to that of a rotary potentiometer goniometer, which showed that the experimental system produced fairly accurate results.

2.2.6 Deterioration of Fiber Optic Cable

One of the most common methods for measuring human bending motions is to use optical fibers. As the fiber bends, light escapes from the fiber at the bend point, causing less light to reach the detector at the other end; based on the amount of decrease of light detected, the amount of bending can be determined. However, since optical fibers are generally used to transmit data, weakening of the signal is an undesired affect, so today's optical fibers are made to have extremely small losses when bent. Therefore, in order to have measurable losses due to bending of optical

fibers, the fiber must be deteriorated to allow extra light to escape at the bend point. This is done by removing the protective cladding on the outside of the fiber near the bend point and removing the outer layer of the fiber.

A previous Space Systems Laboratory (SSL) project was the Joint Angle and Muscle fatigue Sensor (JAMS) system [28] [32]. The goal of this project was to develop a system to measure joint position and fatigue during suited, EVA activities. The JAMS team chose to use a commercially available fiber optic system, the right-handed 5th Glove System from General Reality Corporation in San Jose, CA. The 5th glove is made of double-layered spandex with fiber optic cables sewn in between the layers. The cables span all of the joints for each of the five fingers, so total deflection of each finger is measured, not deflection of each joint in each finger. The cables are etched in a small area over the joint to allow light to escape from the fiber when it is bent. Therefore, signal loss is proportional to the bend angle. There are LEDs and light detectors located in an epoxy casing on the dorsal aspect of the hand, which eliminates the effect of wrist flexion on sensor readings.

While this method of treating the optical fibers has been shown to work well for measuring joint angles, it has two primary drawbacks. The first is that it can be difficult to deteriorate the fiber evenly in one area and uniformly at multiple locations on one fiber or across separate fibers. Varying amounts of fiber erosion will lead to outputs from the light detector that should correspond to the same joint angles, but will instead be incorrectly interpreted as different angles. The second problem with treating the fiber in this manner is that it weakens the optical fiber, making it more prone to breakage.

2.2.7 Sliding Fiber Optic Cable

In response to the problems created by deteriorating optical fibers, Wright and Wright developed a new way to use fiber optic cables for joint angle measurements [33]. A piece of tubing is attached on one side of the joint with a light source directed into the tube. A second length of tubing is placed inside the first tube such that the inner tube can easily slide inside the outer tube, as shown in Figure 2.2.7. One end of the fiber optic cable is attached inside the inner piece of tubing. The fiber optic cable then spans across the joint and is fixed such that the output of the fiber is directed into a light detector. Thus, as the joint bends, the inner tube and fiber optic cable slide along the outer tube, so when the joint is fully bent, the light must travel the length of the outer tube plus the length of the cable, whereas when the joint is fully extended, the light only travels the length of the cable. When the light travels through the tube, it is no longer as tightly directed as it was in the optical fiber, resulting in a multitude of reflections off the surface of the tube. Therefore, the amount of light detected at the output of the fiber will be proportional to the length of the gap between the output of the optical fiber and the light detector, which corresponds to the angle of the joint.

There are many different materials that could be used for the tubing – brass, copper, aluminum, steel, or some plastics. However, depending on the material, the inner surface of the outer tube may need to be chemically treated to linearize the fiber output with respect to the changing joint angle and to reduce or eliminate the effects of a "transitional zone." As the inner tube slides in and out of the outer
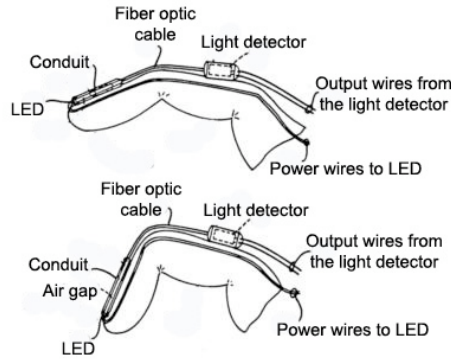
Figure 2.2: Operation of movement detection system
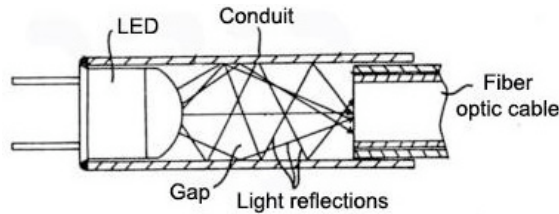
Figure 2.3: Reflections from light source through conduit to fiber

tube, there will be two regions, one where the all of the light entering the fiber comes directly from the light source, and one where the light comes both directly from the light source and from reflections off the inner surface of the outer tube. When the fiber moves between these two regions, non-linearities may be introduced, making it more difficult to correlate the amount of light detected with the correct joint angle. One way to eliminate this problem of the transitional zone is to introduce an offset, so the fiber can never enter the region where all the light comes directly from the light source. However, this can be a relatively large offset and significantly increase the size of the system. A second way to avoid the transitional zone issue is to treat the inner surface of the outer tube so that the light rays are more uniformly disbursed, removing the non-linearities at the point where the fiber moves from one

18

region to another. Wright and Wright state that anodized aluminum, blued steel, or oxidized brass or copper worked well to properly eliminate the non-linearities of the transitional zone. The non-linearities could also be reduced through computer software signal processing, but this can introduce unwanted time delays and added system complexity and expense.

2.2.8 Summary

While vision systems that track retro-reflective markers have been shown to work so well that they are considered by some to be the "gold standard" of motion trackers. Unfortunately, these systems have major disadvantages, including their large size, high cost, and lack of portability. Also, the use of retro-reflective markers would be infeasible for use in underwater zero-G simulation. Vision systems that rely on computer intelligence to recognize and track moving objects without the assistance of markers overcome some of the disadvantages of using markers, but are currently not sufficiently advanced for reliable joint angle measurement.

Exoskeletons are an effective method for measuring human joint angles, but are extremely bulky and currently would be difficult to incorporate into a space suit. Various combinations of gyroscopes and accelerometers have been proven effective for detecting human gait patterns. However, to obtain joint angle information from the angular velocity and acceleration data of these sensors, the signals must be integrated, which can compound errors due to noise, drift and offset of the sensors. FSRs are a small, simple solution for gait detection, but since they measure forces,

are unusable for measuring free-space arm movements.

EMG signals can be used for measuring joint motion, but are not adequate for use in robotic teleoperation. EMG signals can differ between people and locations of the sensors. The signals can also vary during testing of a single subject, since sensor positions can shift as a results of sweat on the skin and EMG signals can change as a person becomes fatigued. Conductive fibers could provide a joint measurement solution that would be small enough to be integrated into a space suit. However, due to their inelastic nature, these fibers may be easily broken if even slightly over-stretched, which could easily happen if sizes of the system are not adjusted properly to accommodate differing arm lengths among users.

Abrasion of fiber optic cable has been shown to be an effective method of measuring joint angles. Optical fibers are small enough to be easily incorporated into a space suit, perhaps even being sewn directly into the LCG or inside of the suit. They directly measure joint angles, without the need for integration. However, without a consistent method for scratching off the outer layer of the optical fiber, large discrepancies in the amount of light that escapes the fiber at a given joint angle could exist. If each fiber is not calibrated properly, this could lead to significant errors. Abrading the fibers also introduces the concern of accelerated wear on the system leading to cable breakage. Allowing a fiber optic cable to slide in and out of a piece of tubing causes the light to reflect off the sides of the tube between exiting the optical fiber and being sensed by a light detector, causing less light to be detected at larger joint angles. This eliminates the need for fiber abrasion and its disadvantages, while retaining the positive features of using optical fibers.

Chapter 3

Getting Started with JAMS

3.1 Introduction

A previous Space Systems Laboratory (SSL) project was the Joint Angle and Muscle fatigue Sensor (JAMS) system [28] [32]. The goal of this project was to develop a system to measure joint position and fatigue during suited, EVA activities. The current JAMSTORM research is not intended as a continuation of Ranniger's system. However, the JAMS technology is similar to that of JAMSTORM, so the operation of JAMS was studied, and some of that project's hardware and software were borrowed for initial evaluation of optical fibers for JAMSTORM.
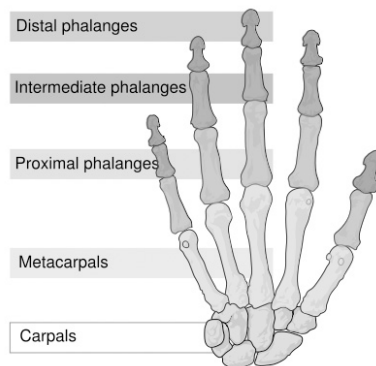
Figure 3.1: Bones of the Human Hand from

http://commons.wikimedia.org/wiki/Image:Human_hand_bones_simple.svg

A variety of methods were considered for measuring motion of the metacar-

pophalangeal and proximal interphalangeal joints of first (thumb), second (index), and third (middle) fingers. Ranniger examined some different types of sensors for use in the JAMS glove. Bend-sensitive resistive elements also respond to changes in joint angles. Unfortunately, they also tend to respond to direct pressure, so they cannot be used in a pressurized EVA glove. Fiber optic sensors are small and can be tuned to respond to small changes in joint angle. They also have the extra benefit that the control electronics do not need to be placed in the same location as the sensors. Therefore, a system of fiber optic sensors was chosen for joint angle measurement in the JAMS system.

3.2   Motion Sensing System

The JAMS team chose to use a commercially available fiber optic system, the right-handed 5th Glove System from General Reality Corporation, a subsidiary of iReality.com, Inc. The 5th Glove is made of double-layered spandex with fiber optic cables sewn in between the layers. The cables span all of the joints on each of the five fingers, so total deflection of each finger is measured, not deflection of each joint in each finger. The cables are etched in a small area over the joint to allow light to escape from the fiber when it is bent. Therefore, signal loss is proportional to the bend angle. There are LEDs and light detectors located in an epoxy casing on the back of the hand, which eliminates the effect of wrist flexion on sensor readings. The joint angle data is processed in a signal conditioning unit, which then connects to the data acquisition system via a serial connection. Due to the double-layered

nature of the 5th Glove, some of the test subjects were unable to fit the spacesuit glove on over the 5th Glove. Therefore, the JAMS team sewed the fiber optic cables directly to the standard comfort glove for the spacesuit, creating its own single-layer, mesh glove using the same fiber optic technology as the 5th Glove.

Figure 3.2: 5DT Data Glove 5 from http://www.ireality.com/p_glove5.html
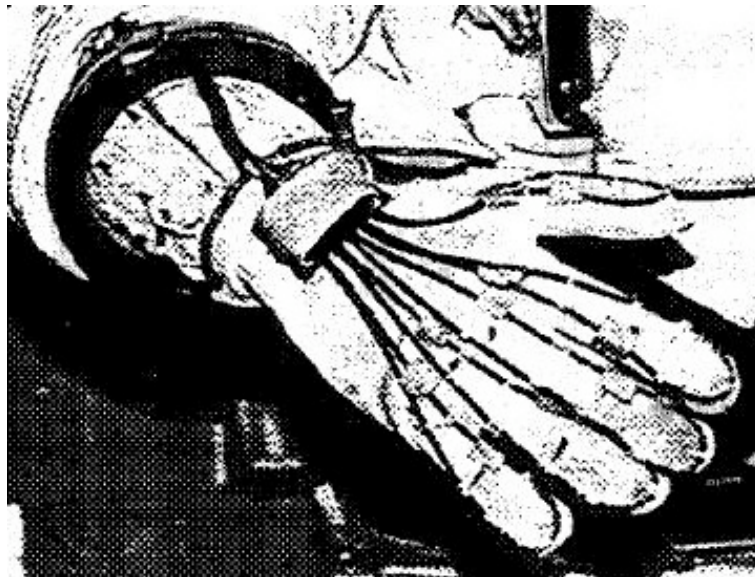
Figure 3.3: JAMS Glove [32]

3.3   Data Acquisition

The data acquisition system for JAMS had three incarnations: one bench-top system and two in-suit systems. The bench-top system used a Mac platform with a National Instruments NB-MIO-16 A/D card and LabView data acquisition and processing software. The in-suit system started as JAMS I, then was later redesigned into the JAMS II. JAMS I used a 386 PC104-form factor PC from AmproComputers, Inc. in Sunnyvale, CA. This PC104 board includes an A/D card, PCMCIA adapter and Ministor 340 MB hard drive, and battery pack capable of providing two voltage lines – unregulated 12 V and regulated 5 V. At system startup, the current draw peaked at 1 A; during data collection, about 0.5 A was required. The system could continuously acquire data for five hours, but it was found to be cumbersome for in-suit use, so the JAMS II system was developed.

JAMS II uses a Tattletale Model 8 data logger by Onset Computer Corporation in Pocasset, MA. This system has seven analog acquisition channels; five channels are used for the joint angles and acquire data at rates of 30 Hz. Joint angle data is the input through the card's serial port and stored onboard on a 20 MB flash memory card. This amount of memory is enough to store about one hour of data per test. The system is powered by eight AA alkaline batteries, which are fused together to eliminate the risk of electric shock to the human subject. Current draw of the JAMS II is much lower than that of the JAMS I system; during bench-top testing, the current draw of the redesigned system did not exceed 350 mA.

3.4 System Integration

The JAMS system is integrated into a vest, which is then worn over the liquid cooling and ventilation garment (LCVG); components are placed in padded pouches that are Velcroed to the vest. The addition of the JAMS hardware does increase the time required to don the spacesuit, but only by about 15 min. The entire JAMS system weighs 2.0 kg.

3.5 Reviving JAMS

Although the current research is not a continuation of the JAMS project, both systems measure joint angles using fiber optic cables. Therefore, it was decided that the 5th Glove and JAMS hardware and software should be used for initial testing of optical fibers. Updated software was downloaded for the 5th Glove from http://www.ireality.com/downloads.html, and the 5th Glove was connected to a PC to test both the glove and the software. The 5th Glove software consists of three programs; the Glove Manager shows graphs of joint angle for all five fingers, the Demo uses the glove movements to enable to the user to "walk" around a simple virtual world, and Glove Mouse enables the 5th Glove to be used in place of a computer mouse. Only the Glove Manager was used for sensor testing, as it provided the clearest knowledge of the sensor outputs. The electronics for the 5th Glove includes two potentiometers for each finger sensor, one for adjusting the gain and one for adjusting the offset of the sensor output. By tuning these potentiometers, each finger of the glove was calibrated to achieve the widest range of joint angle data

without saturating the detection system.
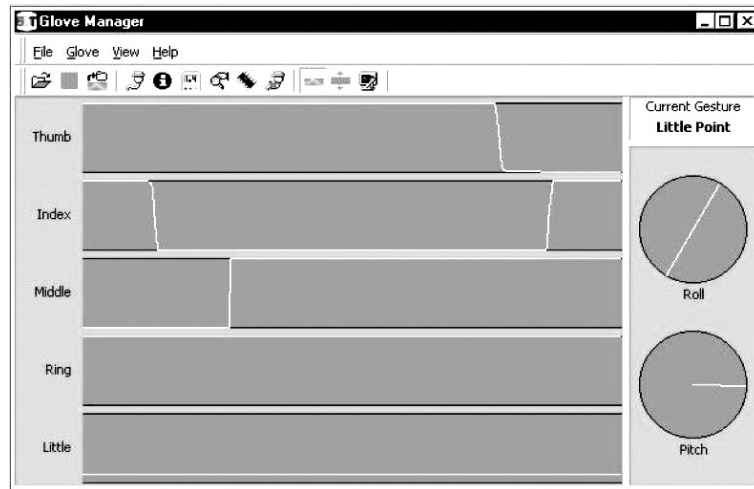
Figure 3.4: Glove Manager Screen Shot

Once the 5th Glove hardware and software were understood, the 5th Glove fiber optic cables were disconnected from the rest of the system and replaced with the JAMS glove. The system needed to be recalibrated for the new sensors, but otherwise, as was expected, the system worked the same with the JAMS glove as it had with the 5th Glove. Next, the 5th Glove software was used to test a variety of fiber optic cables; this series of tests will be discussed in Chapter 4.

Chapter 4

System Design

The final design of the system consists of three fiber optic cables, one each to measure elbow flexion/extension, shoulder flexion/extension, and shoulder abduction/adduction. These are three of the joint movements of the human arm that need to be measured for gesture-based teleoperation of a robotic manipulator. These three motions were chosen as a starting point; in future system revision, detection of more degrees of freedom should be implemented. Measurement of wrist flexion/extension will be similar to that of elbow flexion/extension, and so could easily be added to the system. Shoulder and elbow medial/lateral rotation and forearm supination/pronation are different types of movement from flexion/extension and abduction/adduction, in that they do not cause a change in distance between points on opposite sides of the joint. For example, while points on the upper arm move closer to points on the forearm during elbow flexion, points on the forearm do not move closer to each other or to points on the upper arm or wrist during forearm supination. For this reason, it may be difficult or impossible to use the proposed method of a sliding optical fiber to detect these types of rotational motions. Therefore, measurement of these joint movements are not included in the current system.

One end of each cable is connected to receive direct illumination from an

infrared LED; the other end of the cable is positioned inside a length of brass tubing such that the cable can slide back and forth within the tube. The end of the tube is connected to a photodiode that detects the light transmitted from the LED through the cable and tube. The output current from the photodiode changes relative to the amount of light detected; through the use of a simple voltage divider, this changing current is converted to a changing voltage. This signal is amplified by a gain of about 4.3 and passed to a National Instruments data acquisition (Ni-DAQ) USB-6008 card, which converts the analog voltage into a digital signal. The USB-6008 has eight available single-ended analog input channels that accept voltages in the range of $\pm10\,$V [34]. The analog data are sampled at a maximum rate of $10\,$kS/s and digitized to a resolution of $12\,$bits. This digital signal is then transferred to a computer via USB, where the signal can be viewed in real-time using the LabView data logger software. The details of the development of this design are discussed in this chapter.

4.1   Evaluation of Fiber Optic Cables

The goal of this research is to determine the feasibility of measuring joint angles using fiber optic cables. Therefore, the first step of the design process was to examine the performance of a variety of fiber optic cables. An assortment of cables was obtained from Circuit Specialists, Inc, which contained twelve different types of optical fibers, including glass, plastic, jacketed, and unjacketed fibers. Both glass and plastic fibers were tested, but only those with an outer jacket, as the unjacketed
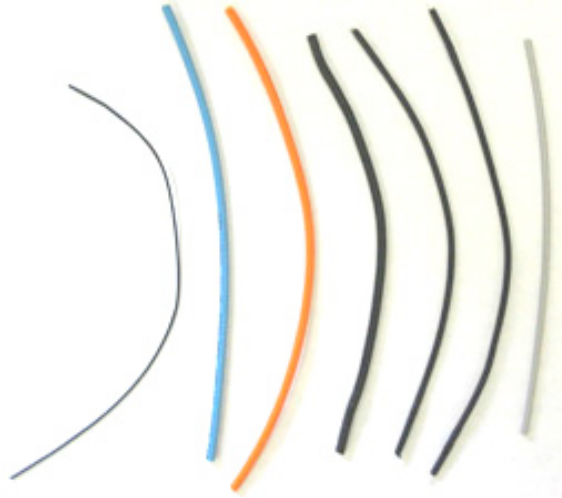
Figure 4.1: Assortment of Optical Fibers Tested

fibers were viewed as more delicate and prone to breakage.

The setup for testing the various fiber optic cables went through several iterations; only those with significant changes will be discussed. When fiber optic cables are used for optical communication, particularly over long distances, it is desirable to have little or no loss associated with bends in the cable. However, for joint angle measurement using optical fibers, the opposite is true; there must be a significant reduction of the light detected that can be correlated to the amount of bending present in the joint.

Therefore, the purpose of the first set of tests was to determine if any of the optical fibers would inherently lose enough light when bent to enable joint angle measurement without damaging the fiber. The 5th Glove signal acquisition electronics and software were used in these tests to evaluate each fiber's performance. First, each fiber was tested in the JAMS setup depicted in Figure 4.1, with one

end of the fiber connected to a LED and the fiber looped around to connect the other end to a photodiode next to the LED. For the second test setup, the fiber was straightened, as shown in Figure 4.1. A LED was powered separately and connected to one end of the fiber; the other end of the fiber was connected to one of the photodiodes of the 5th Glove data acquisition electronics. Of the seven optical fibers tested, only one showed any noticeable changes in light output when bent as compared to unbent. Therefore, untreated fibers were determined to be an infeasible method for joint angle measurement.
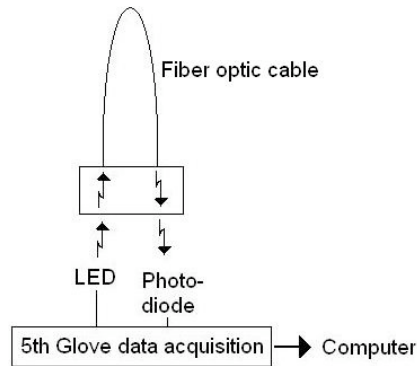
Figure 4.2: Test Setup 1

Due to the disadvantages of the fiber abrasion method discussed in Section 2.2.6 and the ineffectiveness of using untreated fibers for joint angle measurement, it was determined that the sliding tube method discussed in Section 2.2.7 should be used if it could be shown to be feasible. Initial testing was conducted on the index finger. The increase in distance from the top of the metacarpal to the finger tip across the proximal phalanges as the finger was flexed was measured to be about 0.5 in, so brass tubes were cut in lengths of 1.0 in. The test setup was similar to

30
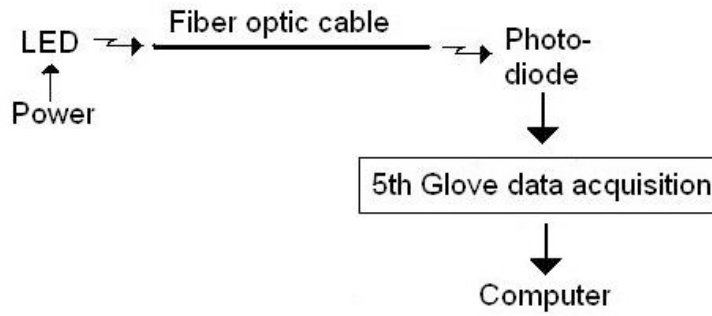
Figure 4.3: Test Setup 2

the previous setup, with the addition of the brass tubes. As in the previous tests, the 5th Glove signal acquisition electronics and software were used to evaluate each fiber's performance. After extensive testing in this configuration, only two of the seven fiber optic cables were determined to have sufficiently consistent results and low errors to be considered for further testing. The first of these two cables was the Super Eska SH1048, which is made up of 48 plastic fibers. Each fiber has a diameter of approximately $265\,\mu$m, and the jacketed cable has a diameter of about $3.0\,$mm. The second cable was the Eska Premier GHV 4001, which consists of a single plastic fiber with a typical diameter of $980\,\mu$m.

The next set of tests simulated elbow flexion/extension using a simple goniometer as shown in Figure 4.5. The increase in distance about the elbow during flexion was measured as about $2.0\,$in, so new pieces of brass tubing were cut in lengths of $2.5\,$in. Using this test setup, even with the gain settings as low as possible, the 5th Glove signal acquisition hardware was saturated. LabView's data logging software and a National Instruments data acquisition (Ni-DAQ) card replaced the 5th Glove

31
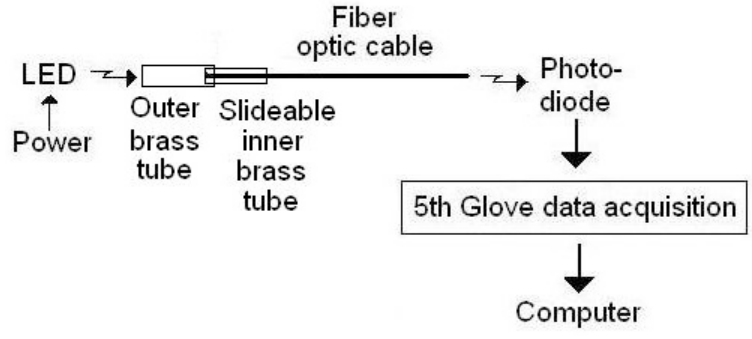
Figure 4.4: Test Setup 3

hardware and software. This change required some additional circuitry at the output of the photodiode, which will be discussed in Section 4.2. The two optical fiber finalists were tested in this basic configuration with a variety of slight alterations, such as transposing the placement of the LED and photodiode, and removing the outer tube and having the cable slide inside the inner tube. Also, different techniques for treating the brass tubing were examined, which will be discussed in Section 4.3.
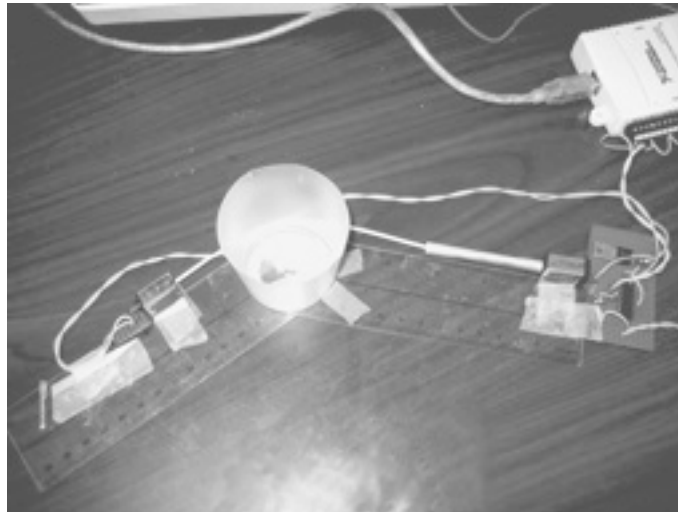
Figure 4.5: Tabletop Test Setup

4.2   Circuit Design

When the 5th Glove hardware and software were no longer being used for data acquisition, some additions to the test circuitry needed to be made. First, a voltage regulator was employed to ensure that a steady voltage is supplied to the LEDs and photodiodes. During some initial testing, it was shown that the power supply being used did not output a constant voltage, and these fluctuations created significant noise in the LED output. A LM317 adjustable voltage regulator by National Semiconductor was chosen to eliminate this problem. Since the voltage output of this regulator is adjustable, resistor values were selected to provide a constant 1.4 V to the rest of the circuit. The calculations to determine the desired resistor values for the voltage regulator sub-circuit can be found in Appendix A.1.

The output current of the photodiode changes as the amount of light detected varies. To measure this fluctuating current, a 1.0 MΩ resistor is connected between the photodiode output and ground. Thus, the voltage across this resistor varies as the current and, therefore, the amount of light detected change. This voltage then becomes the measured sensor output. A 1.0 MΩ value was chosen since the current is quite small; therefore, the larger the resistance, the larger the voltage across that resistor will be. A large initial output voltage requires less amplification and enables smaller variations in current to be distinguished.

Even with the 1.0 MΩ resistor pulling the current to ground, the voltage output from the detection sub-circuit is too small – maximum of 1.8 V – to provide a wide measurement range, so this value had to be amplified before being transmitted

to the computer for processing. A Texas Instruments LM324 operational amplifier (op-amp) was chosen for signal amplification. This op-amp package contains four amplifier circuits, so one chip can be used for the signals from all measured joint angles – shoulder abduction/adduction, shoulder flexion/extension, and elbow flexion/extension. Resistors at the negative input and output are needed to set the gain of the amplifier. The amplifier is to be powered with $9\,\text{V}$, which implies a maximum allowable gain of 5. Therefore, the desired amount of gain is between 4 and 5. The calculations for the resistor values for the amplifier sub-circuit can be found in Appendix A.2. These values provide an amplifier gain of slightly more than 4.3.

4.3   Treatment of Brass Tubing

As mentioned in Section 2.2.7, the inside of the brass tubing needs to be properly oxidized to eliminate the non-linearities in the "transitional zone." This is the region where the optical fiber transitions from acquiring light only directly from the LED to receiving light both directly from the LED and from reflections off the inner surface of the tube. Therefore, brass tubes oxidized using different methods, as well as untreated brass tubing, were examined. An internet search produced two simple techniques for oxidizing brass. The first process used to oxidize the brass tubing was to soak the tube in vinegar [35]. The second procedure was to coat the inside of the tube with a water/baking soda mixture [36].

4.4 Data Analysis

During each test, data were collected at a rate of 4 Hz for approximately 20 sec at each angle. Initially, data were collected for every 15 deg; as potential test variations were eliminated, data were collected every 5 deg. Later, data were also collected at a rate of 50 Hz for 10 sec at each angle. The LabView data logger automatically saves input data into a file of comma-separated values that contains information about program settings, such as number of channels recorded, the date and time when data logging began, and two columns for the data information. The first of these columns contains the values for the x-axis in fractions of seconds that relate to the sampling frequency, so for a sampling rate of 4 Hz, the values in this column increment by 0.25 sec for every data point recorded. The second column is the voltage output from the joint angle measurement system. Data collection was halted between changes in angle, thus creating one file for the data points recorded for each angle in a test run. These files were then combined in Microsoft Excel to form a single file for each test containing one column for the sample number, a second column for the angle measured using the goniometer, and a third column for the voltage measured.

The data for several test runs of a single setup were then combined into one spreadsheet, with one column for the data from each test run. Calculations were then performed within the spreadsheet to determine the maximum, minimum, and average voltages, as well as the standard deviation of the data, for a given angle during a given test. Then the overall maximum and minimum voltages for a set of tests

performed the same day were calculated, along with the averages of the maxima, minima, means, and standard deviations of that day's data. Finally, the maximum and minimum voltages and the averages of the maxima, minima, means, and standard deviations over all of the tests were calculated. These maxima, minima, and means were used to devise a variety of ranges for the voltages to be assigned to each angle. Using IF statements in Excel, each data point was assigned an angle value based on the voltage range to which it belonged. If this assigned value matched the measured angle of that portion of the test, then the variable in the "correct?" column was assigned a 1 and added to the overall correct score for that angle during the given test. Using this number of correct assignments and the total known data points for each angle tested, the percent error for each angle during each test was calculated simply as:

$$PercentError = \left(\frac{total\,points - correctly\,assigned\,points}{total\,points} \right) 100 \qquad (4.1)$$

From these individual errors, the maximum, minimum, and average percent errors over all of the angles across all tests were calculated for a particular set of voltage ranges. The range set that resulted in the lowest overall errors was selected for each test setup. These results were then compared to determine the test setup that had the lowest errors.

4.5   Evaluation Results

After all of the elimination testing, there was only one configuration that was clearly the best, which made the design decision quite simple. The chosen fiber optic

cable was the GHV 4001 Eska Premier. This is a single, plastic, jacketed optical fiber with a typical core diameter of 980 μm and an outer, jacketed diameter of about 2.20 mm [37]. Of the conduit options, the vinegar-treated brass tubing, with the cable able to slide back and forth inside, was selected. The LED is positioned at the input to the optical fiber, and the photodiode is located at the output end of the brass tube. This arrangement showed consistent results with low errors. When discriminating between every 15 deg, the maximum error for any angle was 3.53% and the average error over all angles and all tests was 0.03%. When resolution was increased to 10 deg, the error rose to an average of 5.52% and a maximum of 100%, implying that all of the data points for at least one angle during one test were assigned to incorrect angles. A sample of these error results is given in Table 4.5. These error values were used to compare performance of the system in various setups to choose the configuration to be used in the final system.

It will be noted that, for the tests in which data were sampled at a rate of 50 Hz, the sensor output spans a different total range than in the tests sampled at 4 Hz. As will be seen from later tests sampled at 50 Hz, this difference is not related to the change of sampling rate; it is most likely due to a misadjusted power supply. However, even though these sensor readings span a total range almost 1 V smaller than those of the 4 Hz tests, they still result in much lower errors than the tests sampled a lower frequency. These lower errors are also not due to the increased sampling rate. Instead, the more likely cause is related to the fact that these tests were performed at a later date, at which time the system electronics were finalized and secured inside a box. This keeps all of the sensor components more consistently

aligned from test to test and provides better shielding of the photodiodes from external light. Although sampling at a higher rate does not result in lower errors, it is still preferred. A high sampling rate collects more data points to be averaged together, so outliers have less of an effect on the overall mean value.

Figure 4.6(a) shows the average voltage output of the sensor in the chosen configuration over 15 trials. The small standard deviations for all the angles indicates that the sensor produces repeatable results. Regions that have larger deviations from the mean do not overlap voltages for the adjacent angle regions, so the sensor will still return repeatable, accurate results in these areas. When examining data taken at every 5-degree change in angle, there are some small amounts of voltage overlap at high angles, increasing the likelihood of errors in determining the sensor angle. However, as seen in Figure 4.6(b), this issue of overlapping voltage ranges for a given angle disappears if data from every 10-degree change is inspected instead. Therefore, the system should produce repeatable, accurate results every 10 deg and repeatable results with some errors at high angles of sensor bend every 5 deg.

Angle (deg)	Sampling Rate of 4 Hz Data Every 5 deg Range Bounds 1	Range Bounds 2	Data Every 10 deg Range Bounds 1	Range Bounds 2	Data Every 15 deg Range Bounds 1	Range Bounds 2	Sampling Rate of 50 Hz Data Every 5 deg Range Bounds 1	Range Bounds 2
0	7.5936	7.5936	7.5834	7.5664	7.4967	7.4651	5.8537	5.8540
5	7.5783	7.5936					5.7977	5.7980
10	7.4152	7.4285	7.2317	7.1794			5.7392	5.7407
15	6.9362	7.0585			6.1514	6.2645	5.6883	5.6888
20	6.2380	6.3909	5.8252	5.9903			5.6120	5.6155
25	5.4226	5.5816					5.4796	5.4715
30	4.6888	4.8376	4.3575	4.5379	4.0976	4.2872	5.0165	5.0081
35	4.0568	4.2084					4.0928	4.1638
40	3.5065	3.6580	3.2975	3.4429			3.3853	3.4299
45	3.0937	3.1987			2.7879	2.8681	2.7848	2.8140
50	2.7268	2.8175	2.5993	2.6551			2.2936	2.3275
55	2.4312	2.4767					1.9298	1.9242
60	2.1305	2.2042	2.0286	2.1118	1.9318	2.0313	1.5099	1.5445
65	1.7126	1.9888					1.2554	1.2625
70	1.7534	1.8071	1.6718	1.7330			1.0187	1.0243
75	1.6056	1.6579			1.5088	1.5611	0.8177	0.8175
80	1.4833	1.5356	1.4374	1.4901			0.6421	0.6360
85	1.3967	1.4429					0.5022	0.4945
90								
Minimum Total % Error	11.30	8.51	0.06	0.00	0.00	0.00	0.03	0.06
Average Total % Error	42.02	24.08	9.60	5.62	0.03	1.09	1.74	1.76
Maximum % Error Seen	100.00	100.00	100.00	100.00	3.53	89.41	45.88	54.12

Table 4.1: Comparison of Range Generation Methods
Range Bounds 1 calculated from the absolute minimum and maximum over all tests for each angle
Range Bounds 2 calculated from the average minimum and maximum over all tests for each angle
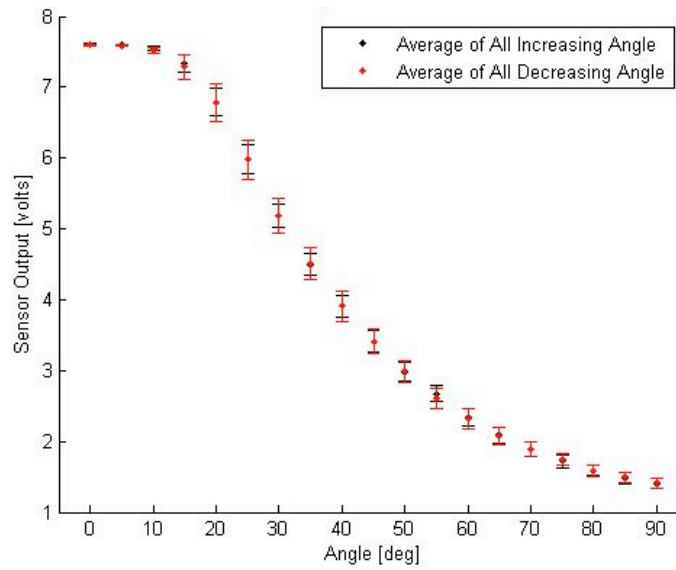
(a) Data Every 5 Degrees
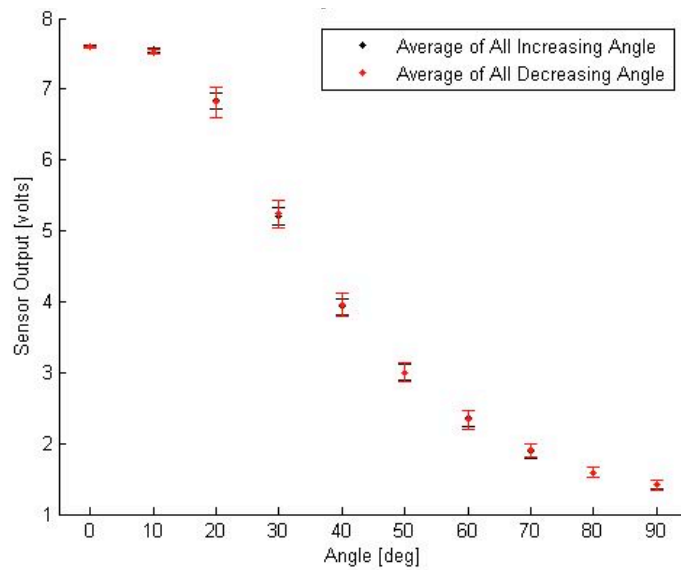
(b) Data Every 10 Degrees

Figure 4.6: Average Voltages Over 15 Tabletop Tests

Tests were performed to characterize the sensor output voltage as a function of the distance the cable slides out of the brass tube. To obtain a nearly continuous curve, data was taken every 0.025 in; this distance was measured accurately using digital calipers. From Figure 4.5 it can be seen that the most linear operating range is from about 0.6 to 1 in. However, with closer inspection in Figure 4.8(b), the range from 1 to 2 in is also shown to be nearly linear. Therefore, if possible, the sensor system should be set up such that the cable does not slide closer to the photodiode than 0.6 in and does not slide out of the tube more than 2 in from the photodiode.
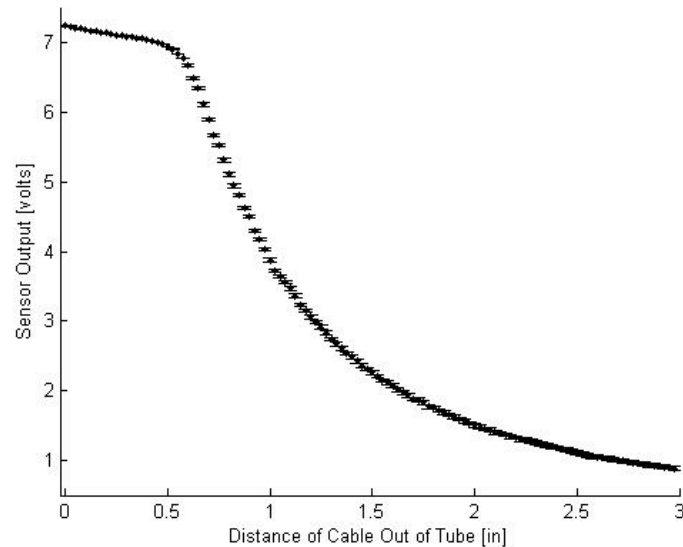
Figure 4.7: All Average Voltages Every 0.025 in For Straight Sliding Tests

Another set of tests was performed to determine the effects, if any, of bend in the cable on sensor output. First, the sensor was set up such that the cable slid straight out of the tube, and data were collected at 0.1-in increments. Next, the sensor was returned to the configuration used in the previous elbow simulation tests. Every 5 deg of bend, the amount of cable that had slid out of the tube was measured.

(a) Data From 0 to 1 in

(b) Data From 1 to 2 in

(c) Data From 2 to 3 in
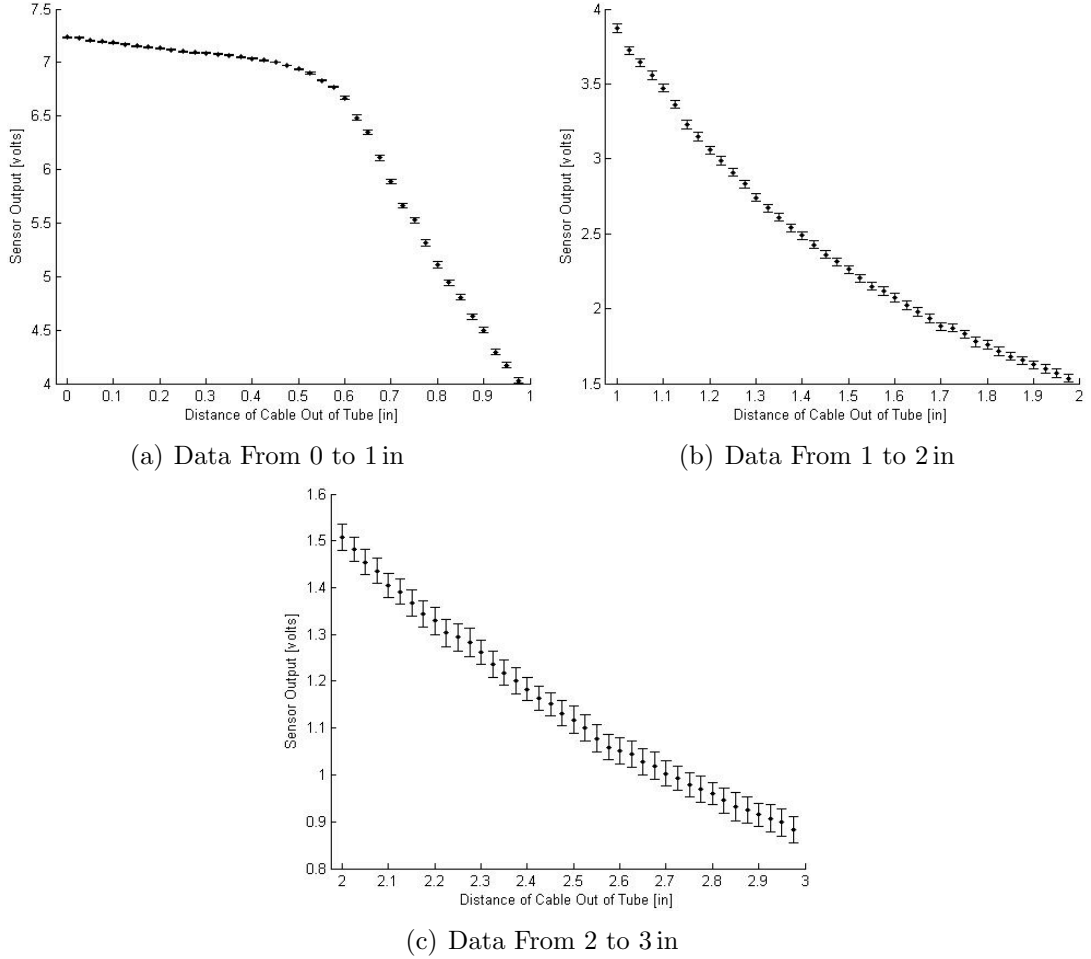
Figure 4.8: Average Voltages Every 0.025 in For Straight Sliding Tests

When the results of the two types of tests were compared in Figure 4.9(a), the output range of the bending tests was much larger than that of the straight sliding tests. This disagreement seemed to suggest that there were some inherent losses as the cable was bent, which decreased the amount of light detected by the photodiode. To try to confirm this, more bending and sliding tests were conducted. However, instead of bending the cable about the 1.8 inch diameter of the goniometer as in the previous tests, the cable was bent around a smaller diameter. The hypothesis was that, if there are light losses associated with just bending the optical fiber,

these losses should increase as the bend diameter decreases. However, as seen in Figure 4.9(b), the results from bending about a smaller diameter match well to those from sliding the cable straight out of the tube. Therefore, another set of tests was performed, this time bending the optical fiber around a larger diameter. Again, if there were significant inherent losses when the optical fiber was bent, bending about a larger diameter should demonstrate lower losses and thus higher sensor output than the cases of straight sliding and sliding and bending around smaller diameters. However, as depicted in Figure 4.9(c), that was not the case. The results from bending about a large diameter corresponded with those from both straight sliding and bending around a small diameter. The tests using the elbow simulation diameter had been performed much earlier in the experimental process than the other tests, so it was next hypothesized that some slight change in the test setup had occurred since that time. A new set of data was collected using the elbow simulation diameter. From Figure 4.10(a), these results are shown to be consistent with the sensor output during straight sliding.
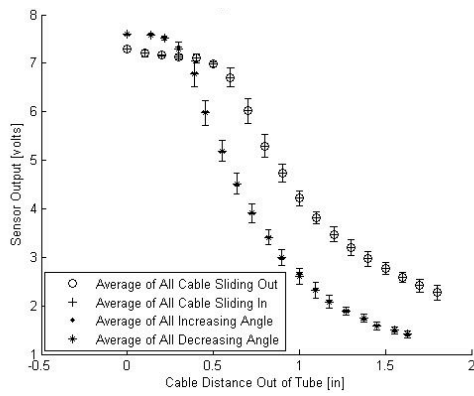
(a) Bending Around 1.8 in Diameter
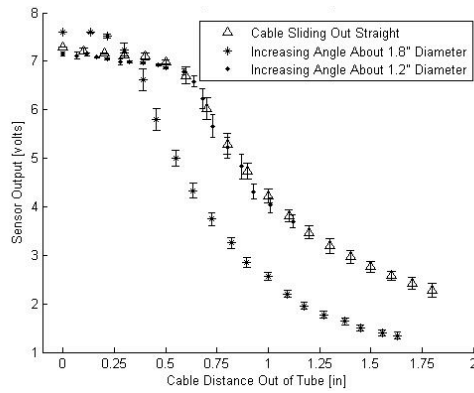
(b) Bending Around 1.8 in Diameter and 1.2 in Diameter
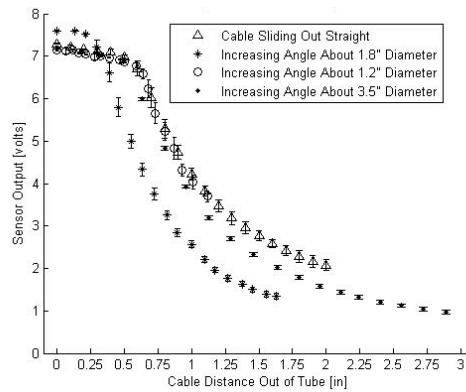
(c) Bending Around 1.8 in Diameter, 1.2 in Diameter, and 3.5 in Diameter

Figure 4.9: Average Voltages for Sliding Straight and Bending Around Various Diameters
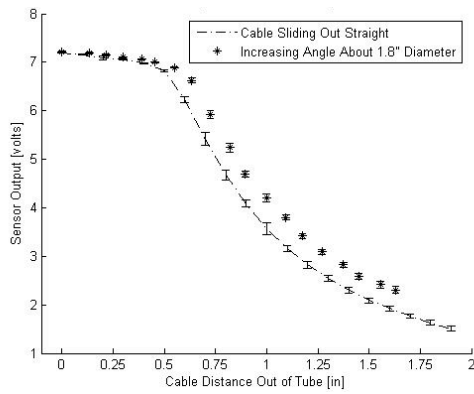
(a) Bending Around 1.8 in Diameter
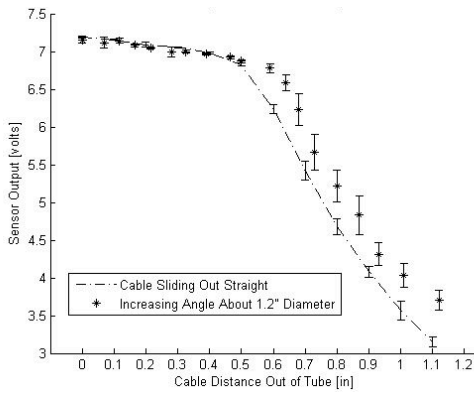
(b) Bending Around 1.2 in Diameter
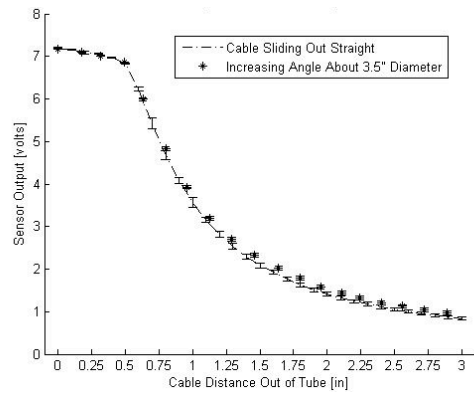
(c) Bending Around 3.5 in Diameter

Figure 4.10: Average Voltages for Sliding Straight and Bending Around Various Diameters

Chapter 5

System Evaluation

5.1 Completed System

The JAMSTORM electronics are attached to a fleece vest and elastic arm-bands. The electronics box is fixed to the upper armband with Velcro. The electronics box contains the power input, the voltage regulator, amplifier, and connectors for the LEDs and photodiodes. Two photodiodes are connected to brass tubes and attached to the upper armband. Two LEDs are sewn into the shoulder of the vest and connected to optical fibers that run into the two tubes. The fibers are positioned to measure shoulder flexion/extension and shoulder abduction/adduction. One photodiode is connected to a brass tube and affixed to the lower armband. An optical fiber runs from this tube across the elbow and into the electronics box to measure elbow flexion/extension. This arrangement is shown in Figures 5.1 and 5.1. As discussed in Chapter 4, the output signals from the amplifier enter a USB-6008 Ni-DAQ card, which transfers the data into the LabView data logger software on a computer. This software then saves the voltage information to a file of comma-separated values for later analysis. The data logger was set to sample the incoming signals at a rate of $50\,\mathrm{Hz}$.
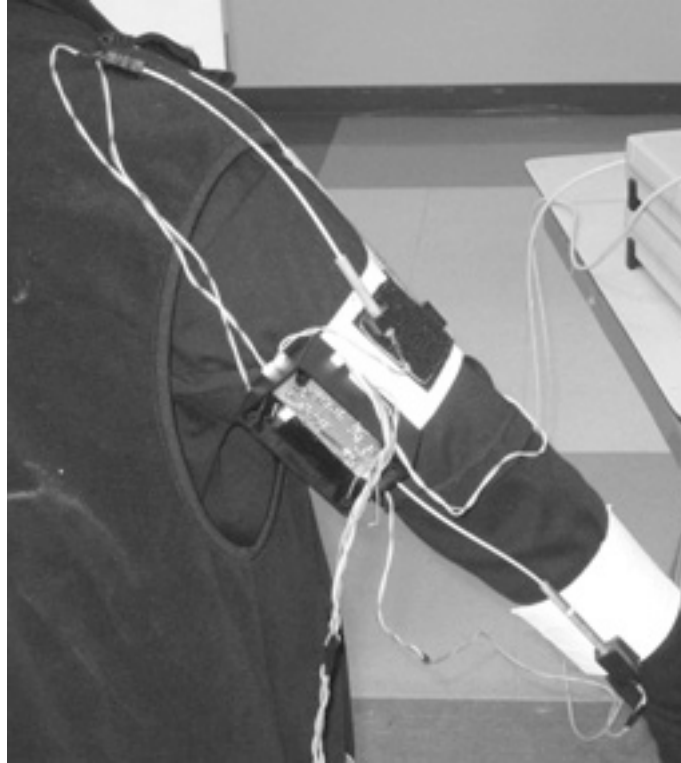
Figure 5.1: Wearable JAMSTORM Vest and Armbands

5.2   Testing using Flock of Birds

It was initially desired to use the Flock of Birds system by Ascension Technology Corporation was used as a verification system for JAMSTORM. The Flock of Birds is a 6-DOF motion tracking system, which would enable observation and comparison of all three JAMSTORM sensors at the same time. The Flock has a transmitter that emits a magnetic field. Two sensors are placed underneath the two elastic armbands that detect the magnetic field and report their positions and orientations relative to the transmitter. The receiver then transfers this data via RS232 serial connection to a PC. The RS232 connection is set up in the winBIRD program

47
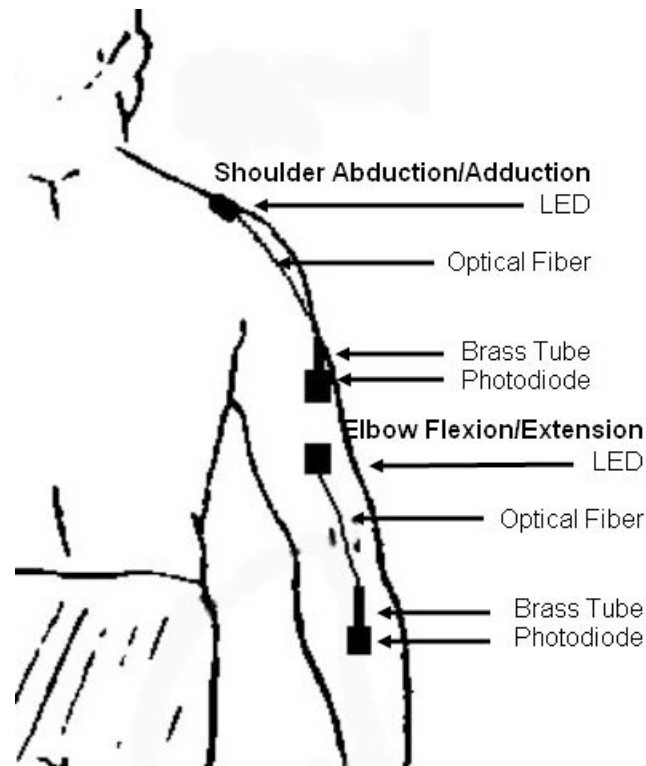
Figure 5.2: Sensor Placement as Viewed from Back

from Ascension Technology; in the current configuration, the number of devices is set to 2 and the baud rate is set to 57600. To achieve a sampling frequency of 50 Hz, the measurement rate must be set to 100 and the samples per record should be 1. WinBIRD records data from the Flock in a text file. For initial attempts at calibration and validation of JAMSTORM, only one type of shoulder motion was performed during a test, and all motions were performed from 0 to 90 deg.

5.2.1   Analysis Using Position Data

The data from both the Flock of Birds and JAMSTORM are saved in the comma-separated values file format and imported into MATLAB for analysis. First,
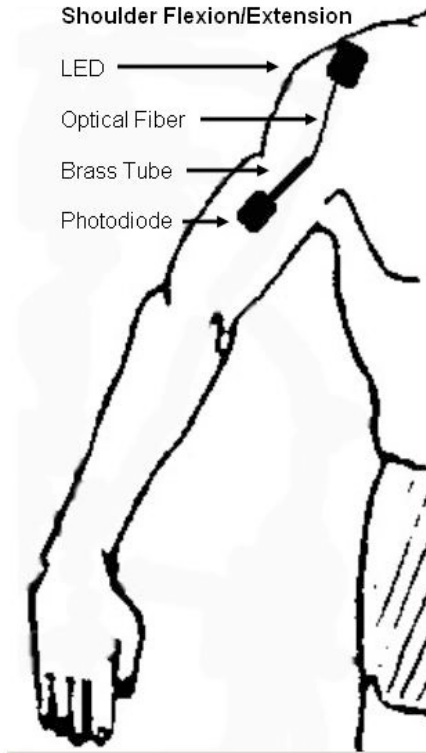
Figure 5.3: Sensor Placement as Viewed from Front

the JAMSTORM data are calibrated to directly match the Flock of Birds rotation angles. Using these joint angle values, the voltage ranges from JAMSTORM are then assigned to joint angles. This calibration is performed for each of the three joint motions, and the ranges are saved for future use.

At first, only position information was obtained from the Flock of Birds sensors. A simple approach to angle calculation was taken. The change in sensor position was determined by the distance formula, using only the two axes in which motion occurs. The change in angle can then be calculated using the law of cosines. For shoulder flexion/extension:

$$c_i = \sqrt{(y_i - y_{i-1})^2 + (z_i - z_{i-1})^2} \tag{5.1}$$

49

For shoulder flexion/extension:

$$c_i = \sqrt{(x_i - x_{i-1})^2 + (y_i - y_{i-1})^2} \tag{5.2}$$

$$c^2 = a^2 + b^2 - 2ab\cos(C) \implies C = \arccos\left(\frac{a^2 + b^2 - c^2}{2ab}\right) \tag{5.3}$$

where C is the desired change in angle

c is the calculated change in position

a and b are the distance measured from the sensor to the center of shoulder rotation

This usage of arccos only provides a positive angle between 0 and 180 deg. Therefore, the sign of the change in angle must then be determined. This is accomplished by subtracting the z-values at the current and previous positions. If the result is positive, the shoulder is in either extension or abduction, and the change in angle is positive; if the result is negative, the shoulder is in flexion or adduction, and the angle change is negative. After a sign is applied to the change in angle, the small change is added to the previous changes to obtain the current, absolute shoulder angle. Most of the shoulder motions appear somewhat feasible, although the data in Figures 5.6(a) and 5.7(a) peak 20-30 deg lower than expected from the observed motion. The cycles of shoulder extension/flexion shown in Figure 5.4(a) do not return to zero between motions, which may imply a problem with the equations used to determine the sign of the changes in angle. The data for elbow motion in the case of shoulder abduction is the closest to plausible of any of the calculated elbow results, and it still peaks about 20-30 deg low, based on the observed motion of 0-90 deg flexion. The behavior seen in Figure 5.6(b) again hint at a potential issue with the calculations of the sign of each small angle change. However, the results

50

in Figures 5.4(b) and 5.7(b) are not easily explained. Due to this strange behavior
of the calculated angles, a new approach was taken.

(a) Sensor on Upper Arm   (b) Sensor on Forearm
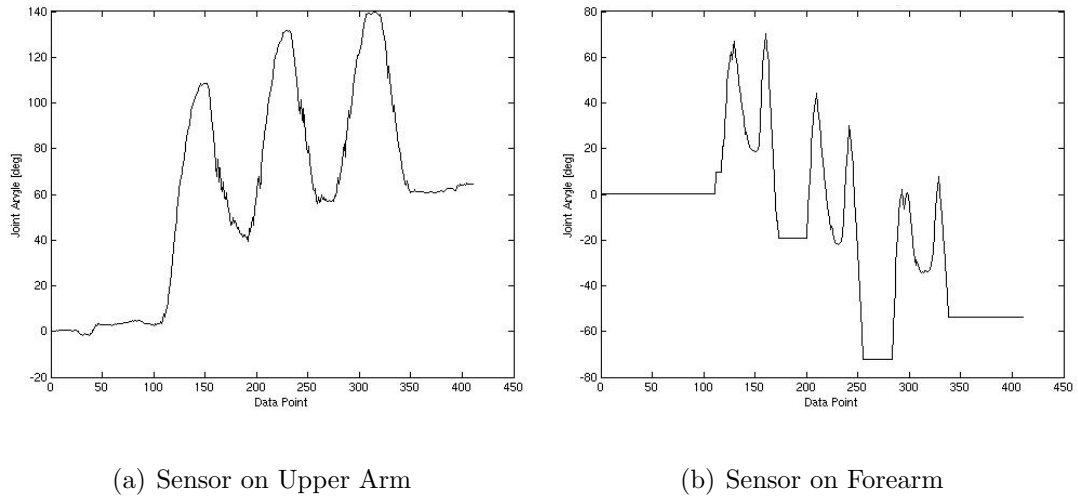
Figure 5.4: Angle Data from Flock of Birds for 3 Cycles of Shoulder Extension/Flexion
Calculated Using the Law of Cosines

(a) Sensor on Upper Arm   (b) Sensor on Forearm
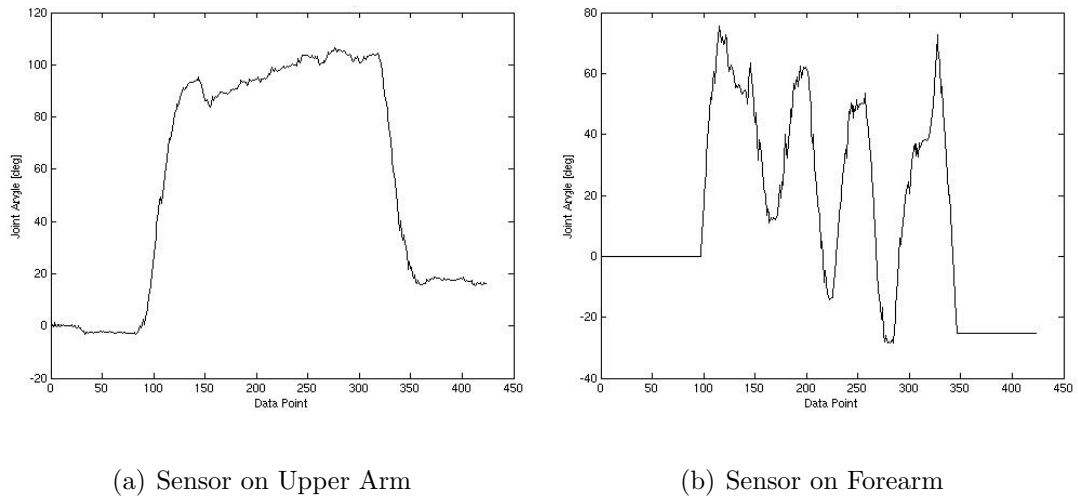
Figure 5.5: Angle Data from Flock of Birds for Shoulder Extension, 3 Cycles of Elbow
Flexion/Extension, Shoulder Flexion Calculated Using the Law of Cosines

51
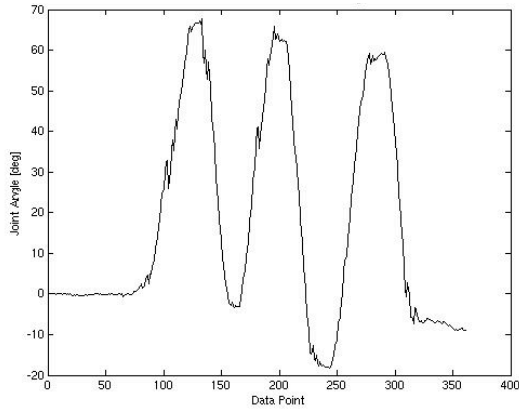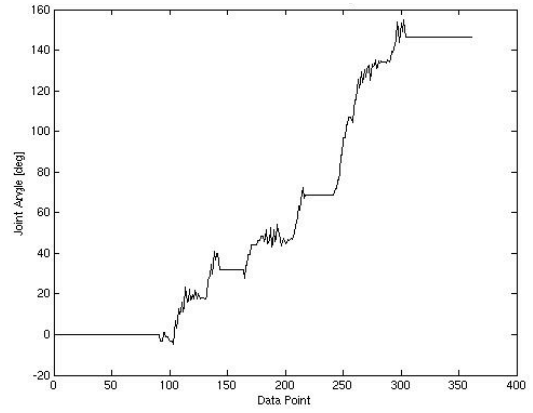
(a) Sensor on Upper Arm   (b) Sensor on Forearm

Figure 5.6: Angle Data from Flock of Birds for 3 Cycles of Shoulder Abduction/Adduction Calculated Using the Law of Cosines

(a) Sensor on Upper Arm   (b) Sensor on Forearm

Figure 5.7: Angle Data from Flock of Birds for Shoulder Abduction, 3 Cycles of Elbow Flexion/Extension, Shoulder Adduction Calculated Using the Law of Cosines

The dot product was next used to obtain the current shoulder angle. This method has significant advantages over the previous approach since it can provide the actual angle instead of a small change in angle that must then be signed and added with all other small changes.

$$\mathbf{v_i} \cdot \mathbf{v_0} = |\mathbf{v_i}|\,|\mathbf{v_0}|\cos(\theta_i) \implies \theta_i = \arccos\left(\frac{\mathbf{v_i} \cdot \mathbf{v_0}}{|\mathbf{v_i}|\,|\mathbf{v_0}|}\right) \tag{5.4}$$

where $\mathbf{v_0}$ is the vector $[x_0 \ y_0 \ z_0]$

$\mathbf{v_i}$ is the vector $[x_i \ y_i \ z_i]$ at the ith position

$|\mathbf{v_0}| = \sqrt{(\mathbf{x_0^2 + y_0^2 + z_0^2})}$

and $|\mathbf{v_i}| = \sqrt{(\mathbf{x_i^2 + y_i^2 + z_i^2})}$

The results using the dot product approach to angle calculation look cleaner and closer to the desired shape than when using the law of cosines. However, the magnitudes of the data are still not correct. According to the dot product calculations, all shoulder motions were less than 16 deg, although they were observed to actually span a 90 deg range. The results of the calculations of elbow angles are also the incorrect magnitudes. For the tests in which there was no significant elbow motion, elbow angles are calculated as 0 to almost 70 deg. In the cases where there was elbow motion, the calculated angles span almost 10 deg at about a 50-60 deg offset. Both of these results for calculated elbow angles suggest that the initial shoulder motion is not being properly removed from the data reported by the sensor on the forearm. The elbow angle equations could be correct, however; since the calculated shoulder angles are extremely low, subtracting them from the forearm sensor data will have little effect on the calculated elbow angles.
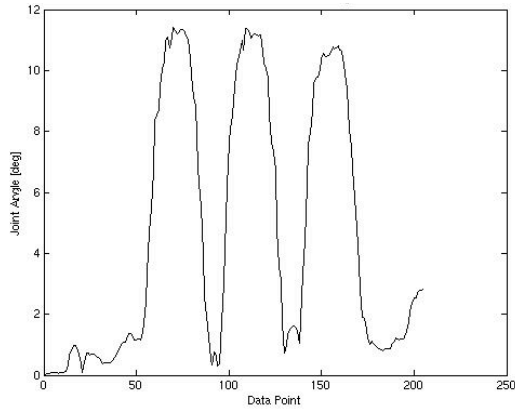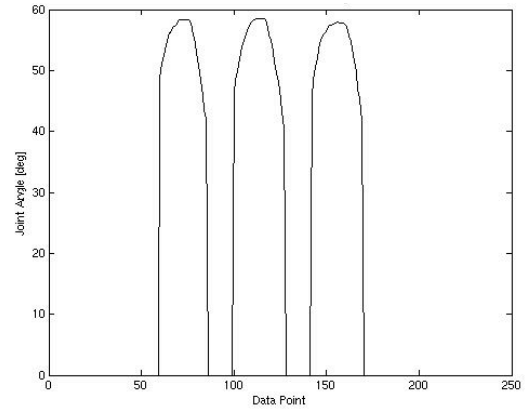
(a) Sensor on Upper Arm   (b) Sensor on Forearm

Figure 5.8: Angle Data from Flock of Birds for 3 Cycles of Shoulder Extension/Flexion
Calculated Using the Dot Product
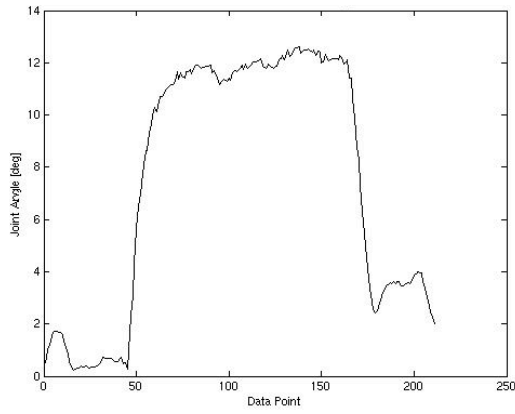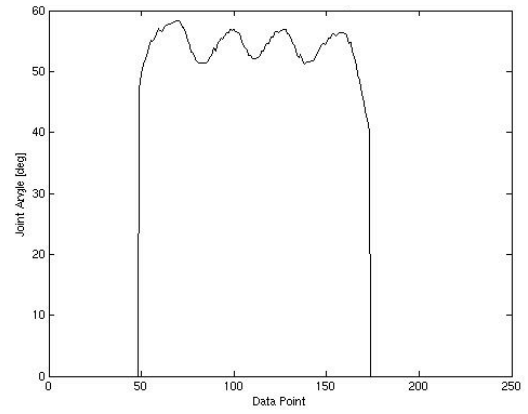
(a) Sensor on Upper Arm   (b) Sensor on Forearm

Figure 5.9: Angle Data from Flock of Birds for Shoulder Extension, 3 Cycles of Elbow
Flexion/Extension, Shoulder Flexion Calculated Using the Dot Product
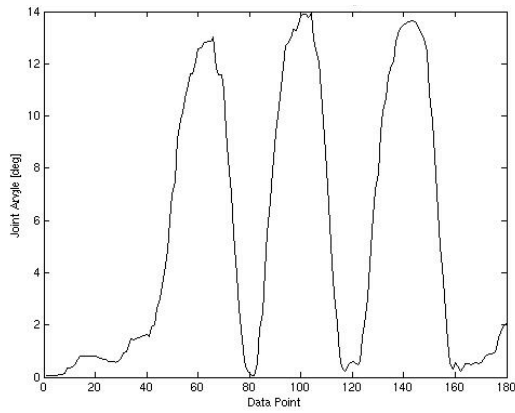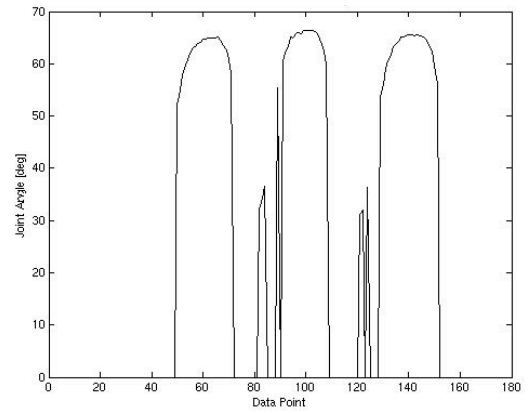
(a) Sensor on Upper Arm   (b) Sensor on Forearm

Figure 5.10: Angle Data from Flock of Birds for 3 Cycles of Shoulder Abduction/Adduction Calculated Using the Dot Product
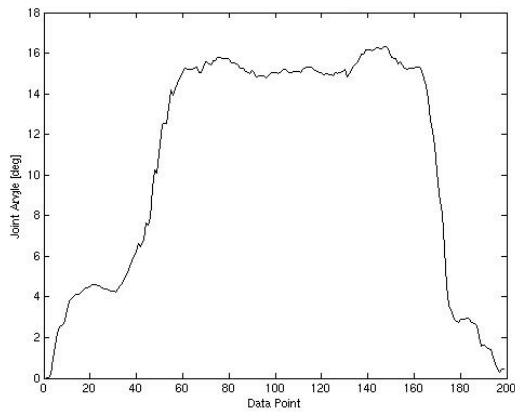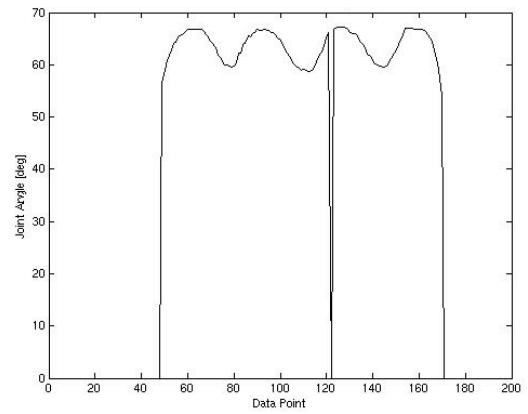
(a) Sensor on Upper Arm   (b) Sensor on Forearm

Figure 5.11: Angle Data from Flock of Birds for Shoulder Abduction, 3 Cycles of Elbow Flexion/Extension, Shoulder Adduction Calculated Using the Dot Product

5.2.2 Analysis Using Orientation Data

Due to the inability to obtain reasonable angle data from the Flock of Birds position information, the orientation information was used. The subject was positioned relative to the Flock transmitter such that the shoulder motion of interest, either flexion/extension or abduction/adduction, was rotating about the transmitter's x-axis and elbow flexion/extension was rotating about the z-axis. Orientation changes about the other axes reported by the Flock sensors then imply either that the subject is not performing perfectly planar motion or that the sensors are not aligned with the transmitter axes. It can be seen from Figures 5.2.2 - 5.2.2 that simply using the raw orientation data reported by the Flock sensors does not provide accurate information. Figures 5.12(a) and 5.13(a) show shoulder extension of 200 deg or more, which is not humanly possible. Figures 5.14(a) and 5.15(a) show shoulder abduction of around 150 deg, which may be possible, but is much larger than the observed motion. Figure 5.13(b) shows elbow flexion of about 100 deg, which could be correct. Figure 5.15(b) depicts large spikes in the data, which are caused by a sign change; otherwise, elbow flexion of around 100 is again reported. However, Figure 5.14(b) also shows 100 deg of elbow flexion when there was no elbow motion.
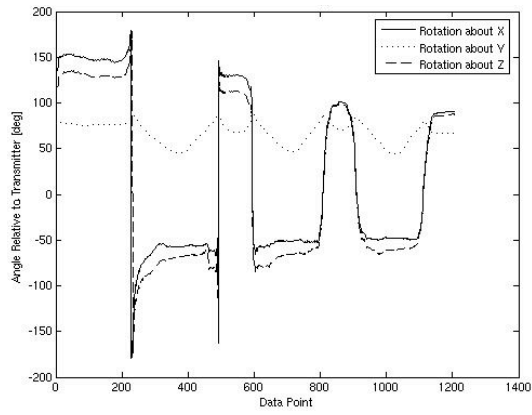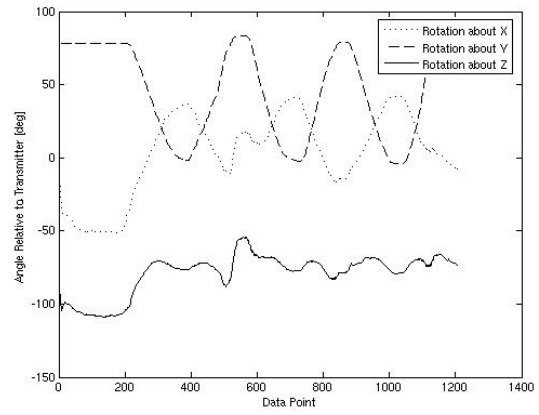
(a) Sensor on Upper Arm   (b) Sensor on Forearm

Figure 5.12: Raw Orientation Data from Flock of Birds for 3 Cycles of Shoulder Extension/Flexion
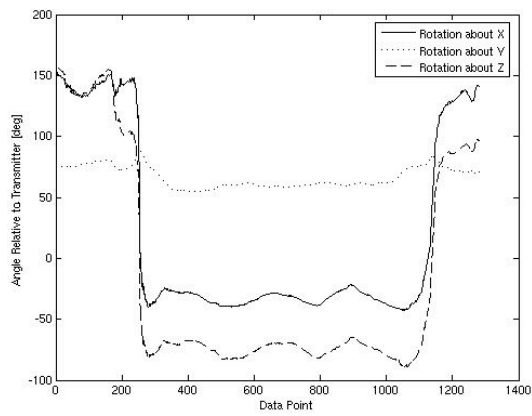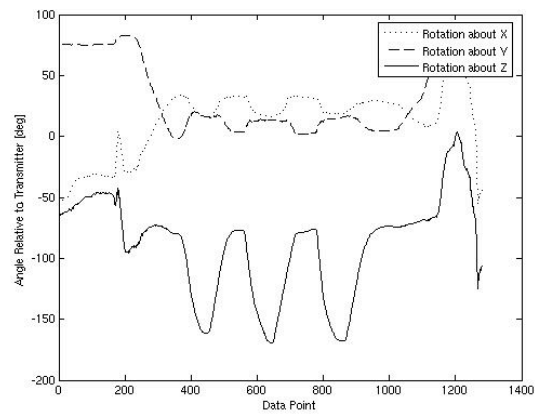
(a) Sensor on Upper Arm   (b) Sensor on Forearm

Figure 5.13: Raw Orientation Data from Flock of Birds for Shoulder Extension, 3 Cycles of Elbow Flexion/Extension, Shoulder Flexion

<div align="center">
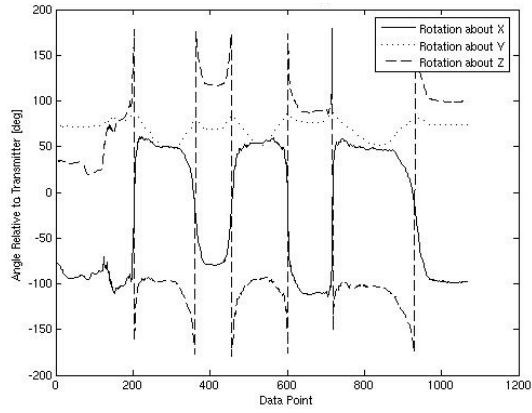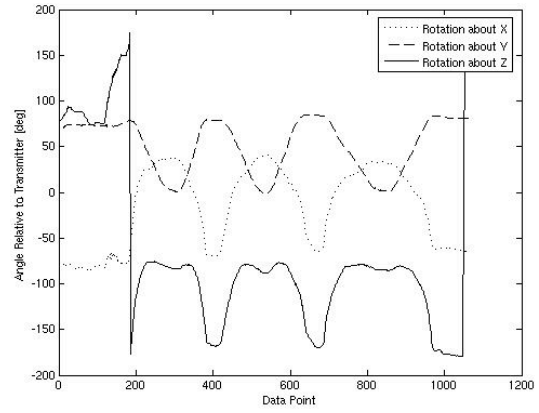
(a) Sensor on Upper Arm   (b) Sensor on Forearm

Figure 5.14: Raw Orientation Data from Flock of Birds for 3 Cycles of Shoulder
Abduction/Adduction

</div>

<div align="center">
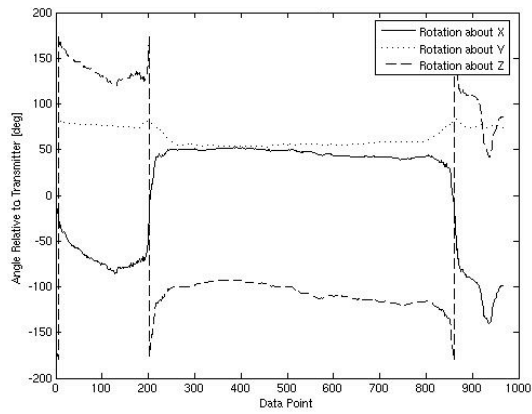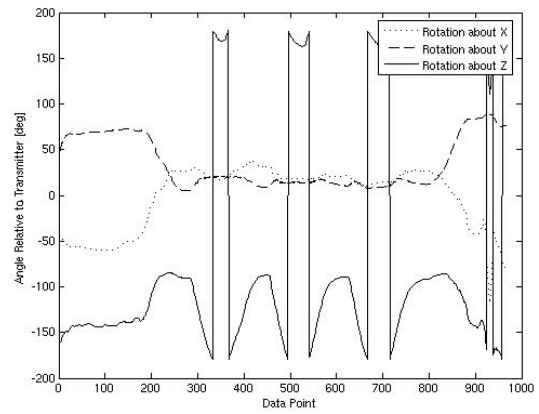
(a) Sensor on Upper Arm   (b) Sensor on Forearm

Figure 5.15: Raw Orientation Data from Flock of Birds for Shoulder Abduction, 3 Cycles of
Elbow Flexion/Extension, Shoulder Adduction

</div>

The orientation of each sensor is reported relative to the three axes of the transmitter. Therefore, in an attempt to resolve the issues discussed previously with using the raw orientation data, this data was transformed to be joint angles relative to the axis of rotation. Since the human motion during testing is not perfectly planar and the orientations of the two Flock of Birds sensors are not perfectly aligned with the transmitter axes, the sensors detect motion about axes other than the axis of primary motion. If the three orientations reported are considered to be X-Y-Z Euler angles, they must be transformed into a single, equivalent angle-axis rotation. This is accomplished using the equation:

$$\theta = cos^{-1}\left(\frac{cos\alpha cos\beta + sin\alpha sin\beta sin\gamma + cos\beta cos\gamma - 1}{2}\right) \qquad (5.5)$$

where:

θ is the equivalent angle of rotation about an arbitrary axis

α is the Euler rotation angle about the x-axis

β is the Euler rotation angle about the y-axis

γ is the Euler rotation angle about the z-axis

for primary rotation about an axis, that Euler angle is set to zero

This results in the portion of the reported angles that are about the primary axis of rotation. This value is then subtracted from the reported angle about the primary axis of rotation to provide the actual rotation angle about that axis. However, this method of angle calculations generated worse results than simply examining the raw sensor information. Shoulder extension and abduction display the same ranges as the raw data. Elbow flexion ranges are also similar to the raw data results for the

cases in which there was elbow flexion/extension. However, changes in elbow motion of up to almost 70 deg are seen for cases in which the subject did not perform any elbow motions.

(a) Sensor on Upper Arm   (b) Sensor on Forearm
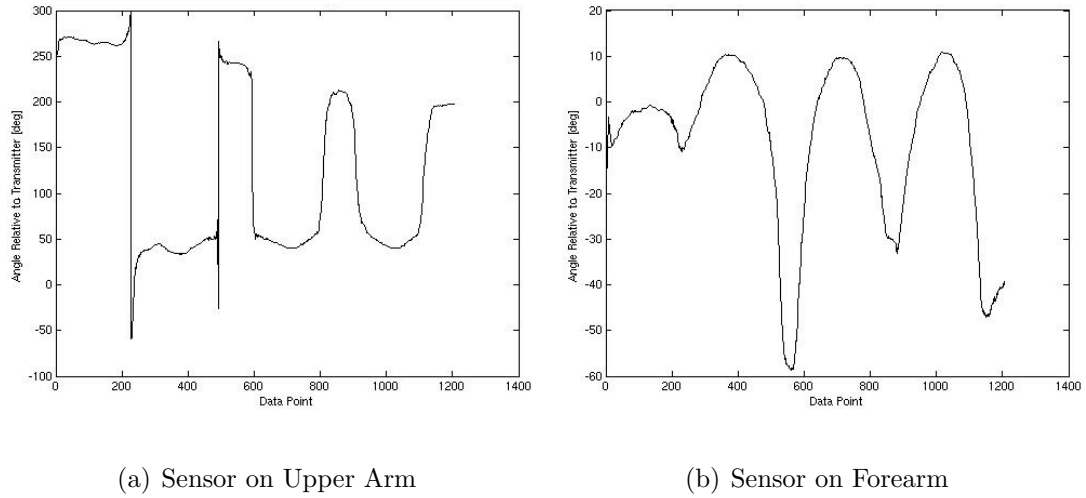
Figure 5.16: Orientation Data from Flock of Birds for 3 Cycles of Shoulder Extension/Flexion

(a) Sensor on Upper Arm   (b) Sensor on Forearm
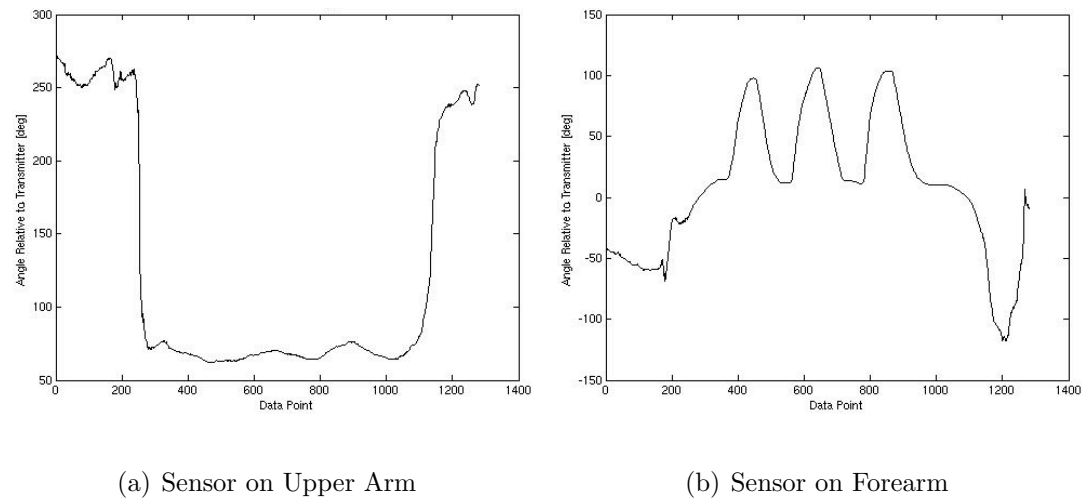
Figure 5.17: Orientation Data from Flock of Birds for Shoulder Extension, 3 Cycles of Elbow Flexion/Extension, Shoulder Flexion
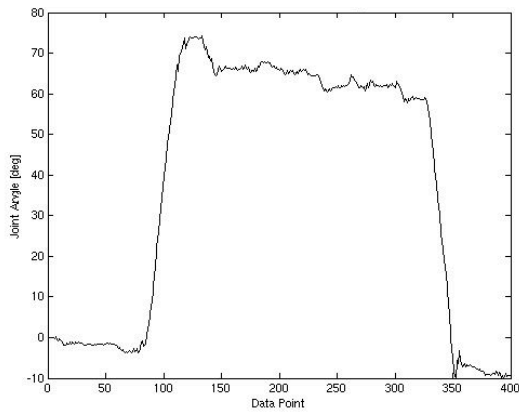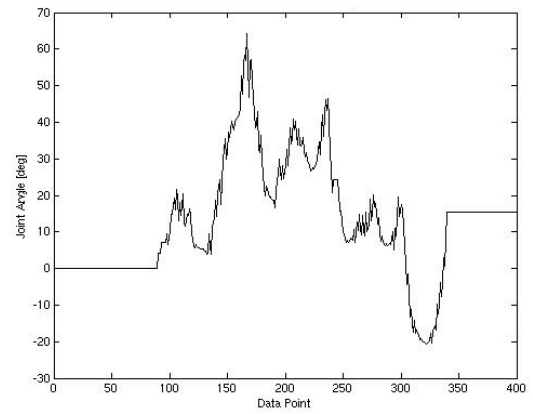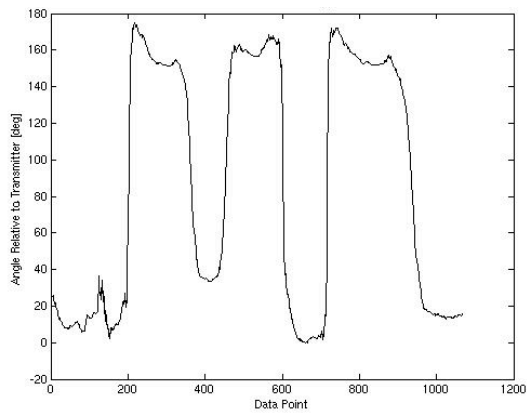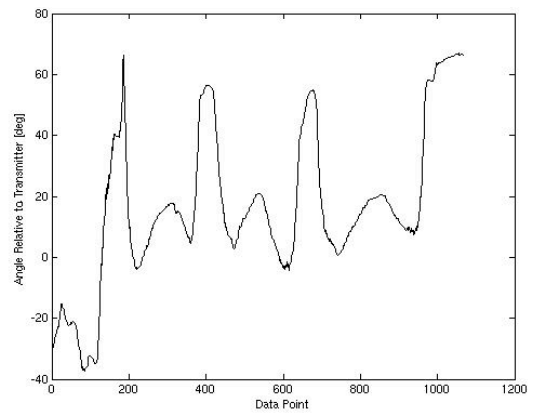
(a) Sensor on Upper Arm　　　　　　(b) Sensor on Forearm

Figure 5.18: Orientation Data from Flock of Birds for 3 Cycles of Shoulder Abduction/Adduction
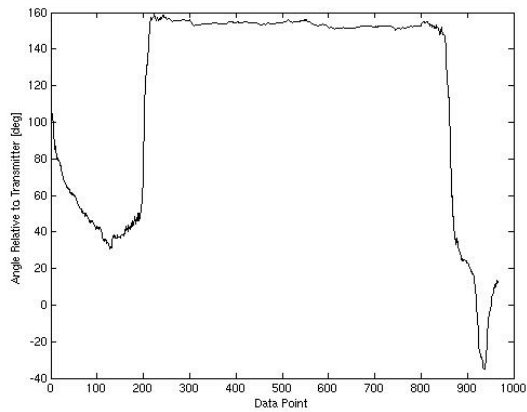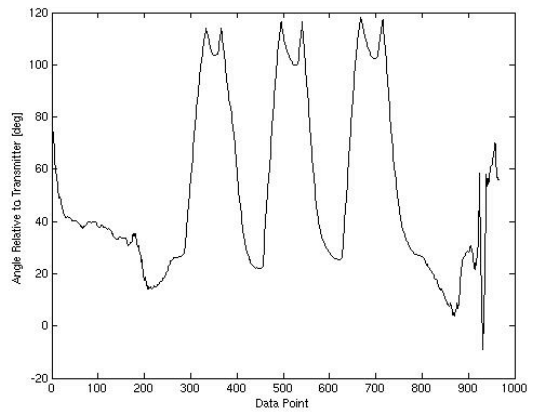
(a) Sensor on Upper Arm　　　　　　(b) Sensor on Forearm

Figure 5.19: Orientation Data from Flock of Birds for Shoulder Abduction, 3 Cycles of Elbow Flexion/Extension, Shoulder Adduction

5.3   Testing using Whiteboard

Due to an inability to diagnose the problem with the Flock of Birds system, a new method for verifying JAMSTORM was devised. The new test equipment involves the use of a whiteboard with angles every 5 deg from 0 to 90 deg marked on it using a protractor. The user moves his/her arm parallel to the whiteboard, keeping level with the angle lines, as depicted in Figure 5.3. This only allows evaluation of motion of a single joint at a time; however, this was deemed sufficient for the current phase of testing. This "whiteboard method" of angle measurement has a ± 2 deg error for each angle due to the thickness of the dry-erase marker used to draw the angles.
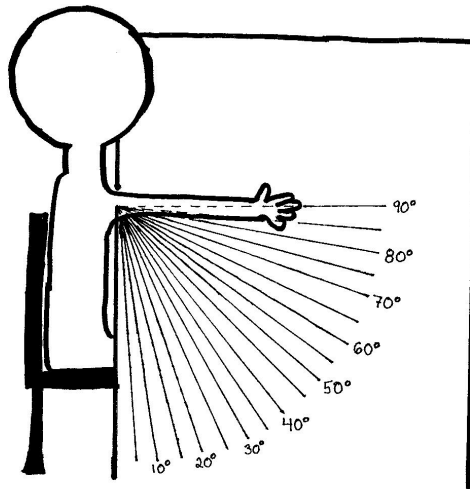
Figure 5.20: Test Setup Using "Whiteboard Method"

5.3.1 Data Analysis

The LabView data logger is used to save 100 data points at each of the 19 angles (0, 5, 10, 15, 20, 25, 30, 35, 40, 45, 50, 55, 60, 65, 70, 75, 80, 85, 90) as the user moves his/her arm up and down. Data collection is stopped during joint motion; therefore, at the end of a calibration run, two files, each containing 100 points, exist for each angle. These files are then imported into MATLAB. This code can be found in Appendix E.

5.3.2 Test Results and Discussion

As discussed previously, the original wearable design of JAMSTORM included two elastic armbands, one Velcroed about the subject's upper arm, the other on the forearm. However, it was found to be challenging to fasten the armbands sufficiently tight; during testing, the armbands tended to shift slightly down the subject's arm. This slippage caused the repeatability demonstrated in the tabletop tests to disappear. To fix this problem, the sensors were removed from the elastic armbands and secured directly to the subject's arm using medical tape. Since the locations of the sensors on the subject were not exactly the same for the two types of sensor attachments, the voltage output values are not the same for the two sets of tests; however, repeatability can still be compared. Taping the sensors to the subject's arm improved repeatability, as shown in Figures 5.3.2-5.3.2. These results show more voltage range overlaps between adjacent sensor angles than the tabletop test results. However, as with the tabletop values, these overlaps diminish or disappear

when data taken every 10 deg is examined instead of every 5 deg.

(a) Shoulder Abduction   (b) Shoulder Adduction
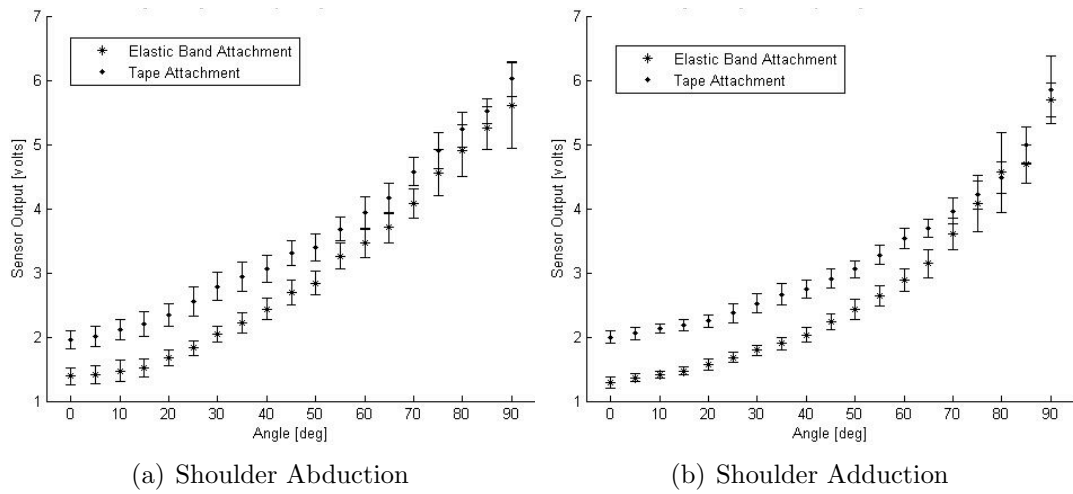
Figure 5.21: Average Voltages at Each Angle for Shoulder Abduction/Adduction

(a) Shoulder Extension   (b) Shoulder Flexion
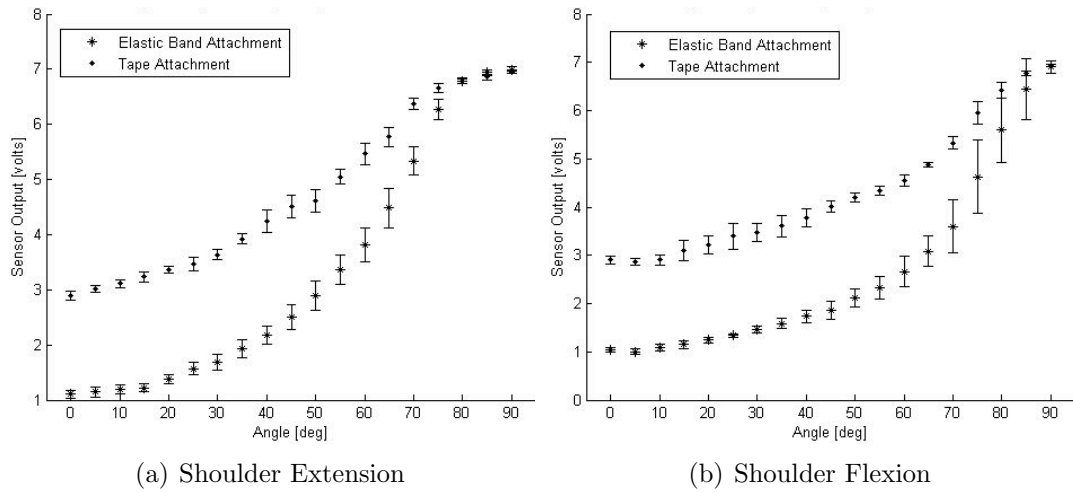
Figure 5.22: Average Voltages at Each Angle for Shoulder Flexion/Extension

(a) Elbow Flexion
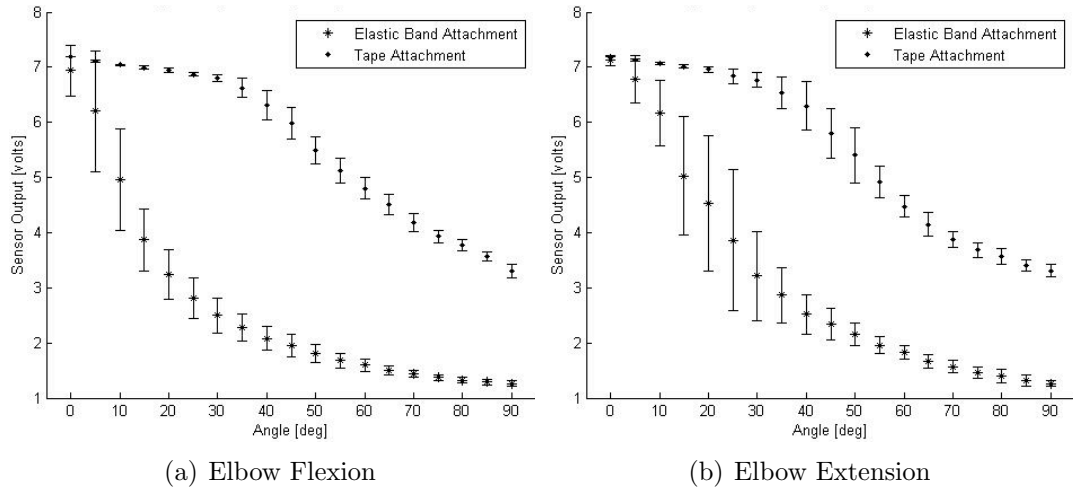
(b) Elbow Extension

Figure 5.23: Average Voltages at Each Angle for Elbow Flexion/Extension

(a) Shoulder Abduction and Adduction

(b) Shoulder Flexion and Extension

(c) Elbow Flexion and Extension
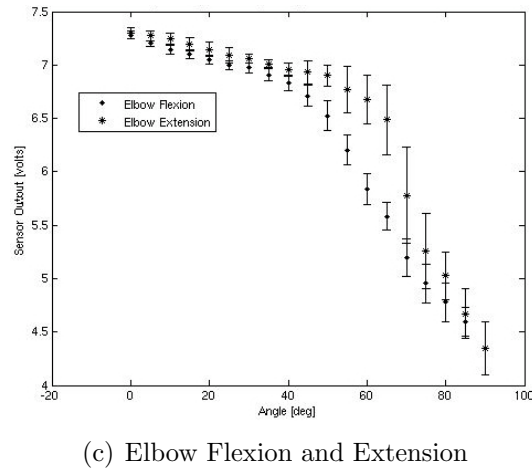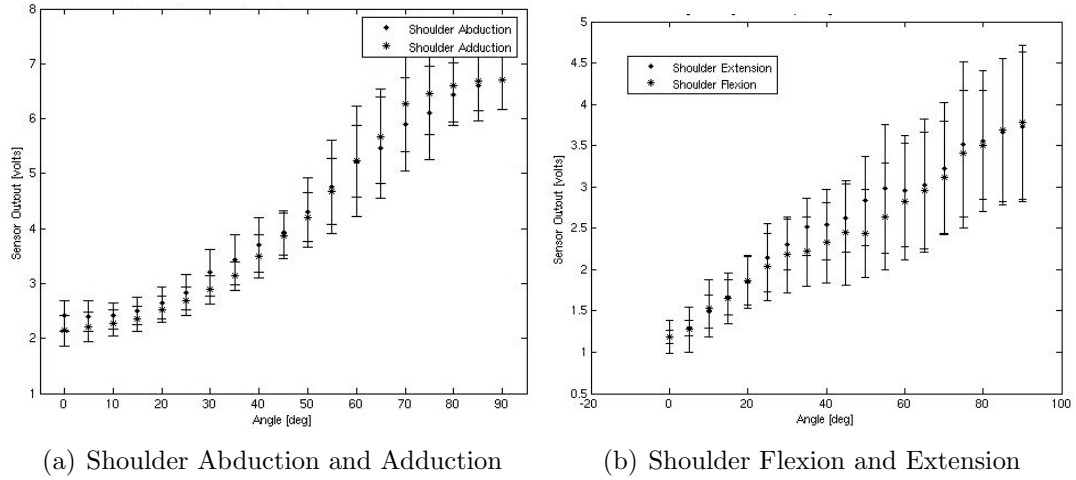
Figure 5.24: Average Voltages at Each Angle Showing Slight Hysteresis Between
Flexion/Extension and Abduction/Adduction During Tape Tests

As the comparison between elastic band and tape sensor attachment shows, there are large variations in sensor output from installation to installation. This means that the system must currently be calibrated before every set of tests since the output voltages are dependent on the exact positioning of the tubes and armbands relative to the optical fibers. While the need for frequent calibration does not make the system unusable, it is not a desirable trait. Therefore, a series of tests were performed to determine the repeatability of sensor attachment. For each of the three arm motions, the sensors were attached to the test subject using medical tape, and the sensor positions were marked. The subject performed one complete test run, with data taken every 5 deg. The sensors were then removed and reattached; using the markings, an effort was made to reattach the sensors in the same place as in the previous test. The subject completed another test run. This test cycle was performed five times for each of the three arm motions of interest.

Figure 5.3.2 shows that even with marking sensor position on the subject's arm, subsequent sensor installations for detecting shoulder flexion/extension are not highly consistent. It may also be noted that the output voltages are not monotonically increasing or decreasing. This issue was not seen in previous tests (see Figure 5.3.2) and is attributed to unintentional posture adjustments by the test subject, possibly combined with some slight scapula motions. With the sensors directly fixed to the subject's skin, these movements could affect sensor position and alignment more than when they were attached to the vest and armbands. Sensor installations for detecting shoulder abduction/adduction are more repeatable, and for elbow motion are even more consistent, as seen in Figures 5.3.2 and 5.3.2. Scapula

movement may have less of an effect on shoulder abduction/adduction than flexion/extension, or the exact locations of the sensors for abduction/adduction may just lend themselves to being easier to duplicate than for flexion/extension. Since no other arm motions are coupled with elbow flexion/extension, sensor attachments for these motions should be the most repeatable.

(a) Shoulder Abduction   (b) Shoulder Adduction
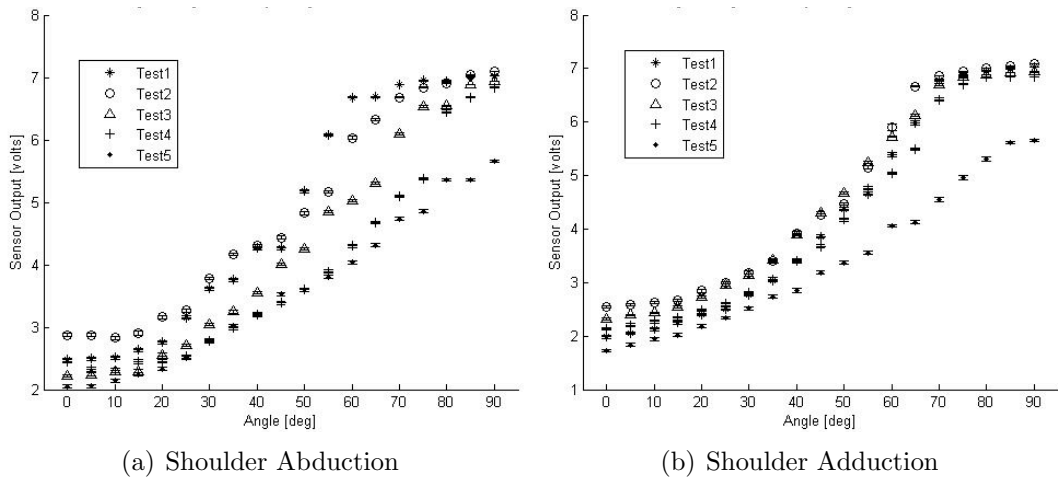
Figure 5.25: Average Voltages During Shoulder Abduction/Adduction for 5 Sensor Installations

(a) Shoulder Extension   (b) Shoulder Flexion
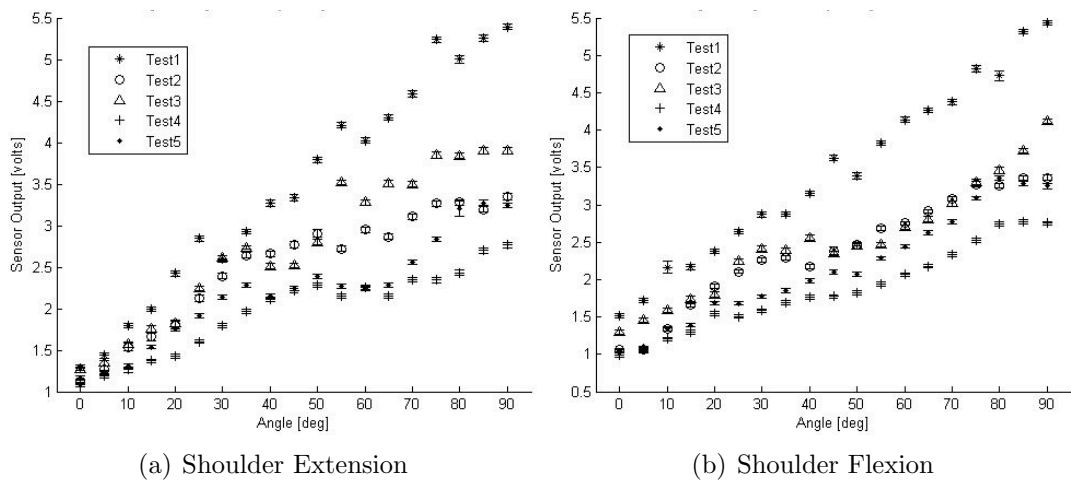
Figure 5.26: Average Voltages During Shoulder Flexion/Extension for 5 Sensor Installations

(a) Elbow Flexion	(b) Elbow Extension
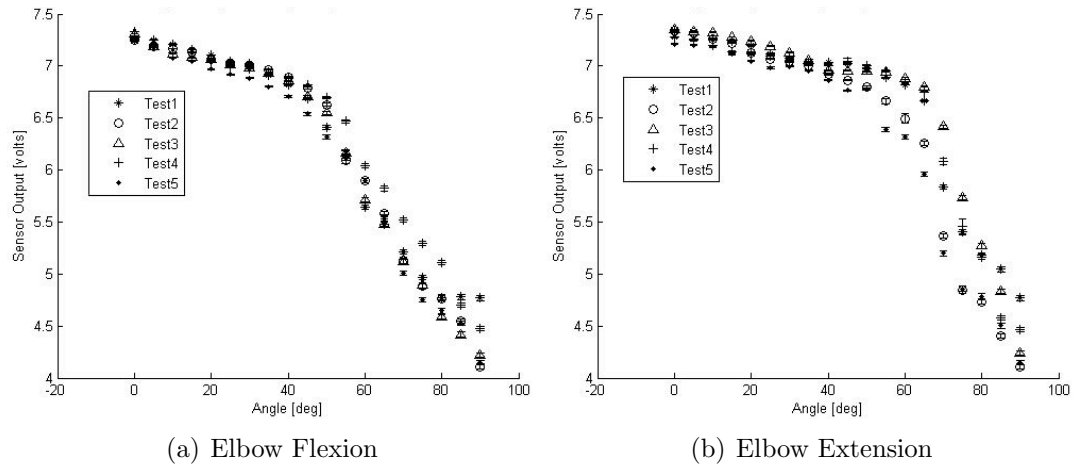
Figure 5.27: Average Voltages During Elbow Flexion/Extension for 5 Sensor Installations

Taping sensors directly to the system user's arm is not the preferred attachment technique for a final system. Sewing the sensors to a sleeved, tight-fitting garment could produce the same repeatability results. It may also be questioned what degree of repeatability is actually necessary for application in gesture-based control. Depending on the desired method of control, knowledge of absolute joint position may not be required. For many uses, only relative joint motion may be needed, which all of the previous data have shown, this system can provide.

Until this point, all tests had been static – move to an angle, start data collection, stop data collection, move to the next angle. Although dynamic results could not be compared with a second system due to previously discussed problems with the Flock of Birds, a basic understanding of the sensor output during continuous motion is desired. To achieve this, a series of elbow flexion/extension tests were performed at three speed levels. At the slowest speed, the test subject flexed the elbow 90 deg over approximately 11 sec, paused, then extended the elbow at the same

68

rate. At the fastest speed, the test subject flexed and extended the elbow 90 deg in 1 sec. A middle speed was also tested, at which the subject moved 90 deg in about 4 sec. The results of these motions can be seen in Figure 5.3.2. A rate of 90 deg in 11 sec equates to a steady motion of about 8 deg each second; a rate of 90 deg in 4 sec corresponds to moving 22.5 deg every second. Since the sampling rate is 50 Hz, extremely rough rounding yields 25 samples every 5 deg for the slow motion, 12 samples every 5 deg for medium speed of motion, and 3 samples every 5 deg for fast motion. To test if 3 samples taken for every 5 deg is an adequate sampling rate, data from a previous elbow flexion/extension test were used. Instead of averaging 100 samples at each angle and comparing between several tests, one test was chosen and 5 groups of 3 samples each were averaged for each angle and compared. Figure 5.3.2 shows that even with this much lower number of samples, the overall results are not significantly different from those in which all of the samples were used. This implies that high rates of motion are possible, and the system can still distinguish among changes of 5 deg.

(a) 90 Deg Motion in About 11 Sec

(b) 90 Deg Motion in About 4 Sec

(c) 90 Deg Motion in About 1 Sec
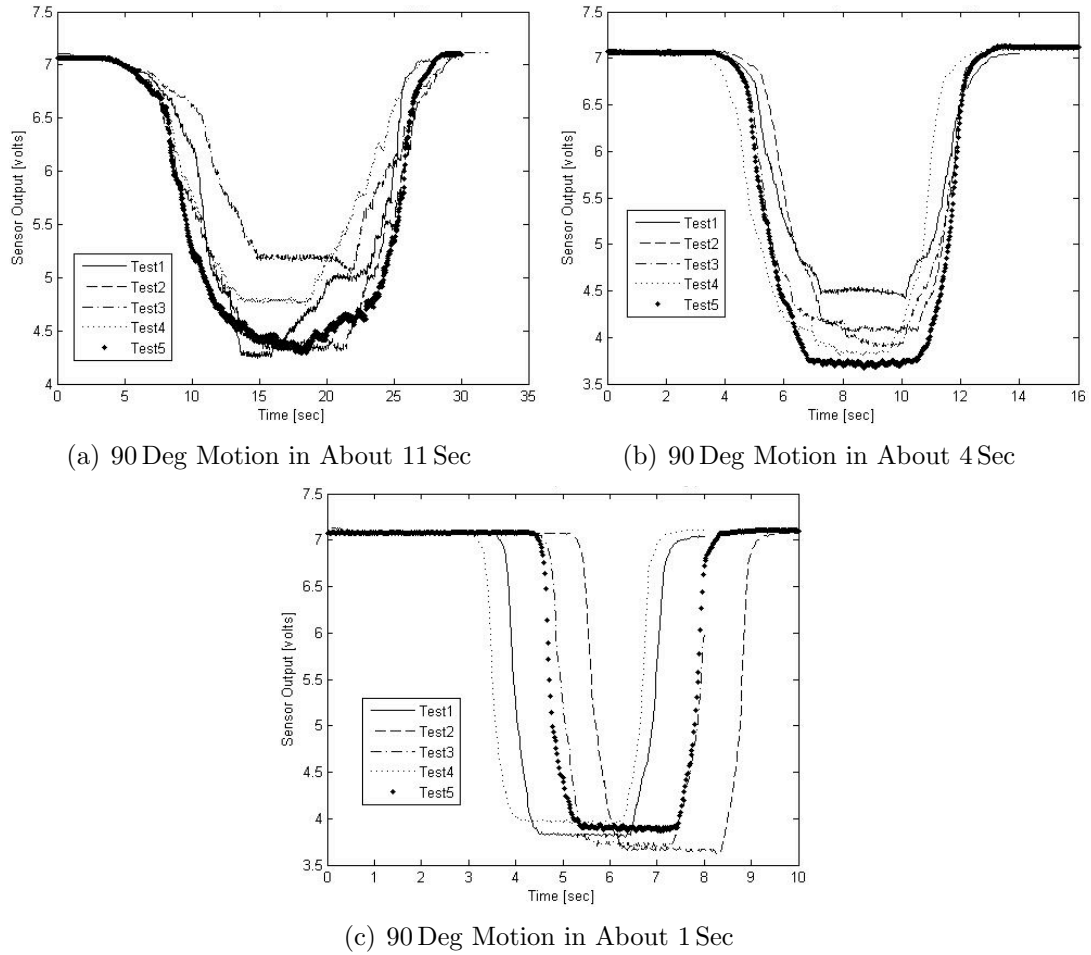
Figure 5.28: Continuous Motion at Three Different Speeds

(a) Voltage Averages Over 5 Sample Groups of 3 Samples per Angle

(b) Voltage Averages of All Samples per Angle
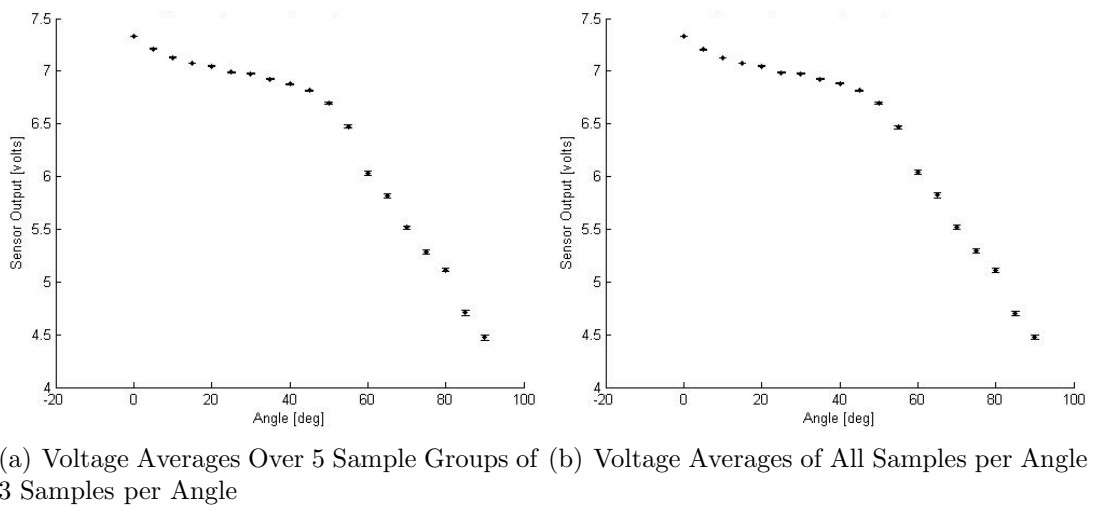
Figure 5.29: Voltage Averages for an Elbow Flexion Test

Chapter 6

Future Work and Conclusions

6.1   Future Work

Currently, the main area for improvement is related to the sensitivity of the sensors to their locations and orientations on the arm. If the photodiode is positioned slightly farther from the LED, a completely different set of voltage ranges will be generated. The elastic armbands were shown to cause problems due to their tendency to shift positions during arm motion. As discussed previously, this problem could be lessened or eliminated by attaching all of the sensors to a sleeved garment, instead of the vest. This would allow for better anchoring of photodiodes, LEDs, and tubing, and would help to keep the sensors aligned relative to each other and the directions of joint motion. Attaching the sensors to be more close-fitting to the body will improve performance as well, since the output voltages are also highly correlated to how well the sensors line up perpendicular to the axis of joint rotation, and this alignment is better maintained when the sensors are not able to shift during motion.

Sewing the sensors into a sleeve could also reduce the need for system calibration after each donning. With the current two attachment methods explored – vest/elastic bands and tape – the system must be calibrated each time a user puts it on. However, with the sensors in more fixed locations, it may be possible to

only calibrate the system once for a given user. Calibration will most likely still be required when switching to a new user, as the sensors will line up differently based on the user's shoulder width, arm length, and arm size. The changes in sensor outputs based on these physical variations should be studied to determine the amount of variation in user size that the system can accommodate without needing to be recalibrated.

As is clear from previous plots of sensor output voltages, sensor behavior is highly nonlinear. However, there generally is a portion of the output that is within a relatively linear range. Since the nonlinear regions occur at the endpoints of motion, it may be possible to operate only in the linear range by adjusting the distance between the photodiode and the end of the optical fiber at full arm extension or abduction. This might solve the problem at one extreme of motion, but it also could cause the sensor to reach the other nonlinear end more quickly, resulting in a smaller range of motion that can be measured. More research is necessary to quantify the nonlinear behavior and understand the causes. Once the behavior is understood, it may not even be necessary to remove the nonlinearities, but instead factor them into the motion analysis.

The next obvious steps are to add measurement of more joint motions, such as wrist flexion/extension and shoulder and forearm medial/lateral rotation. The addition of rotational movements will require research and testing to determine if and how this can be accomplished using the current method of allowing the fiber optic cable to slide within a piece of tubing. Also, further testing is needed to determine what, if any, effects the movement of one joint has on the sensor readings

for the other joints.

After measurement of all of the desired joint motions have been implemented, the system outputs must be integrated with the control software for the Ranger dexterous manipulator. Since the output information from JAMSTORM is a set of joint angles, these values can be directly communicated to the Ranger control software. During this integration, tests of the system can be run using the Ranger computer simulation, which requires fewer human resources than full Ranger operations and is safer for initial evaluation. After proving the system in simulation, tests can be performed using the 1-G version of Ranger. Before underwater research can begin, all of the JAMSTORM electronics must be sealed and waterproofed. Finally, the JAMSTORM electronics may be incorporated into MARS suit. Performance of the sensors in the pressurized suit will need to be evaluated. Since the sensors operate in a more repeatable manner when they are unable to shift position during motion, pressurization may improve overall system repeatability as the pressure may help keep the sensors rigidly positioned on the user. However, there is the possibility that the pressure will be large enough that the optical fibers will be unable to slide in and out of the tubes, which would render JAMSTORM unusable. Once these potential issues have been studied and addressed, JAMSTORM will be ready for underwater, suited, gestural teleoperation of Ranger.

6.2 Conclusions

Most robotic teleoperation is performed using multiple hand controllers and several cameras to obtain as many views of the robot and workspace as possible. This can be a difficult task and often requires two people: one to operate the robot and the other to manipulate the available cameras to obtain the necessary views. Therefore, there exists a need for a method for robotic teleoperation that is more intuitive and easier to use than the current hand controller approach. The use of gestures for robotic control is one option for an alternative teleoperation technique; however, most systems that can recognize human motion tend to either be too large for use outside of a designated research area, useable only for detecting human gait without being adaptable to detect arm movements, or are in other ways unsuitable for applications in the area of space robotics.

The goal of the research presented in the thesis was to evaluate optical fibers for use in a joint measurement system. JAMSTORM was developed as a wearable system that can be integrated with control software to teleoperate a robotic manipulator using gestures. The system uses fiber optic cables that slide within pieces of brass tubing and are attached to a vest and elastic armbands. Three fiber optic sensors are implemented, one each to measure shoulder abduction/adduction, shoulder flexion/extension, and elbow flexion/extension. Tests were performed to determine accuracy and repeatability of the system. As mentioned previously, the system does not reliably provide absolute angle information, such as would be necessary for characterizing body motion for biomedical research. However, for robotic

control, only information regarding relative motion from one point in time to the next is necessary. From the test results presented in this thesis, it is clear that a system using sliding optical fibers is capable of providing reliable relative joint angle information for gesture-based robot control.

Appendix A

Circuit Calculations

A.1 Calculation of resistor values for voltage regulation sub-circuit

For the adjustable voltage regulator LM317 [38]

$$
\begin{aligned}
V_{out} &= 1.25\left(1 + \frac{R_2}{R_1}\right) + I_{adj}R_2 \\
&= 1.25 + \frac{1.25}{R_1}R_2 + I_{adj}R_2 \\
&= 1.25 + R_2\left(\frac{1.25}{R_1} + I_{adj}\right)
\end{aligned}
\tag{A.1}
$$

$$
R_2\left(\frac{1.25}{R_1} + I_{adj}\right) = V_{out} - 1.25
\tag{A.2}
$$

$$
R_2 = \frac{V_{out} - 1.25}{\frac{1.25}{R_1} + I_{adj}}
\tag{A.3}
$$

Typical $I_{adj} = 50\,\mu\text{A}$ and maximum $I_{adj} = 100\,\mu\text{A}$

Set $R_1 = 500\,\Omega$ For WP7113SF4C infrared LED and QSD2030 infrared photodiode,

$V_{out} = V_{supply} = 1.4\,\text{V}$ [39][40] For $I_{adj} = 50\,\mu\text{A}$:

$$
R_2 = \frac{1.4 - 1.25}{\frac{1.25}{240} + 50 \times 10^{-6}} = 58.824\,\Omega
\tag{A.4}
$$

For $I_{adj} = 100\,\mu\text{A}$:

$$
R_2 = \frac{1.4 - 1.25}{\frac{1.25}{240} + 100 \times 10^{-6}} = 57.692\,\Omega
\tag{A.5}
$$

Based on available resistor values, choose $R_1 = 499\,\Omega$ and $R_2 = 51\,\Omega$, which results

in $V_{out} = 1.38\,\text{V}$

A.2 Calculation of resistor values for amplifier sub-circuit

For the operational amplifier LM324 [41]

$$V_O = \frac{R_s + R_f}{R_s} V_g \tag{A.6}$$

$$\frac{V_O}{V_g} \geq \frac{R_s + R_f}{R_s} \tag{A.7}$$

$$\frac{V_O}{V_g} R_s \geq R_s + R_f \tag{A.8}$$

$$\left(\frac{V_O}{V_g} - 1 \right) R_s \geq R_f \tag{A.9}$$

Set $V_{CC^+} = 9\,\text{V} = V_O$

Based on testing, without amplification, the maximum voltage out of the photodiode

is $1.8\,\text{V}$, so set $V_g = 1.8\,\text{V}$

$$\left(\frac{9}{1.8} - 1 \right) R_s \geq R_f \tag{A.10}$$

$$4R_s \geq R_f \tag{A.11}$$

choose $R_s = 10\,k\Omega$ and $R_f = 33\,k\Omega$, which results in a maximum $V_O = 7.74\,\text{V}$

Appendix B

Schematic
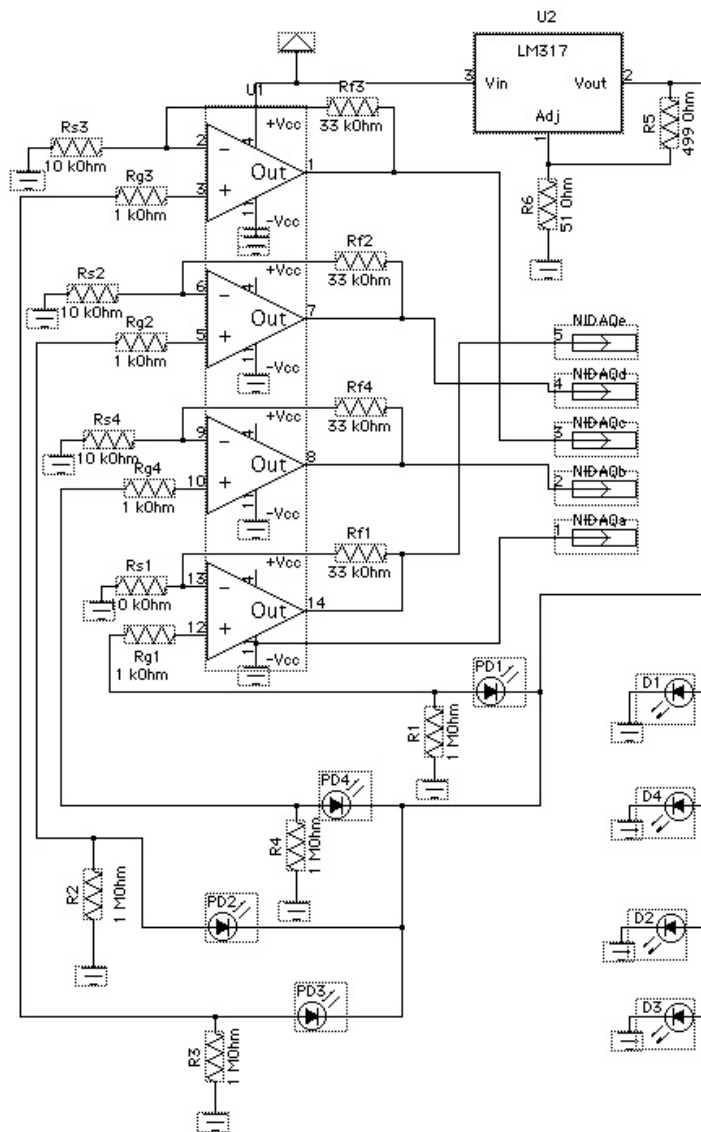
Figure B.1: Circuit Schematic

Appendix C

Example Spreadsheets

This appendix contains excerpts from the spreadsheets generated for data analysis. This data is from three days of testing, five tests per day, for the GHV 4001 Eska Premier optical fiber slideably positioned in a vinegar-treated brass tube with the LED directed into the input end of the fiber and the photodiode positioned at the output end of the brass tube. The system is powered with a $9\,\mathrm{V}$ supply.

The "Calc" column is the angle calculated from the predetermined voltage ranges. The equation for this assignment is shown below. The "Cor?" column contains a 1 if the assigned angle is correct and 0 if the angle is incorrect. This value is determined by using a simple IF statement in Excel to compare the value in the "Calc" column with the value in the "Actual" column, which contains the known value of the angle during data collection.

calc =

IF(AND(BD3<=C7,C7<BB3),90,

IF(AND(BB3<=C7,C7<AZ3),85,

IF(AND(AZ3<=C7,C7<AX3),80,

IF(AND(AX3<=C7,C7<AV3),75,

IF(AND(AV3<=C7,C7<AT3),70,

IF(AND(AT3<=C7,C7<AR3),65,

IF(AND(AR3<=C7,C7<AP3),60,

IF(AND(AP3<=C7,C7<AN3),55,

IF(AND(AN3<=C7,C7<AL3),50,

IF(AND(AL3<=C7,C7<AJ3),45,

IF(AND(AJ3<=C7,C7<AH3),40,

IF(AND(AH3<=C7,C7<AF3),35,

IF(AND(AF3<=C7,C7<AD3),30,

IF(AND(AD3<=C7,C7<AB3),25,

IF(AND(AB3<=C7,C7<Z3),20,

IF(AND(Z3<=C7,C7<X3),15,

IF(AND(X3<=C7,C7<V3),10,

IF(AND(V3<=C7,C7<T3),5,0))))))

where $C7$ is the value of the data point,

$BD3$ is the lowest range value and $AF3 = 0.00$,

and $T3$ is the highest range value

For this example, which is from the final tests that determined the optical fiber and test configuration choices,

$$BD3 = 1.510$$

$$BB3 = 1.371$$

$$AZ3 = 1.459$$

$$AX3 = 1.576$$

80

$$AV3 = 1.707$$

$$AT3 = 1.875$$

$$AR3 = 2.069$$

$$AP3 = 2.333$$

$$AN3 = 2.684$$

$$AL3 = 3.039$$

$$AJ3 = 3.483$$

$$AH3 = 4.018$$

$$AF3 = 4.639$$

$$AD3 = 5.369$$

$$AB3 = 6.166$$

$$Z3 = 6.865$$

$$X3 = 7.349$$

$$V3 = 7.551$$

$$T3 = 7.596$$

C.1 Example Spreadsheet of Compiled Raw Sensor Data (in Volts)

		10/17/2006	10/26/2006			10/17/2006	10/26/2006
point#	angle	test1	test15	point#	angle	test1	test15
1	0	7.619051	7.598667	1616	90	1.462906	1.320213
2	0	7.608859	7.578282	1617	90	1.462906	1.25906
3	0	7.619051	7.588475	1618	90	1.442521	1.289637
4	0	7.598667	7.588475	1619	90	1.462906	1.320213
5	0	7.608859	7.588475	1620	90	1.452713	1.320213
86	5	7.598667	7.578282	1701	85	1.544444	1.360983
87	5	7.588475	7.578282	1702	85	1.544444	1.35079
88	5	7.588475	7.578282	1703	85	1.513867	1.360983
89	5	7.598667	7.578282	1704	85	1.554636	1.360983
90	5	7.598667	7.578282	1705	85	1.524059	1.340598
171	10	7.557898	7.445782	1786	80	1.625982	1.48329
172	10	7.557898	7.455975	1787	80	1.61579	1.452713
173	10	7.547705	7.455975	1788	80	1.656559	1.452713
174	10	7.557898	7.445782	1789	80	1.625982	1.411944
175	10	7.547705	7.445782	1790	80	1.646367	1.452713
256	15	7.405013	6.936168	1871	75	1.829828	1.575021
257	15	7.394821	6.925975	1872	75	1.819636	1.605598
258	15	7.405013	6.94636	1873	75	1.829828	1.585213
259	15	7.405013	6.925975	1874	75	1.809444	1.605598
260	15	7.394821	6.956552	1875	75	1.819636	1.595405
341	20	6.956552	6.202323	1956	70	1.97252	1.666751
342	20	6.966745	6.222707	1957	70	1.982713	1.707521
343	20	6.956552	6.243092	1958	70	1.982713	1.676944
344	20	6.966745	6.212515	1959	70	1.97252	1.656559
345	20	6.966745	6.232899	1960	70	2.003097	1.687136
426	25	6.202323	5.4379	2041	65	2.227328	1.819636
427	25	6.202323	5.417516	2042	65	2.227328	1.850213
428	25	6.19213	5.417516	2043	65	2.186558	1.850213
429	25	6.212515	5.417516	2044	65	2.217135	1.84002
430	25	6.19213	5.448093	2045	65	2.186558	1.829828
511	30	5.295208	4.693863	2126	60	2.512712	2.054059
512	30	5.285016	4.734632	2127	60	2.512712	2.013289
513	30	5.295208	4.72444	2128	60	2.492327	2.043866
514	30	5.285016	4.72444	2129	60	2.471943	2.064251
515	30	5.285016	4.714247	2130	60	2.482135	2.054059
596	35	4.622517	4.072133	2211	55	2.757327	2.288481
597	35	4.602132	4.072133	2212	55	2.757327	2.319058
598	35	4.612325	4.082325	2213	55	2.736942	2.278289
599	35	4.642901	4.061941	2214	55	2.767519	2.298674
600	35	4.622517	4.092518	2215	55	2.72675	2.319058
681	40	4.082325	3.521749	2296	50	3.12425	2.655404
682	40	4.082325	3.521749	2297	50	3.144634	2.665596
683	40	4.082325	3.48098	2298	50	3.114057	2.655404
684	40	4.072133	3.521749	2299	50	3.12425	2.604443
685	40	4.092518	3.531941	2300	50	3.144634	2.635019
766	45	3.562518	3.103865	2381	45	3.531941	3.022327
767	45	3.57271	3.12425	2382	45	3.531941	3.012134
768	45	3.562518	3.073288	2383	45	3.531941	2.99175
769	45	3.57271	3.103865	2384	45	3.531941	3.022327
770	45	3.562518	3.073288	2385	45	3.542134	3.042711

point#	angle	10/17/2006 test1	10/26/2006 test15	point#	angle	10/17/2006 test1	10/26/2006 test15
851	50	3.165019	2.72675	2466	40	4.092518	3.399441
852	50	3.185403	2.72675	2467	40	4.112902	3.430018
853	50	3.154826	2.736942	2468	40	4.112902	3.430018
854	50	3.175211	2.696173	2469	40	4.072133	3.430018
855	50	3.134442	2.736942	2470	40	4.092518	3.430018
936	55	2.798096	2.451558	2551	35	4.642901	3.980402
937	55	2.808288	2.410789	2552	35	4.632709	4.000787
938	55	2.808288	2.431174	2553	35	4.602132	3.97021
939	55	2.787904	2.420981	2554	35	4.632709	3.980402
940	55	2.808288	2.410789	2555	35	4.632709	3.990595
1021	60	2.563673	2.145789	2636	30	5.254439	4.622517
1022	60	2.563673	2.125405	2637	30	5.234055	4.642901
1023	60	2.573866	2.115212	2638	30	5.254439	4.632709
1024	60	2.584058	2.125405	2639	30	5.264631	4.602132
1025	60	2.573866	2.135597	2640	30	5.264631	4.59194
1106	65	2.247712	1.901174	2721	25	6.080015	5.376747
1107	65	2.227328	1.870597	2722	25	6.080015	5.417516
1108	65	2.257904	1.901174	2723	25	6.039246	5.407324
1109	65	2.227328	1.860405	2724	25	6.080015	5.407324
1110	65	2.257904	1.911366	2725	25	6.049438	5.386939
1191	70	1.97252	1.697328	2806	20	6.94636	6.19213
1192	70	1.982713	1.717713	2807	20	6.956552	6.212515
1193	70	1.97252	1.697328	2808	20	6.936168	6.212515
1194	70	1.992905	1.697328	2809	20	6.936168	6.19213
1195	70	1.962328	1.707521	2810	20	6.94636	6.19213
1276	75	1.819636	1.575021	2891	15	7.384629	6.844437
1277	75	1.819636	1.564828	2892	15	7.384629	6.834245
1278	75	1.850213	1.575021	2893	15	7.374436	6.844437
1279	75	1.84002	1.544444	2894	15	7.384629	6.834245
1280	75	1.829828	1.585213	2895	15	7.374436	6.824052
1361	80	1.646367	1.422136	2976	10	7.506936	7.415206
1362	80	1.676944	1.462906	2977	10	7.517129	7.405013
1363	80	1.646367	1.452713	2978	10	7.506936	7.405013
1364	80	1.666751	1.422136	2979	10	7.506936	7.394821
1365	80	1.697328	1.48329	2980	10	7.506936	7.415206
1446	85	1.564828	1.299829	3061	5	7.56809	7.557898
1447	85	1.554636	1.320213	3062	5	7.56809	7.557898
1448	85	1.575021	1.320213	3063	5	7.578282	7.557898
1449	85	1.554636	1.340598	3064	5	7.578282	7.557898
1450	85	1.564828	1.330406	3065	5	7.56809	7.56809
1531	90	1.452713	1.289637	3146	0	7.578282	7.598667
1532	90	1.462906	1.269252	3147	0	7.56809	7.598667
1533	90	1.442521	1.299829	3148	0	7.56809	7.598667
1534	90	1.442521	1.289637	3149	0	7.578282	7.598667
1535	90	1.452713	1.279444	3150	0	7.578282	7.598667

C.2 Example Spreadsheet to Check Correctness of Calculated Angle

voltage ranges for every 5 degrees

	0		5		10		15		20		25	
9.000		7.596		7.551		7.349		6.865		6.166		5.369
	30		35		40		45		50		55	
	4.639		4.018		3.483		3.039		2.684		2.333	
60		65		70		75		80		85		90
2.069		1.875		1.707		1.576		1.459		1.371		0.000

	test1				test15			
actual	60-90?	55-30?	25-0?	correct?	60-90?	55-30?	25-0?	correct?
0	0	0	0	1	0	0	0	1
0	0	0	0	1	0	0	5	0
0	0	0	0	1	0	0	5	0
0	0	0	0	1	0	0	5	0
0	0	0	0	1	0	0	5	0
5	0	0	0	0	0	0	5	1
5	0	0	5	1	0	0	5	1
5	0	0	5	1	0	0	5	1
5	0	0	0	0	0	0	5	1
5	0	0	0	0	0	0	5	1
10	0	0	5	0	0	0	10	1
10	0	0	5	0	0	0	10	1
10	0	0	10	1	0	0	10	1
10	0	0	5	0	0	0	10	1
10	0	0	10	1	0	0	10	1
15	0	0	10	0	0	0	15	1
15	0	0	10	0	0	0	15	1
15	0	0	10	0	0	0	15	1
15	0	0	10	0	0	0	15	1
15	0	0	10	0	0	0	15	1
20	0	0	15	0	0	0	20	1
20	0	0	15	0	0	0	20	1
20	0	0	15	0	0	0	20	1
20	0	0	15	0	0	0	20	1
20	0	0	15	0	0	0	20	1
25	0	0	20	0	0	0	25	1
25	0	0	20	0	0	0	25	1
25	0	0	20	0	0	0	25	1
25	0	0	20	0	0	0	25	1
25	0	0	20	0	0	0	25	1
30	0	30	0	1	0	30	0	1
30	0	30	0	1	0	30	0	1
30	0	30	0	1	0	30	0	1
30	0	30	0	1	0	30	0	1
30	0	30	0	1	0	30	0	1
35	0	35	0	1	0	35	0	1
35	0	35	0	1	0	35	0	1
35	0	35	0	1	0	35	0	1
35	0	30	0	0	0	35	0	1
35	0	35	0	1	0	35	0	1

actual	test1				test15			
	60-90?	55-30?	25-0?	correct?	60-90?	55-30?	25-0?	correct?
40	0	35	0	0	0	40	0	1
40	0	35	0	0	0	40	0	1
40	0	35	0	0	0	45	0	0
40	0	35	0	0	0	40	0	1
40	0	35	0	0	0	40	0	1
45	0	40	0	0	0	45	0	1
45	0	40	0	0	0	45	0	1
45	0	40	0	0	0	45	0	1
45	0	40	0	0	0	45	0	1
45	0	40	0	0	0	45	0	1
50	0	45	0	0	0	50	0	1
50	0	45	0	0	0	50	0	1
50	0	45	0	0	0	50	0	1
50	0	45	0	0	0	50	0	1
50	0	45	0	0	0	50	0	1
55	0	50	0	0	0	55	0	1
55	0	50	0	0	0	55	0	1
55	0	50	0	0	0	55	0	1
55	0	50	0	0	0	55	0	1
55	0	50	0	0	0	55	0	1
60	0	55	0	0	60	0	0	1
60	0	55	0	0	60	0	0	1
60	0	55	0	0	60	0	0	1
60	0	55	0	0	60	0	0	1
60	0	55	0	0	60	0	0	1
65	60	0	0	0	65	0	0	1
65	60	0	0	0	70	0	0	0
65	60	0	0	0	65	0	0	1
65	60	0	0	0	70	0	0	0
65	60	0	0	0	65	0	0	1
70	65	0	0	0	75	0	0	0
70	65	0	0	0	70	0	0	1
70	65	0	0	0	75	0	0	0
70	65	0	0	0	75	0	0	0
70	65	0	0	0	70	0	0	1
75	70	0	0	0	80	0	0	0
75	70	0	0	0	80	0	0	0
75	70	0	0	0	80	0	0	0
75	70	0	0	0	80	0	0	0
75	70	0	0	0	75	0	0	1
80	75	0	0	0	85	0	0	0
80	75	0	0	0	80	0	0	1
80	75	0	0	0	85	0	0	0
80	75	0	0	0	85	0	0	0
80	75	0	0	0	80	0	0	1
85	80	0	0	0	90	0	0	0
85	80	0	0	0	90	0	0	0
85	80	0	0	0	90	0	0	0
85	80	0	0	0	90	0	0	0
85	80	0	0	0	90	0	0	0
90	85	0	0	0	90	0	0	1
90	80	0	0	0	90	0	0	1
90	85	0	0	0	90	0	0	1
90	85	0	0	0	90	0	0	1
90	85	0	0	85 0	90	0	0	1

C.3 Example Spreadsheet of Calculated Minima, Maxima, Means, and Standard Deviations

	0 deg	5 deg	10 deg	15 deg	20 deg	25 deg	30 deg
test1							
max	7.6191	7.5987	7.5579	7.4152	6.9973	6.2329	5.3360
min	7.5681	7.5681	7.5069	7.3642	6.9158	6.0392	5.2341
average	7.5898	7.5831	7.5316	7.3908	6.9532	6.1341	5.2828
std dev	0.0145	0.0087	0.0182	0.0139	0.0188	0.0708	0.0258
test2							
max	7.6496	7.6191	7.5681	7.4254	7.0687	6.2329	5.3971
min	7.5681	7.5681	7.5273	7.3948	6.8444	6.0698	5.2748
average	7.6036	7.5944	7.5455	7.4133	6.9596	6.1536	5.3407
std dev	0.0253	0.0176	0.0129	0.0055	0.0964	0.0617	0.0339
test3							
max	7.5885	7.5885	7.5477	7.4152	7.0585	6.3246	5.4379
min	7.5681	7.5681	7.5171	7.3642	6.8954	6.0596	5.2646
average	7.5783	7.5783	7.5301	7.3869	6.9784	6.1921	5.3515
std dev	0.0043	0.0046	0.0063	0.0162	0.0619	0.1124	0.0647
test4							
max	7.5885	7.5987	7.5375	7.4152	7.0687	6.2635	5.4991
min	7.5579	7.5681	7.5171	7.3744	6.8648	6.0902	5.2748
average	7.5788	7.5780	7.5298	7.3975	6.9667	6.1711	5.3852
std dev	0.0052	0.0044	0.0056	0.0096	0.0840	0.0631	0.0923
test5							
max	7.5885	7.5987	7.5477	7.4152	7.0687	6.2431	5.4379
min	7.5681	7.5579	7.5171	7.3846	6.9260	6.1310	5.3156
average	7.5770	7.5773	7.5320	7.4018	6.9953	6.1898	5.3740
std dev	0.0043	0.0051	0.0060	0.0059	0.0488	0.0398	0.0346
test6							
max	7.6496	7.6292	7.5987	7.3948	6.9056	6.1412	5.2442
min	7.5885	7.5885	7.5375	7.3133	6.7221	5.9169	5.1321
average	7.6120	7.6108	7.5667	7.3543	6.8145	6.0221	5.1857
std dev	0.0163	0.0118	0.0139	0.0236	0.0654	0.0816	0.0287
test7							
max	7.6191	7.6191	7.5579	7.3948	6.8342	6.0392	5.2850
min	7.5783	7.5885	7.5273	7.3031	6.7629	5.8456	5.0812
average	7.6013	7.6015	7.5467	7.3530	6.7986	5.9439	5.1835
std dev	0.0080	0.0075	0.0077	0.0278	0.0151	0.0714	0.0582
test8							
max	7.6191	7.6292	7.5783	7.4356	7.0075	6.2431	5.4583
min	7.5885	7.5885	7.5375	7.3439	6.8852	6.1717	5.2850
average	7.6045	7.6047	7.5572	7.3940	6.9473	6.2056	5.3745
std dev	0.0063	0.0069	0.0114	0.0286	0.0380	0.0143	0.0630
test9							
max	7.6191	7.6191	7.6089	7.3948	6.8342	6.0189	5.2850
min	7.5783	7.5783	7.5375	7.3337	6.7833	5.9475	5.1627
average	7.5988	7.5954	7.5754	7.3643	6.8161	5.9901	5.2279
std dev	0.0083	0.0072	0.0194	0.0156	0.0115	0.0149	0.0363

	0 deg	5 deg	10 deg	15 deg	20 deg	25 deg	30 deg
test10							
max	7.6089	7.6089	7.5987	7.4050	6.7935	6.0291	5.2544
min	7.5783	7.5783	7.5273	7.2929	6.7017	5.8558	5.0608
average	7.5907	7.5887	7.5619	7.3471	6.7476	5.9422	5.1558
std dev	0.0064	0.0065	0.0235	0.0409	0.0226	0.0541	0.0703
test11							
max	7.6191	7.6191	7.5681	7.3439	6.8241	6.1208	5.3258
min	7.5783	7.5885	7.4967	7.3133	6.7629	5.9271	5.0914
average	7.6047	7.6044	7.5369	7.3297	6.7944	6.0273	5.2107
std dev	0.0059	0.0060	0.0178	0.0062	0.0136	0.0709	0.0905
test12							
max	7.6089	7.6191	7.5375	7.3642	6.8241	6.0392	5.2035
min	7.5885	7.5783	7.5171	7.2929	6.6712	5.8150	5.0506
average	7.6029	7.6015	7.5291	7.3288	6.7432	5.9298	5.1301
std dev	0.0058	0.0058	0.0067	0.0243	0.0522	0.0837	0.0455
test13							
max	7.6089	7.6191	7.5579	7.3439	6.7833	5.9475	5.1627
min	7.5783	7.5885	7.4764	7.1910	6.6304	5.8456	5.0404
average	7.6015	7.6002	7.5181	7.2692	6.7088	5.8934	5.1034
std dev	0.0068	0.0062	0.0266	0.0594	0.0522	0.0291	0.0338
test14							
max	7.6191	7.6089	7.5171	7.1808	6.5183	5.7029	4.9385
min	7.5783	7.5579	7.4050	6.8444	6.1514	5.3462	4.6531
average	7.5975	7.5828	7.4586	7.0190	6.3336	5.5203	4.7900
std dev	0.0066	0.0131	0.0442	0.1481	0.1535	0.1513	0.1145
test15							
max	7.6089	7.5885	7.4662	6.9667	6.2533	5.4583	4.7550
min	7.5783	7.5477	7.3948	6.8037	6.1717	5.3666	4.5716
average	7.5981	7.5701	7.4257	6.8865	6.2152	5.4064	4.6715
std dev	0.0062	0.0101	0.0235	0.0547	0.0176	0.0241	0.0581
overall total							
max	7.6496	7.6292	7.6089	7.4356	7.0687	6.3246	5.4991
min	7.5579	7.5477	7.3948	6.8037	6.1514	5.3462	4.5716
avg avg	7.5960	7.5914	7.5297	7.3091	6.7848	5.9814	5.1845
avg st dev	0.0087	0.0081	0.0162	0.0320	0.0501	0.0629	0.0567
overall average							
avg max	7.6143	7.6109	7.5565	7.3541	6.8560	6.0691	5.2680
avg min	7.5762	7.5742	7.5029	7.2610	6.7126	5.8952	5.0995

	35 deg	40 deg	45 deg	50 deg	55 deg	60 deg
test1						
max	4.6429	4.1129	3.6033	3.1956	2.8287	2.5943
min	4.5919	4.0619	3.4912	3.1039	2.7268	2.4618
average	4.6228	4.0890	3.5485	3.1468	2.7732	2.5293
std dev	0.0137	0.0137	0.0280	0.0240	0.0269	0.0423
test2						
max	4.7041	4.1435	3.5931	3.1752	2.8185	2.5433
min	4.6021	3.9906	3.5319	3.0733	2.7675	2.4618
average	4.6551	4.0693	3.5629	3.1228	2.7882	2.4975
std dev	0.0296	0.0534	0.0145	0.0318	0.0135	0.0175
test3						
max	4.7958	4.1027	3.6033	3.1854	2.8083	2.5229
min	4.5919	4.0314	3.5319	3.1243	2.7369	2.4312
average	4.6898	4.0653	3.5698	3.1558	2.7714	2.4706
std dev	0.0749	0.0171	0.0134	0.0134	0.0140	0.0251
test4						
max	4.8060	4.1231	3.5829	3.2058	2.8491	2.5229
min	4.6531	4.0314	3.5014	3.0835	2.7573	2.4618
average	4.7356	4.0801	3.5396	3.1454	2.7934	2.4957
std dev	0.0570	0.0246	0.0167	0.0297	0.0204	0.0153
test5						
max	4.7244	4.1333	3.6237	3.1854	2.8287	2.5229
min	4.6021	4.0619	3.4810	3.0937	2.7471	2.4414
average	4.6686	4.0910	3.5494	3.1403	2.7826	2.4818
std dev	0.0351	0.0154	0.0487	0.0204	0.0153	0.0187
test6						
max	4.5206	3.9294	3.4504	3.0121	2.6146	2.3904
min	4.4492	3.8479	3.3587	2.9204	2.5433	2.2375
average	4.4852	3.8882	3.4051	2.9718	2.5847	2.3099
std dev	0.0162	0.0185	0.0169	0.0228	0.0171	0.0405
test7						
max	4.6123	3.9600	3.5014	3.0325	2.7981	2.3700
min	4.4289	3.8275	3.3791	2.8898	2.5637	2.2681
average	4.5229	3.8915	3.4416	2.9641	2.6821	2.3210
std dev	0.0579	0.0382	0.0304	0.0423	0.0772	0.0247
test8						
max	4.7652	4.1435	3.6033	3.1446	2.7268	2.3598
min	4.6633	3.9906	3.5014	3.0325	2.5637	2.2783
average	4.7130	4.0618	3.5524	3.0841	2.6488	2.3181
std dev	0.0256	0.0441	0.0221	0.0253	0.0471	0.0188
test9						
max	4.5512	3.9498	3.4810	2.9816	2.6044	2.3598
min	4.4594	3.8479	3.3077	2.8796	2.4923	2.2375
average	4.5013	3.9019	3.3936	2.9305	2.5495	2.3007
std dev	0.0230	0.0231	0.0492	0.0237	0.0262	0.0305

	35 deg	40 deg	45 deg	50 deg	55 deg	60 deg
test10						
max	4.5308	3.9804	3.4300	3.0325	2.7166	2.3191
min	4.4492	3.7460	3.3383	2.8898	2.5637	2.2171
average	4.4922	3.8648	3.3821	2.9630	2.6419	2.2674
std dev	0.0182	0.0824	0.0224	0.0427	0.0456	0.0251
test11						
max	4.6021	4.0517	3.5116	3.0019	2.6554	2.3496
min	4.4085	3.8173	3.2873	2.8796	2.4923	2.2171
average	4.5091	3.9312	3.3971	2.9448	2.5737	2.2764
std dev	0.0634	0.0878	0.0796	0.0307	0.0496	0.0326
test12						
max	4.5206	3.9091	3.3994	2.9714	2.7166	2.2987
min	4.3167	3.7460	3.2975	2.8796	2.5637	2.2069
average	4.4165	3.8282	3.3543	2.9284	2.6373	2.2537
std dev	0.0760	0.0521	0.0217	0.0227	0.0417	0.0220
test13						
max	4.4798	3.8581	3.4096	3.0121	2.6044	2.2579
min	4.3677	3.7766	3.2873	2.8083	2.4719	2.1764
average	4.4207	3.8182	3.3413	2.9093	2.5369	2.2113
std dev	0.0268	0.0172	0.0294	0.0668	0.0335	0.0195
test14						
max	4.2760	3.7052	3.2058	2.7777	2.6044	2.1968
min	4.0517	3.4504	3.0121	2.6350	2.2885	2.0337
average	4.1657	3.5770	3.1083	2.7062	2.4464	2.1111
std dev	0.0791	0.0975	0.0634	0.0417	0.1170	0.0507
test15						
max	4.1027	3.5421	3.1243	2.7573	2.4516	2.1458
min	3.9702	3.3892	2.9816	2.6044	2.2681	1.9929
average	4.0372	3.4644	3.0515	2.6872	2.3604	2.0783
std dev	0.0410	0.0448	0.0418	0.0433	0.0645	0.0445
overall total						
max	4.8060	4.1435	3.6237	3.2058	2.8491	2.5943
min	3.9702	3.3892	2.9816	2.6044	2.2681	1.9929
avg avg	4.5090	3.9081	3.4132	2.9867	2.6380	2.3282
avg st dev	0.0425	0.0420	0.0332	0.0321	0.0407	0.0285
overall average						
avg max	4.5756	3.9763	3.4749	3.0447	2.7084	2.3836
avg min	4.4404	3.8411	3.3526	2.9265	2.5698	2.2749

	65 deg	70 deg	75 deg	80 deg	85 deg	90 deg
test1						
max	2.2681	2.0133	1.8502	1.6973	1.5954	1.4833
min	2.1764	1.9419	1.7789	1.6056	1.5037	1.4221
average	2.2286	1.9728	1.8204	1.6554	1.5512	1.4525
std dev	0.0202	0.0146	0.0160	0.0217	0.0197	0.0134
test2						
max	2.2579	2.0643	1.8604	1.7075	1.6056	1.4731
min	2.1866	1.9419	1.7789	1.6158	1.5139	1.4119
average	2.2203	1.9993	1.8191	1.6627	1.5568	1.4476
std dev	0.0186	0.0280	0.0209	0.0176	0.0214	0.0138
test3						
max	2.2375	2.0235	1.8400	1.6871	1.5852	1.4731
min	2.1662	1.9521	1.7789	1.6158	1.5037	1.4018
average	2.2031	1.9883	1.8120	1.6536	1.5422	1.4400
std dev	0.0158	0.0159	0.0149	0.0151	0.0151	0.0159
test4						
max	2.2477	2.0235	1.8604	1.6871	1.5750	1.4731
min	2.1764	1.9419	1.7789	1.6056	1.5037	1.4018
average	2.2076	1.9840	1.8211	1.6531	1.5377	1.4443
std dev	0.0148	0.0166	0.0175	0.0198	0.0152	0.0155
test5						
max	2.2477	2.0439	1.8706	1.6973	1.5750	1.4629
min	2.1560	1.9318	1.7585	1.6056	1.4935	1.4018
average	2.2047	1.9800	1.8219	1.6617	1.5316	1.4386
std dev	0.0208	0.0316	0.0271	0.0188	0.0173	0.0152
test6						
max	2.1050	1.9725	1.8094	1.6973	1.5750	1.4731
min	2.0133	1.7891	1.6668	1.5037	1.4119	1.3814
average	2.0616	1.8826	1.7352	1.6024	1.4972	1.4357
std dev	0.0196	0.0553	0.0349	0.0588	0.0498	0.0208
test7						
max	2.1152	1.9623	1.7993	1.6769	1.5852	1.5139
min	2.0235	1.8502	1.6158	1.5037	1.4935	1.4323
average	2.0771	1.9053	1.7166	1.5941	1.5380	1.4749
std dev	0.0216	0.0227	0.0579	0.0535	0.0202	0.0190
test8						
max	2.1254	1.9012	1.7891	1.6362	1.5648	1.4833
min	2.0439	1.7993	1.6668	1.5444	1.4629	1.4018
average	2.0873	1.8504	1.7343	1.5889	1.5137	1.4399
std dev	0.0194	0.0249	0.0256	0.0219	0.0235	0.0195
test9						
max	2.1356	1.9318	1.7891	1.6260	1.5546	1.4731
min	2.0337	1.8400	1.6464	1.5343	1.4629	1.3916
average	2.0825	1.8888	1.7175	1.5835	1.5097	1.4349
std dev	0.0216	0.0199	0.0419	0.0229	0.0191	0.0182

	65 deg	70 deg	75 deg	80 deg	85 deg	90 deg
test10						
max	2.1968	1.9929	1.8502	1.6871	1.5444	1.4731
min	2.0133	1.8400	1.7075	1.5852	1.4425	1.3916
average	2.1079	1.9234	1.7784	1.6321	1.4979	1.4422
std dev	0.0589	0.0408	0.0400	0.0230	0.0241	0.0168
test11						
max	2.0846	1.9318	1.7483	1.6158	1.5139	1.4018
min	1.9623	1.8094	1.6769	1.5139	1.3916	1.2998
average	2.0240	1.8692	1.7126	1.5540	1.4554	1.3544
std dev	0.0269	0.0294	0.0179	0.0196	0.0260	0.0229
test12						
max	2.1152	2.0235	1.7789	1.6362	1.5343	1.4629
min	1.9827	1.7585	1.6362	1.5546	1.4323	1.3814
average	2.0488	1.8871	1.7124	1.5918	1.4762	1.4192
std dev	0.0328	0.1029	0.0368	0.0200	0.0206	0.0206
test13						
max	2.0133	1.8502	1.7177	1.5648	1.4833	1.4323
min	1.9114	1.7177	1.6260	1.4527	1.4119	1.3508
average	1.9667	1.7822	1.6664	1.5084	1.4473	1.3926
std dev	0.0230	0.0337	0.0221	0.0248	0.0177	0.0177
test14						
max	1.9318	1.7483	1.6056	1.4833	1.3610	1.2693
min	1.7993	1.6464	1.5037	1.3610	1.2794	1.1877
average	1.8747	1.7014	1.5501	1.4206	1.3189	1.2261
std dev	0.0359	0.0256	0.0202	0.0282	0.0178	0.0190
test15						
max	1.9216	1.7483	1.6464	1.4935	1.4018	1.3406
min	1.7891	1.6362	1.5241	1.4119	1.2896	1.2591
average	1.8568	1.6976	1.5781	1.4526	1.3399	1.3017
std dev	0.0359	0.0258	0.0256	0.0188	0.0260	0.0175
overall total						
max	2.2681	2.0643	1.8706	1.7075	1.6056	1.5139
min	1.7891	1.6362	1.5037	1.3610	1.2794	1.1877
avg avg	2.0835	1.8875	1.7331	1.5877	1.4876	1.4096
avg st dev	0.0257	0.0325	0.0280	0.0256	0.0222	0.0177
overall average						
avg max	2.1336	1.9487	1.7877	1.6396	1.5370	1.4459
avg min	2.0289	1.8264	1.6763	1.5343	1.4398	1.3678

C.4 Example Spreadsheet to Calculate Percent Error in Calculated Angles

ranges from each separate section

	test1			**test15**		
increasing angle						
	# correct	# incorrect	% error	# correct	# incorrect	% error
0 deg	78	7	8.24	66	19	22.35
5 deg	62	23	27.06	85	0	0.00
10 deg	65	20	23.53	85	0	0.00
15 deg	0	85	100.00	85	0	0.00
20 deg	0	85	100.00	85	0	0.00
25 deg	0	85	100.00	85	0	0.00
30 deg	85	0	0.00	85	0	0.00
35 deg	63	22	25.88	85	0	0.00
40 deg	0	85	100.00	77	8	9.41
45 deg	0	85	100.00	85	0	0.00
50 deg	0	85	100.00	85	0	0.00
55 deg	0	85	100.00	85	0	0.00
60 deg	0	85	100.00	85	0	0.00
65 deg	0	85	100.00	55	30	35.29
70 deg	0	85	100.00	63	22	25.88
75 deg	0	85	100.00	12	73	85.88
80 deg	0	85	100.00	35	50	58.82
85 deg	0	85	100.00	0	85	100.00
90 deg	0	85	100.00	85	0	0.00
decreasing angle						
90 deg	0	85	100.00	85	0	0.00
85 deg	0	85	100.00	33	52	61.18
80 deg	0	85	100.00	42	43	50.59
75 deg	0	85	100.00	67	18	21.18
70 deg	0	85	100.00	11	74	87.06
65 deg	0	85	100.00	0	85	100.00
60 deg	0	85	100.00	0	85	100.00
55 deg	0	85	100.00	0	85	100.00
50 deg	0	85	100.00	2	83	97.65
45 deg	0	85	100.00	7	78	91.76
40 deg	0	85	100.00	0	85	100.00
35 deg	78	7	8.24	13	72	84.71
30 deg	85	0	0.00	5	80	94.12
25 deg	85	0	0.00	73	12	14.12
20 deg	0	85	100.00	85	0	0.00
15 deg	0	85	100.00	0	85	100.00
10 deg	85	0	0.00	85	0	0.00
5 deg	85	0	0.00	82	3	3.53
0 deg	0	85	100.00	73	12	14.12
total:	771	2459	76.13	1991	1239	38.36

min total % error:	12.54
avg total % error:	50.97

Appendix D

Example MATLAB Code for Tabletop Evaluation of Optical Fibers
D.1   Results of Tabletop Tests Every 5 Deg

```
% b. teresa buchholz 2007
% tabletoptesting_incby5_analysis.m

clear all
close all

% READ IN DATA FROM FILES FOR BENDING WHILE SLIDING TESTS
read1_up0 = csvread('bending&sliding/main_diameter/10_17_2006/one_tube_v_9Vtest1/up0one1.csv',21,0);
read1_up90 = csvread('bending&sliding/main_diameter/10_17_2006/one_tube_v_9Vtest1/up90one1.csv',21,0);

read1_down0 = csvread('bending&sliding/main_diameter/10_17_2006/one_tube_v_9Vtest1/down0one1.csv',21,0);
read1_down90 = csvread('bending&sliding/main_diameter/10_17_2006/one_tube_v_9Vtest1/down90one1.csv',21,0);

% SIMILAR CODE FOR OTHER ANGLES AND OTHER TESTS
% ORGANIZE DATA FROM JAMSTORM SENSORS
up1_0 = read1_up0(1:total_points,2);
up1_90 = read1_up90(1:total_points,2);
down1_0 = read1_down0(1:total_points,2);
down1_90 = read1_down90(1:total_points,2);

% SIMILAR CODE FOR OTHER ANGLES AND OTHER TESTS
% FIND AVERAGE FOR EACH ANGLE SECTION PER TEST
avgup1_0 = mean(up1_0);
avgup1_90 = mean(up1_90);

avgup2_0 = mean(up2_0);
avgup2_90 = mean(up2_90);

avgup3_0 = mean(up3_0);
avgup3_90 = mean(up3_90);

avgup4_0 = mean(up4_0);
avgup4_90 = mean(up4_90);

avgup5_0 = mean(up5_0);
avgup5_90 = mean(up5_90);

avgup_day1_0 = mean([avgup1_0;avgup2_0;avgup3_0;avgup4_0;avgup5_0]);
avgup_day1_90 = mean([avgup1_90;avgup2_90;avgup3_90;avgup4_90;avgup5_90]);
avgup_day1 = [avgup_day1_0;avgup_day1_5;avgup_day1_10;avgup_day1_15;avgup_day1_20;avgup_day1_25;avgup_day1_30;
        avgup_day1_35;avgup_day1_40;avgup_day1_45;avgup_day1_50;avgup_day1_55;avgup_day1_60;avgup_day1_65;
        avgup_day1_70;avgup_day1_75;avgup_day1_80;avgup_day1_85;avgup_day1_90];

% SIMILAR CODE FOR OTHER ANGLES AND OTHER TESTS
avgup_day3_0 = mean([avgup11_0;avgup12_0;avgup13_0;avgup14_0;avgup15_0]);
avgup_day3_90 = mean([avgup11_90;avgup12_90;avgup13_90;avgup14_90;avgup15_90]);
avgup_day3 = [avgup_day3_0;avgup_day3_5;avgup_day3_10;avgup_day3_15;avgup_day3_20;avgup_day3_25;avgup_day3_30;
        avgup_day3_35;avgup_day3_40;avgup_day3_45;avgup_day3_50;avgup_day3_55;avgup_day3_60;avgup_day3_65;
        avgup_day3_70;avgup_day3_75;avgup_day3_80;avgup_day3_85;avgup_day3_90];

avgup_0 = mean([avgup_day1_0;avgup_day2_0;avgup_day3_0]);
avgup_90 = mean([avgup_day1_90;avgup_day2_90;avgup_day3_90]);
```

```
% SIMILAR CODE FOR OTHER ANGLES
avgup = [avgup_0;avgup_5;avgup_10;avgup_15;avgup_20;avgup_25;avgup_30;avgup_35;avgup_40;avgup_45;
        avgup_50;avgup_55;avgup_60;avgup_65;avgup_70;avgup_75;avgup_80;avgup_85;avgup_90];

stdup1_0 = std(up1_0);
stdup1_90 = std(up1_90);

stdup2_0 = std(up2_0);
stdup2_90 = std(up2_90);

stdup3_0 = std(up3_0);
stdup3_90 = std(up3_90);

stdup4_0 = std(up4_0);
stdup4_90 = std(up4_90);

stdup5_0 = std(up5_0);
stdup5_90 = std(up5_90);

% SIMILAR CODE FOR OTHER ANGLES AND OTHER TESTS
stdup_0 = std([up1_0;up2_0;up3_0;up4_0;up5_0;up6_0;up7_0;up8_0;
        up9_0;up10_0;up11_0;up12_0;up13_0;up14_0;up15_0]);
stdup_90 = std([up1_90;up2_90;up3_90;up4_90;up5_90;up6_90;up7_90;up8_90;
        up9_90;up10_90;up11_90;up12_90;up13_90;up14_90;up15_90]);

% SIMILAR CODE FOR OTHER ANGLES
stdup = [stdup_0;stdup_5;stdup_10;stdup_15;stdup_20;stdup_25;stdup_30;stdup_35;stdup_40;stdup_45;
        stdup_50;stdup_55;stdup_60;stdup_65;stdup_70;stdup_75;stdup_80;stdup_85;stdup_90];

% SIMILAR CODE FOR DECREASING ANGLES
% PLOT VOLTAGES
angle = [0;5;10;15;20;25;30;35;40;45;50;55;60;65;70;75;80;85;90];

figure
errorbar(angle,avgup,stdup,'.k')
hold on
errorbar(angle,avgdown,stddown,'.r')
title('Averages from All Tests')
xlabel('Angle [deg]')
ylabel('Sensor Output [volts]')
legend('Average of All Increasing Angle','Average of All Decreasing Angle')
```

D.2 Results of Tabletop Tests Every 10 Deg

```
% b. teresa buchholz 2007
% tabletoptesting_incby10_analysis.m

clear all
close all

% READ IN DATA FROM FILES
read1_up0 = csvread('10_17_2006/one_tube_v_9Vtest1/up0one1.csv',21,0);
read1_up90 = csvread('10_17_2006/one_tube_v_9Vtest1/up90one1.csv',21,0);

read1_down0 = csvread('10_17_2006/one_tube_v_9Vtest1/down0one1.csv',21,0);
read1_down90 = csvread('10_17_2006/one_tube_v_9Vtest1/down90one1.csv',21,0);

% SIMILAR CODE FOR OTHER ANGLES AND OTHER TESTS
% ORGANIZE DATA FROM JAMSTORM SENSORS
up1_0 = read1_up0(1:total_points,2);
up1_90 = read1_up90(1:total_points,2);

down1_0 = read1_down0(1:total_points,2);
down1_90 = read1_down90(1:total_points,2);
```

```
% SIMILAR CODE FOR OTHER ANGLES AND OTHER TESTS
% FIND AVERAGE FOR EACH ANGLE SECTION PER TEST
avgup1_0 = mean(up1_0);
avgup1_90 = mean(up1_90);

avgup2_0 = mean(up2_0);
avgup2_90 = mean(up2_90);

avgup3_0 = mean(up3_0);
avgup3_90 = mean(up3_90);

avgup4_0 = mean(up4_0);
avgup4_90 = mean(up4_90);

avgup5_0 = mean(up5_0);
avgup5_90 = mean(up5_90);

% SIMILAR CODE FOR OTHER ANGLES AND OTHER TESTS
avgup_day1_0 = mean([avgup1_0;avgup2_0;avgup3_0;avgup4_0;avgup5_0]);
avgup_day1_90 = mean([avgup1_90;avgup2_90;avgup3_90;avgup4_90;avgup5_90]);
avgup_day2_0 = mean([avgup6_0;avgup7_0;avgup8_0;avgup9_0;avgup10_0]);
avgup_day2_90 = mean([avgup6_90;avgup7_90;avgup8_90;avgup9_90;avgup10_90]);
avgup_day3_0 = mean([avgup11_0;avgup12_0;avgup13_0;avgup14_0;avgup15_0]);
avgup_day3_90 = mean([avgup11_90;avgup12_90;avgup13_90;avgup14_90;avgup15_90]);

% SIMILAR CODE FOR OTHER ANGLES AND OTHER TESTS
avgup_0 = mean([avgup_day1_0;avgup_day2_0;avgup_day3_0]);
avgup_90 = mean([avgup_day1_90;avgup_day2_90;avgup_day3_90]);

% SIMILAR CODE FOR OTHER ANGLES
avgup = [avgup_0;avgup_10;avgup_20;avgup_30;avgup_40;avgup_50;avgup_60;avgup_70;avgup_80;avgup_90];

stdup1_0 = std(up1_0);
stdup1_90 = std(up1_90);

stdup2_0 = std(up2_0);
stdup2_90 = std(up2_90);

stdup3_0 = std(up3_0);
stdup3_90 = std(up3_90);

stdup4_0 = std(up4_0);
stdup4_90 = std(up4_90);

stdup5_0 = std(up5_0);
stdup5_90 = std(up5_90);

% SIMILAR CODE FOR OTHER ANGLES AND OTHER TESTS
stdup_0 = std([up1_0;up2_0;up3_0;up4_0;up5_0;up6_0;up7_0;up8_0;
        up9_0;up10_0;up11_0;up12_0;up13_0;up14_0;up15_0]);
stdup_90 = std([up1_90;up2_90;up3_90;up4_90;up5_90;up6_90;up7_90;up8_90;
        up9_90;up10_90;up11_90;up12_90;up13_90;up14_90;up15_90]);

% SIMILAR CODE FOR OTHER ANGLES
stdup = [stdup_0;stdup_10;stdup_20;stdup_30;stdup_40;stdup_50;stdup_60;stdup_70;stdup_80;stdup_90];

% SIMILAR CODE FOR DECREASING ANGLES
% PLOTS
angle = [0;10;20;30;40;50;60;70;80;90];

figure
errorbar(angle,avgup,stdup,'.k')
hold on
errorbar(angle,avgdown,stddown,'.r')
title('Averages from All Tests')
xlabel('Angle [deg]')
ylabel('Sensor Output [volts]')
legend('Average of All Increasing Angle','Average of All Decreasing Angle')
```

D.3 Compare Sliding While Straight and Bending for 3 Different Bend Radii

```
% b. teresa buchholz 2007
% compare3diameters_bendvsstraight2_every01in.m

clear all
close all

% STRAIGHT SLIDING TESTS
% Read in Data From Files
out1_00 = csvread('slidingstraight/5_3_2007/test1/out00_test1.csv',6,2);
out1_09 = csvread('slidingstraight/5_3_2007/test1/out09_test1.csv',6,2);
out1_10 = csvread('slidingstraight/5_3_2007/test1/out10_test1.csv',6,2);
out1_29 = csvread('slidingstraight/5_3_2007/test1/out29_test1.csv',6,2);
out1_30 = csvread('slidingstraight/5_3_2007/test1/out30_test1.csv',6,2);

% SIMILAR CODE FOR OTHER DISTANCES AND OTHER TESTS
% Find Average and Standard Deviation for Each Distance for Each Test
avgout1_00 = mean(out1_00);
avgout1_29 = mean(out1_29);
avgout1_30 = mean(out1_30);

% SIMILAR CODE FOR OTHER DISTANCES AND OTHER TESTS
avgout_00 = mean([avgout1_00;avgout2_00;avgout3_00;avgout4_00;avgout5_00]);
avgout_20 = mean([avgout1_20;avgout2_20;avgout3_20;avgout4_20;avgout5_20]);
avgout_30 = mean([avgout1_30;avgout2_30;avgout3_30;avgout4_30;avgout5_30]);

% SIMILAR CODE FOR OTHER DISTANCES
avgout = [avgout_00,avgout_01,avgout_02,avgout_03,avgout_04,avgout_05,avgout_06,avgout_07,avgout_08,avgout_09,
        avgout_10,avgout_11,avgout_12,avgout_13,avgout_14,avgout_15,avgout_16,avgout_17,avgout_18,avgout_19,
        avgout_20,avgout_21,avgout_22,avgout_23,avgout_24,avgout_25,avgout_26,avgout_27,avgout_28,avgout_29,avgout_30];

stdout1_00 = std(out1_00);
stdout1_19 = std(out1_19);
stdout1_20 = std(out1_20);
stdout1_30 = std(out1_30);

% SIMILAR CODE FOR OTHER DISTANCES AND OTHER TESTS
stdout_00 = std([out1_00;out2_00;out3_00;out4_00;out5_00]);
stdout_19 = std([out1_19;out2_19;out3_19;out4_19;out5_19]);
stdout_20 = std([out1_20;out2_20;out3_20;out4_20;out5_20]);
stdout_30 = std([out1_30;out2_30;out3_30;out4_30;out5_30]);

% SIMILAR CODE FOR OTHER DISTANCES
stdout = [stdout_00,stdout_01,stdout_02,stdout_03,stdout_04,stdout_05,stdout_06,stdout_07,stdout_08,stdout_09,
        stdout_10,stdout_11,stdout_12,stdout_13,stdout_14,stdout_15,stdout_16,stdout_17,stdout_18,stdout_19,
        stdout_20,stdout_21,stdout_22,stdout_23,stdout_24,stdout_25,stdout_26,stdout_27,stdout_28,stdout_29,stdout_30];

% BENDING WHILE SLIDING TESTS: MIDDLE DIAMETER (1.8in)
% SAME CODE AS IN tabletoptesting_incby5_analysis.m
% BENDING WHILE SLIDING TESTS: SMALL DIAMETER (1.2in)
% SIMILAR CODE AS FOR MIDDLE DIAMETER
% BENDING WHILE SLIDING TESTS: LARGE DIAMETER (3.5 in)
% SIMILAR CODE AS FOR MIDDLE DIAMETER
% PLOT VOLTAGES
dist = [0;0.1;0.2;0.3;0.4;0.5;0.6;0.7;0.8;0.9;1;1.1;1.2;1.3;1.4;1.5;1.6;1.7;1.8;1.9;2;2.1;2.2;2.3;2.4;2.5;2.6;2.7;2.8;2.9;3];
angledist = [0;0.135;0.215;0.297;0.390;0.455;0.550;0.635;0.725;0.820;0.895;1.000;1.095;1.175;1.270;1.375;1.450;1.555;1.630];
smallangledist = [0;0.068;0.117;0.165;0.215;0.280;0.325;0.390;0.465;0.500;0.590;0.640;0.680;0.730;0.800;0.870;0.930;1.010;1.120];
bigangledist = [0;0.18;0.32;0.49;0.63;0.80;0.96;1.13;1.29;1.46;1.64;1.80;1.95;2.11;2.24;2.40;2.56;2.72;2.89];

figure
errorbar(dist,avgout,stdout,'.k')
```

```
hold on;
errorbar(angledist,avgup_day3,stdup_day3,'.r')
errorbar(smallangledist,avgsmallup,stdsmallup,'.b')
errorbar(bigangledist,avgbigup,stdbigup,'.g')
xlim([-0.1 3.1])
set(gca,'XTick',0:0.25:3)
title('Averages from 5 Tests on Day3')
xlabel('Cable Distance Out of Tube [in]')
ylabel('Sensor Output [volts]')
legend('Cable Sliding Out Straight','Increasing Angle About 1.8" Diameter','Increasing Angle About 1.2" Diameter','Increasing Angle About 3.5" Diameter')
```

Appendix E

Example MATLAB Code for Evaluating JAMSTORM Data
E.1   Compare Sensor Attachments for Shoulder Abduction/Adduction

```
% b. teresa buchholz 2007
% calibrate sensors for shoulder abduction/adduction
% read in voltages for each angle, contatenate for complete motion, and compare between tests
% and different methods of sensor attachment

clear all
close all

% READ IN DATA FROM ELASTIC BAND TESTS
reade1_up0 = csvread('4_19_2007/shoulder_abad_test1/up0deg_test1.csv',6,2);
reade1_up45 = csvread('4_19_2007/shoulder_abad_test1/up45deg_test1.csv',6,2);
reade1_up90 = csvread('4_19_2007/shoulder_abad_test1/up90deg_test1.csv',6,2);

reade1_down0 = csvread('4_19_2007/shoulder_abad_test1/down5deg_test1.csv',6,2);
reade1_down45 = csvread('4_19_2007/shoulder_abad_test1/down45deg_test1.csv',6,2);
reade1_down90 = csvread('4_19_2007/shoulder_abad_test1/down90deg_test1.csv',6,2);

% SIMILAR CODE FOR OTHER ANGLES AND OTHER TESTS
% READ IN DATA FROM TAPE TESTS
readt1_up0 = csvread('4_25_2007/shoulder_abad_test1/up0deg_test1.csv',6,2);
readt1_up45 = csvread('4_25_2007/shoulder_abad_test1/up45deg_test1.csv',6,2);
readt1_up90 = csvread('4_25_2007/shoulder_abad_test1/up90deg_test1.csv',6,2);

readt1_down0 = csvread('4_25_2007/shoulder_abad_test1/down0deg_test1.csv',6,2);
readt1_down45 = csvread('4_25_2007/shoulder_abad_test1/down45deg_test1.csv',6,2);
readt1_down90 = csvread('4_25_2007/shoulder_abad_test1/down90deg_test1.csv',6,2);

% SIMILAR CODE FOR OTHER ANGLES AND OTHER TESTS
% ORGANIZE DATA FROM ELASTIC BAND TESTS: Sensor for shoulder ab/adduction is on channel 2
upe1_0 = reade1_up0(1:length(reade1_up0),3);
upe1_45 = reade1_up45(1:length(reade1_up45),3);
upe1_90 = reade1_up90(1:length(reade1_up90),3);

downe1_0 = reade1_down0(1:length(reade1_down0),3);
downe1_45 = reade1_down45(1:length(reade1_down45),3);
downe1_90 = reade1_down90(1:length(reade1_down90),3);

% SIMILAR CODE FOR OTHER ANGLES AND OTHER TESTS
% ORGANIZE DATA FROM TAPE TESTS: Sensor for shoulder ab/adduction is on channel 3
upt1_0 = readt1_up0(1:length(readt1_up0),4);
upt1_45 = readt1_up45(1:length(readt1_up45),4);
upt1_90 = readt1_up90(1:length(readt1_up90),4);

downt1_0 = readt1_down0(1:length(readt1_down0),4);
downt1_45 = readt1_down45(1:length(readt1_down45),4);
downt1_90 = readt1_down90(1:length(readt1_down90),4);

% SIMILAR CODE FOR OTHER ANGLES AND OTHER TESTS
% FIND AVERAGE AND STANDARD DEVIATION OF VOLTAGES FOR EACH ANGLE
% Elastic Band Tests
avgupe_0 = mean([upe1_0;upe2_0;upe3_0;upe4_0;upe5_0]);
stdupe_0 = std([upe1_0;upe2_0;upe3_0;upe4_0;upe5_0]);
avgupe_45 = mean([upe1_45;upe2_45;upe3_45;upe4_45;upe5_45]);
```

```
stdupe_45 = std([upe1_45;upe2_45;upe3_45;upe4_45;upe5_45]);
avgupe_90 = mean([upe1_90;upe2_90;upe3_90;upe4_90;upe5_90]);
stdupe_90 = std([upe1_90;upe2_90;upe3_90;upe4_90;upe5_90]);

% SIMILAR CODE FOR OTHER ANGLES
avgupe = [avgupe_0;avgupe_5;avgupe_10;avgupe_15;avgupe_20;avgupe_25;avgupe_30;avgupe_35;avgupe_40;
        avgupe_45;avgupe_50;avgupe_55;avgupe_60;avgupe_65;avgupe_70;avgupe_75;avgupe_80;avgupe_85;avgupe_90];
stdupe = [stdupe_0;stdupe_5;stdupe_10;stdupe_15;stdupe_20;stdupe_25;stdupe_30;stdupe_35;stdupe_40;
        stdupe_45;stdupe_50;stdupe_55;stdupe_60;stdupe_65;stdupe_70;stdupe_75;stdupe_80;stdupe_85;stdupe_90];

avgdowne_0 = mean([downe1_0;downe2_0;downe3_0;downe4_0;downe5_0]);
stddowne_0 = std([downe1_0;downe2_0;downe3_0;downe4_0;downe5_0]);
avgdowne_45 = mean([downe1_45;downe2_45;downe3_45;downe4_45;downe5_45]);
stddowne_45 = std([downe1_45;downe2_45;downe3_45;downe4_45;downe5_45]);
avgdowne_90 = mean([downe1_90;downe2_90;downe3_90;downe4_90;downe5_90]);
stddowne_90 = std([downe1_90;downe2_90;downe3_90;downe4_90;downe5_90]);

% SIMILAR CODE FOR OTHER ANGLES
avgdowne = [avgdowne_0;avgdowne_5;avgdowne_10;avgdowne_15;avgdowne_20;avgdowne_25;avgdowne_30;
        avgdowne_35;avgdowne_40;avgdowne_45;avgdowne_50;avgdowne_55;avgdowne_60;
        avgdowne_65;avgdowne_70;avgdowne_75;avgdowne_80;avgdowne_85;avgdowne_90];
stddowne = [stddowne_0;stddowne_5;stddowne_10;stddowne_15;stddowne_20;stddowne_25;stddowne_30;
        stddowne_35;stddowne_40;stddowne_45;stddowne_50;stddowne_55;stddowne_60;
        stddowne_65;stddowne_70;stddowne_75;stddowne_80;stddowne_85;stddowne_90];

% Tape Tests
avgupt_0 = mean([upt1_0;upt2_0;upt3_0;upt4_0;upt5_0]);
stdupt_0 = std([upt1_0;upt2_0;upt3_0;upt4_0;upt5_0]);
avgupt_45 = mean([upt1_45;upt2_45;upt3_45;upt4_45;upt5_45]);
stdupt_45 = std([upt1_45;upt2_45;upt3_45;upt4_45;upt5_45]);
avgupt_90 = mean([upt1_90;upt2_90;upt3_90;upt4_90;upt5_90]);
stdupt_90 = std([upt1_90;upt2_90;upt3_90;upt4_90;upt5_90]);

% SIMILAR CODE FOR OTHER ANGLES
avgupt = [avgupt_0;avgupt_5;avgupt_10;avgupt_15;avgupt_20;avgupt_25;avgupt_30;avgupt_35;avgupt_40;
        avgupt_45;avgupt_50;avgupt_55;avgupt_60;avgupt_65;avgupt_70;avgupt_75;avgupt_80;avgupt_85;avgupt_90];
stdupt = [stdupt_0;stdupt_5;stdupt_10;stdupt_15;stdupt_20;stdupt_25;stdupt_30;stdupt_35;stdupt_40;
        stdupt_45;stdupt_50;stdupt_55;stdupt_60;stdupt_65;stdupt_70;stdupt_75;stdupt_80;stdupt_85;stdupt_90];

avgdownt_0 = mean([downt1_0;downt2_0;downt3_0;downt4_0;downt5_0]);
stddownt_0 = std([downt1_0;downt2_0;downt3_0;downt4_0;downt5_0]);
avgdownt_45 = mean([downt1_45;downt2_45;downt3_45;downt4_45;downt5_45]);
stddownt_45 = std([downt1_45;downt2_45;downt3_45;downt4_45;downt5_45]);
avgdownt_90 = mean([downt1_90;downt2_90;downt3_90;downt4_90;downt5_90]);
stddownt_90 = std([downt1_90;downt2_90;downt3_90;downt4_90;downt5_90]);

% SIMILAR CODE FOR OTHER ANGLES
avgdownt = [avgdownt_0;avgdownt_5;avgdownt_10;avgdownt_15;avgdownt_20;avgdownt_25;avgdownt_30;
        avgdownt_35;avgdownt_40;avgdownt_45;avgdownt_50;avgdownt_55;avgdownt_60;
        avgdownt_65;avgdownt_70;avgdownt_75;avgdownt_80;avgdownt_85;avgdownt_90];
stddownt = [stddownt_0;stddownt_5;stddownt_10;stddownt_15;stddownt_20;stddownt_25;stddownt_30;
        stddownt_35;stddownt_40;stddownt_45;stddownt_50;stddownt_55;stddownt_60;
        stddownt_65;stddownt_70;stddownt_75;stddownt_80;stddownt_85;stddownt_90];

% PLOT
angles = [0;5;10;15;20;25;30;35;40;45;50;55;60;65;70;75;80;85;90];

figure
errorbar(angles,avgupe,stdupe,'.b')
hold on
errorbar(angles,avgupt,stdupt,'.r')
xlim([-5 95])
set(gca,'XTick',0:10:90)
title('Voltage Averages for Every 5 Deg of Shoulder Abduction')
xlabel('Angle [deg]')
ylabel('Sensor Output [volts]')
legend('Elastic Band Attachment','Tape Attachment')
```

```
figure
errorbar(angles,avgdowne,stddowne,'.b')
hold on
errorbar(angles,avgdownt,stddownt,'.r')
xlim([-5 95])
set(gca,'XTick',0:10:90)
title('Voltage Averages for Every 5 Deg of Shoulder Adduction')
xlabel('Angle [deg]')
ylabel('Sensor Output [volts]')
legend('Elastic Band Attachment','Tape Attachment')
```

E.2 Compare Sensor Attachments for Shoulder Flexion/Extension

```
% b. teresa buchholz 2007
% calibrate sensors for shoulder flexion/extension
% read in voltages for each angle, contatenate for complete motion, and compare between tests
% and different methods of sensor attachment

clear all
close all

% READ IN DATA FROM ELASTIC BAND TESTS
% READ IN DATA FROM TAPE TESTS
% ORGANIZE DATA FROM ELASTIC BAND TESTS: Sensor for shoulder flexion/extension is on channel 3
% ORGANIZE DATA FROM TAPE TESTS: Sensor for shoulder flexion/extension is on channel 2
% FIND AVERAGE AND STANDARD DEVIATION OF VOLTAGES FOR EACH ANGLE
% Elastic Band Tests
% Tape Tests

% PLOT

% SIMILAR CODE TO THAT FOR SHOULDER ABDUCTION/ADDUCTION
```

E.3 Compare Sensor Attachments for Elbow Flexion/Extension

```
% b. teresa buchholz 2007
% elbow flexion/extension
% read in voltages for each angle, contatenate for complete motion, and compare between tests
% and different methods of sensor attachment

clear all
close all

% READ IN DATA FROM ELASTIC BAND TESTS
% READ IN DATA FROM TAPE TESTS
% ORGANIZE DATA FROM ELASTIC BAND TESTS: Sensor for elbow flexion/extension is on channel 1
% ORGANIZE DATA FROM TAPE TESTS: Sensor for elbow flexion/extension is on channel 0
% FIND AVERAGE AND STANDARD DEVIATION OF VOLTAGES FOR EACH ANGLE
% Elastic Band Tests
% Tape Tests

% PLOT

% SIMILAR CODE TO THAT FOR SHOULDER ABDUCTION/ADDUCTION
```

Bibliography

[1] "Remote manipulator system," accessed Mar 16, 2007. [Online]. Available: http://prime.jsc.nasa.gov/ROV/rms.html

[2] S. J. Hoffman, "Advanced eva capabilities: A study for nasa's revolutionary aerospace systems concept program, Tech. Rep. NASA/TP–2004-212068, Apr 2004.

[3] D. Akin, "Ranger laboratory operations," May 2003, accessed Feb 16, 2007. [Online]. Available: http://spacecraft.ssl.umd.edu/SSL.photos/SSLprojects.photos/LabRobots /030515.AFD-SLP/030507.AFD-SLP.01.jpg

[4] "Ranger telerobotic shuttle experiment october 1996 to june 2002," Jul 2002, accessed Mar 16, 2007. [Online]. Available: http://www.ssl.umd.edu/projects/rangertsx/

[5] S. Jacobs, "Maryland advance research/simulation (mars) suit," accessed Feb 16, 2007. [Online]. Available: http://ssl.umd.edu/projects/MARSsuit/index.shtml

[6] D. Akin, "Mars suit mx-2 - november 11, 2005 low-cost glove testing," Nov 2005, accessed Feb 16, 2007. [Online]. Available: http://spacecraft.ssl.umd.edu/SSL.photos /SSLprojects.photos/MARS_Suit/051111.MARS/051111.MARS.11.jpg

[7] ——, "Dual-arm hst ecu changeout april 14, 2004," Apr 2004, accessed Feb 16, 2007. [Online]. Available: http://spacecraft.ssl.umd.edu/SSL.photos/SSLprojects.photos /LabRobots/040414.2armECU/040414.AFD-SLP.48.jpg

[8] B. A. Marcus, B. An, and B. Eberman, "Exos research on master controllers for robotic devices," in *Fifth Annual Workshop on Space Operations Applications and Research*, ser. NASA Conference Publication, vol. 1, no. 3127, Jul 1991, pp. 238–245.

[9] G. L. Harris, *The Origins and Technology of the Advance Extravehicular Space Suit*, ser. AAS History Series. American Astronautical Society, 2001, vol. 24.

[10] "Mars exploration rover mission: Spacecraft: Surface operations: Rover: How the robotic arm works," Jun 2005, accessed Mar 16, 2007. [Online]. Available: http://marsrovers.jpl.nasa.gov/mission/sc_rover_arm_move.html

[11] "Canadarm description," MacDonald, Dettwiler and Associates Ltd., 2006, accessed Mar 16, 2007. [Online]. Available: http://sm.mdacorporation.com/what_we_do/can_description.html

[12] S. Roderick, "Joint soft stops," sroderick@ssl.umd.edu, Mar 2006, accessed Mar 6, 2006.

[13] Y. Ogura, H. Aikawa, K. Shimomura, H. Kondo, A. Morishima, H. ok Lim, and A. Takanishi, "Development of a new humanoid robot wabian-2." IEEE International Conference on Robotics and Automation, May 2006, pp. 76–81.

[14] K. Kaneko, F. Kanehiro, S. Kajita, H. Hirukawa, T. Kawasaki, M. Hirata, K. Akachi, and T. Isozumi, "Humanoid robot hrp-2." IEEE International Conference on Robotics and Automation, Apr 2004, pp. 1083–1090.

[15] L. Wang, W. Hu, and T. Tan, "Recent developments in human motion analysis," *Pattern Recognition*, vol. 36, pp. 585–601, 2003.

[16] "Weta digital ltd," accessed Jan 9, 2007. [Online]. Available: http://www.wetadigital.com

[17] "Weta digital," Jan 2007, accessed Jan 9, 2007. [Online]. Available: http://en.wikipedia.org/wiki/Weta_Digital

[18] "The polar express production notes," accessed Jan 9, 2007. [Online]. Available: http://polarexpressmovie.warnerbros.com/movie_prodnotes.html

[19] K. Tong and M. H. Granat, "A practical gait analysis system using gyroscopes," *Medical Engineering and Physics*, vol. 21, pp. 87–94, 1999.

[20] I. P. I. Pappas, M. R. Popovic, T. Keller, V. Dietz, and M. Morari, "A reliable gait phase detection system," *IEEE Transactions on Neural Systems and Rehabilitation Engineering*, vol. 9, pp. 113–125, Jun 2001.

[21] T. Liu, Y. Inoue, K. Shibata, and H. Morioka, "Development of wearable sensor combinations for human lower extremity motion analysis." IEEE International Conference on Robotics and Automation, May 2006, pp. 1655–1660.

[22] D. W. Repperger, S. J. Remis, and G. Merrill, "Performance measures of teleoperation using an exoskeleton device," ser. International Conference on Robotics and Automation, vol. 1. IEEE, May 1990, pp. 552–557.

[23] C. Carignan, M. Liszka, and S. Roderick, "Design of an arm exoskeleton with scapula motion for shoulder rehabilitation," in *Proceedings of the 12th International Conference on Advanced Robotics*, Jul 2005, pp. 524–531.

[24] J. K. Perng, B. Fisher, S. Hollar, and K. S. J. Pister, "Acceleration sensing glove (asg)." IEEE International Symposium on Wearable Computers, 1999, pp. 178–180.

[25] R. Williamson and B. J. Andrews, "Gait event detection for fes using accelerometers and supervised machine learning," *IEEE Transactions on Rehabilitation Engineering*, vol. 8, no. 3, pp. 312–319, Sep 2000.

[26] R. Barbieri, E. Farella, L. Benini, B. Ricco, and A. Acquaviva, "A low-power motion capture system with integrated accelerometers." IEEE Consumer Communications and Networking Conference, Jan 2004, pp. 418–423.

[27] H. Dejnabadi, B. M. Jolles, and K. Aminian, "A new approach to accurate measurement of uniaxial joint angles based on a combination of accelerometers and gyroscopes," *IEEE Transactions on Biomedical Engineering*, vol. 52, no. 8, pp. 1478–1484, Aug 2005.

[28] C. U. Ranniger, E. A. Sorenson, and D. L. Akin, "Development and applications of a self-contained, non-invasive eva joint angle and muscle fatigue sensor system." AIAA Life Sciences and Space Medicine Conference, Apr 1995.

[29] O. Fukuda, T. Tsuji, M. Kaneko, and A. Otsuka, "A human-assisting manipulator teleoperated by emg signals and arm motions," *IEEE Transactions on Robotics and Automation*, vol. 19, no. 2, pp. 210–222, Apr 2003.

[30] P. K. Artemiadis and K. J. Kyriakopoulos, "Emg-based teleoperation of a robot arm in planar catching movements using armax model and trajectory monitoring techniques." IEEE International Conference on Robotics and Automation, May 2006, pp. 3244–3249.

[31] P. Gibbs and H. H. Asada, "Wearable conductive fiber sensors for measuring joint movements." IEEE International Conference on Robotics and Automation, Apr 2004, pp. 4753–4758.

[32] C. U. Ranniger, D. L. Akin, C. G. Henshaw, S. W. Sell, and E. A. Sorenson, "Joint angle and muscle fatigue detection in the hand during eva simulation operations." AIAA Space Programs and Technologies Conference, Sept 1996.

[33] S. M. Wright and R. E. Wright, "Optical attenuator movement detection system," Patent 5 184 009, Feb, 1993. [Online]. Available: http://patft.uspto.gov/netacgi/nph-Parser?Sect1=PTO1&Sect2=HITOFF&d =PALL&p=1&u=%2Fnetahtml%2FPTO%2Fsrchnum.htm&r=1&f=G&l=50& s1=5184009.PN.&OS=PN/5184009&RS=PN/5184009

[34] *Low-Cost Multifunction DAQ for USB*, National Instruments, 2006.

[35] "How to oxidize brass," accessed Aug 30, 2006. [Online]. Available: http://www.ehow.com/how_13285_oxidize-brass.html

[36] R. A. Chernich and B. Streigler, "Model internal combustion engines frequently asked questions: How do i make my new, bright, and shiny brass bits look less new, bright, and shiny?" accessed Aug 1, 2006. [Online]. Available: http://modelenginenews.org/faq/index.html#qa12

[37] *GHV 4001*, Mitsubishi Rayon Co., Ltd. Eska Optical Fiber Division, Jul 2001.

[38] *LM117/LM317A/LM317 3-Terminal Adjustable Regulator*, National Semiconductor, Jun 2006.

[39] H. Q. Yuan, *T-1 3/4 (5mm) Infra-red Emitting Diode*, Kingbright, Apr 2005.

[40] *QSD2030 Plastic Silicon Photodiode*, Fairchild Semiconductor, Oct 2001.

[41] *LM124, LM124A, LM224, LM224A, LM324, LM324A, LM2902, LM2902V, LM224K, LM224KA, LM324K, LM324KA, LM2902K, LM2902KV, LM2902AV Quadruple Operational Amplifers*, Texas Instruments Incorporated, Jan 2005.